(12) LEVEL II

DNA 4816

DEVELOPMENT OF A LATERALLY ISOLATED DIAPHRAGM-TYPE SOIL-STRUCTURE INTERFACE STRESS GAGE

U.S. Army Engineer Waterways Experiment Station
Structures Laboratory
P.O. Box 631
Vicksburg, Mississippi 39180

1 December 1977

Final Report for Period 1 November 1975—1 December 1977

MIPR 77-577

THIS WORK SPONSORED BY THE DEFENSE NUCLEAR AGENCY
UNDER RDT&E RMSS CODE B344077462 H11CAXSX33273 H2590D.

Prepared for
Director
DEFENSE NUCLEAR AGENCY
Washington, D. C. 20305

Destroy this report when it is no longer needed. Do not return to sender.

PLEASE NOTIFY THE DEFENSE NUCLEAR AGENCY, ATTN: STTI, WASHINGTON, D.C. 20305, IF YOUR ADDRESS IS INCORRECT, IF YOU WISH TO BE DELETED FROM THE DISTRIBUTION LIST, OR IF THE ADDRESSEE IS NO LONGER EMPLOYED BY YOUR ORGANIZATION.

UNCLASSIFIED

SECURITY CLASSIFICATION OF THIS PAGE (When Data Entered)

REPORT DOCUMENTATION PAGE

READ INSTRUCTIONS BEFORE COMPLETING FORM

1. REPORT NUMBER: DNA 4816F	2. GOVT ACCESSION NO.: A089 719
3. RECIPIENT'S CATALOG NUMBER:	
4. TITLE (and Subtitle): DEVELOPMENT OF A LATERALLY ISOLATED DIAPHRAGM-TYPE SOIL-STRUCTURE INTERFACE STRESS GAGE	5. TYPE OF REPORT & PERIOD COVERED: Final Report. ~~For Period~~ 1 Nov 75—1 Dec 77
	6. PERFORMING ORG. REPORT NUMBER:
7. AUTHOR(s): Andres/Peekna	8. CONTRACT OR GRANT NUMBER(s): MIPR-77-577
9. PERFORMING ORGANIZATION NAME AND ADDRESS: U.S. Army Engineer Waterways Experiment Station, Structures Laboratory, P.O. Box 631, Vicksburg, Mississippi 39180	10. PROGRAM ELEMENT, PROJECT, TASK AREA & WORK UNIT NUMBERS: Subtask H11CAXSX352-73 / H11CAXS
11. CONTROLLING OFFICE NAME AND ADDRESS: Director, Defense Nuclear Agency, Washington, D.C. 20305	12. REPORT DATE: 1 December 1977
	13. NUMBER OF PAGES: 96
14. MONITORING AGENCY NAME & ADDRESS(if different from Controlling Office): X352	15. SECURITY CLASS. (of this report): UNCLASSIFIED
	15a. DECLASSIFICATION/DOWNGRADING SCHEDULE:

16. DISTRIBUTION STATEMENT (of this Report)

Approved for public release; distribution unlimited.

17. DISTRIBUTION STATEMENT (of the abstract entered in Block 20, if different from Report)

18. SUPPLEMENTARY NOTES

This work sponsored by the Defense Nuclear Agency under RDT&E RMSS Code B344077462 H11CAXSX35273 H2590D.

19. KEY WORDS (Continue on reverse side if necessary and identify by block number)

Gage Mount	Strain Rate
Gage	Stress
Peak Stress	Lateral Stress
Soil	Interface Pressure

20. ABSTRACT (Continue on reverse side if necessary and identify by block number)

The measurement package consists of a modified commercially available gage together with a mounting system that anchors the gage close to the outer surface of the structure and isolates it from lateral stresses in the structure. This package is suitable for soil-structure interface stress measurement with full-scale gage ratings from 1.4 MPa to 20.7 MPa.

DD FORM 1 JAN 73 1473 EDITION OF 1 NOV 65 IS OBSOLETE

UNCLASSIFIED

SECURITY CLASSIFICATION OF THIS PAGE (When Data Entered)

411415

JQB

PREFACE

This project was sponsored by the Defense Nuclear Agency under Subtask L11CAXSX352, "Development of Field Instrumentation," Work Unit 49, "Development of a Soil-Structure Interface Stress Gage," and Work Unit 65, "Soil Structure Interaction Gage," and under Subtask H11CAXSX352, "Development of Field Instrumentation, Work Unit 73, "Soil Structure Interaction Gage." The work was accomplished during the period November 1975 through December 1977. Mr. T. E. Kennedy was technical monitor.

This project was under the general supervision of Mr. W. J. Flathau, Chief, Structures Laboratory (SL), Waterways Experiment Station (WES), Mr. J. T. Ballard, Chief, Structural Mechanics Division (SMD), SL.

This project was conducted by Dr. A. Peekna, the principal investigator. Mr. F. Glaser, Exchange Scientist, Federal Republic of Germany, participated in the early stages of the project. Evaluation of lateral sensitivity and the gage registration tests with sand were performed at the Soil Dynamics Division, SL. SP-5 J. V. Getchell, who supervised some of these test, also helped prepare this report.

Directors of WES during this period were COL G. H. Hilt, Director, and COL J. L. Cannon, Commander and Director. Mr. F. R. Brown was Technical Director.

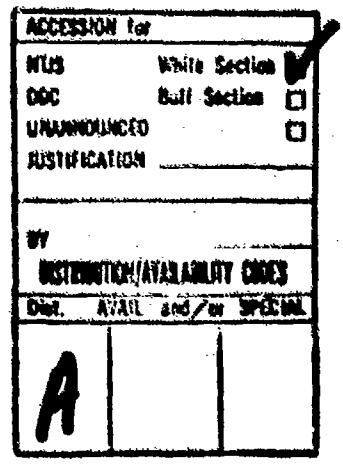

CONTENTS

TABLES

FIGURES

CONVERSION FACTORS, U. S. CUSTOMARY TO METRIC (SI)
UNITS OF MEASUREMENT

U. S. customary units of measurement used in this report can be converted to metric (SI) units as follows:

Multiply	By	To Obtain
inches	2.54	centimetres
feet	0.3048	metres
pounds (mass)	453.59237	grams
pounds (force)	4.448222	newtons
pounds (mass) per cubic inch	27.68	grams per cubic cm
pounds (force) per square inch	.006894757	megapascals
g (acceleration of gravity)	9.18	metres per sec^2
microns	10^{-6}	metres

DEVELOPMENT OF A LATERALLY ISOLATED DIAPHRAGM-TYPE SOIL-STRUCTURE INTERFACE STRESS GAGE

CHAPTER 1

INTRODUCTION

1.1 BACKGROUND

The type of gage that has been most commonly used to measure compressive stress exerted by an explosion-generated stress wave on a soil-structure interface is basically a strain-gaged load column. Force exerted on a flush-mounted piston is transmitted to a column supporting the piston along the sensing axis; readout is from strain gages on this column. Experience with this type of gage has indicated several shortcomings. For example, any significant friction between the piston and casing affects the measured results. Such friction can arise when interface shear stress forces the piston against one side, or when slightly eccentric loading misaligns the piston, or as a result of injection of granular material into the space between piston and casing just above the O-ring. Output time-histories which indicate friction in the gage have been observed. The necessity of carefully disassembling and cleaning this type of gage between each use is a nuisance and creates a quality control problem.

Further considerations have also revealed other fundamental shortcomings. Generally, a soil stress gage will not indicate exactly the same stress that would occur if the gage were not present in the medium. For example, if a soil stress gage is placed in the free field or on a structure made of relatively stiff material such that it sticks out into the external medium, the gage will tend to overregister if its active deflecting portion is stiffer than the medium, and to underregister if it is less stiff than the medium. Reference 1 is a thorough review of the interaction between soils and pressure cells. A flush-mounted stress gage is surrounded on its sides by the structure material, and the approach of attempting to have the axial gage stiffness

match or exceed the stiffness of the structure material has sometimes been taken. Such an approach is fallacious because it ignores the effect of lateral stresses in the structure wall. Because Poisson's ratio of the wall material is not zero, the lateral stresses in the wall also influence the strains in the wall in the normal direction. Therefore, it is easy to see that motion of the piston face with respect to the outer surface of the structure depends not only on the stiffness of the strain-gaged column and the structure material but also on the lateral stresses in the structure wall. Since the lateral stresses often greatly exceed the normal stresses being measured, sometimes by an order of magnitude, their effect should not be ignored. The deeper the anchoring of the gage column within the structure wall, the greater the predicted effect of lateral stresses on gage registration. Clearly, this sort of situation in which gage registration is significantly affected not only by soil properties but also by the lateral stresses at its specific location in the structure is to be avoided as much as possible.

1.2 PURPOSE

The objective was to develop an improved soil-structure interface stress gage suitable for static and dynamic measurements in a stress wave environment in the range below 35 MPa (5000 psi).

1.3 SCOPE

Investigations of alternative gage concepts and the results of a survey of commercial gages are documented in Chapter 2; emphasis is on comparison of the column and diaphragm concepts. The design of the lateral isolation system is documented in Chapter 3, and its experimental evaluation in Chapter 4. Prediction and experimental determination acceleration sensitivity are in Chapter 5. Results of gage registration tests with three different kinds of sand are presented in Chapter 6. The findings are summarized in Chapter 7; the reader may wish to proceed directly to Chapter 7 in a first reading

CHAPTER 2

ALTERNATIVE GAGE CONCEPTS AND SURVEY OF INDUSTRY

2.1 GENERAL REQUIREMENTS

When making measurements on a structure interface, it must be kept in mind that the lateral stresses in the structure often greatly exceed the normal stresses being measured. Clearly, the gage and its mounting system must be such that the lateral stresses exerted on the mount do not in themselves give rise to significant output. In addition, the lateral stresses also tend to influence the interaction of the gage with the external medium (soil) by way of influencing the strains in the wall in the normal direction; this has already been mentioned in Chapter 1. It is worthwhile to consider the stresses and strains in the wall in somewhat greater detail.

Given an orthogonal coordinate system with the x-direction along the gage sensing axis (the normal to the surface) and considering the structure wall material in the vicinity as elastic with Young's modulus E and Poisson's ratio ν, the fundamental equation relating the axial strain ε_x to the axial stress σ_x and the lateral stresses σ_y and σ_z is (from Reference 2).

$$\varepsilon_x = \frac{1}{E}\left[\sigma_x - \nu\,(\sigma_y + \sigma_z)\right] \qquad (2.1)$$

In hardened structures, the concrete is usually a fairly stong mix; denoting its unconfined compressive strength by σ, typical properties are as follows:

$$\sigma = 40 \text{ MPa } (\approx 6000 \text{ psi})$$
$$E = 40{,}000 \text{ MPa } (\approx 6{,}000{,}000 \text{ psi})$$
$$\nu = 0.18 \qquad (2.2)$$

The test environment for hardened structures is usually designed to approach the threshold of destruction. For example, at the center of a square two-way slab, the lateral stresses would be axisymmetric, with $\sigma_y = \sigma_z \approx -\sigma$ at the loaded face; tensile stresses and extensional strains are considered positive. With the properties (2.2) Equation 2.1

predicts an extensional strain of $360(10^{-6})$ for the contribution of lateral stresses to the strain in the axial direction. If the magnitude of the normal stress applied by the soil is 2 MPa (≈300 psi), its contribution is a compressive strain of magnitude $50(10^{-6})$. The total axial strain would thus be $360(10^{-6})$ minus $50(10^{-6})$, i.e., an extensional strain of $310(10^{-6})$ at the center of the slab. By contrast, at some other locations in the same slab, such as near a simply supported edge, the lateral stresses may be negligible; at such locations the axial strain would be of magnitude $50(10^{-6})$ and compressive. The futility of attempting to match gage stiffness to the deformation of the structure material in the axial direction should be fully apparent from this example.

Considering a gage anchored at depth d from the outer surface of the structure, the axial elongation of the structure material around the gage due to lateral stresses is the depth d times the contribution of lateral stresses to the strain in the axial direction. Again, with $\sigma_y = \sigma_z = -\sigma$ and the properties (2.2), this is $360(10^{-6})d$. Since the gage column itself is isolated from lateral stresses, this is also the magnitude of the resultant inward motion of the gage face with respect to the outer surface of the structure. If the structure were loaded with a fluid, this inward motion would have no adverse consequences, but with soil this gives rise to arching effects which alter the stresses exerted on the gage face. Comparison with the magnitude of the gage deflection δ due to the normal stress p acting on the gage gives an estimate of the relative significance of the effect of lateral stresses on the interaction of the gage with the soil. For a column gage with external sensing face area A_e and a column with cross-sectional area A_c, length L, and made of a material with Young's modulus E_c, this is given by:

$$\delta = \frac{pA_eL}{A_cE_c} \tag{2.3}$$

As an example, consider the aluminum column gage described in Figure 3.13 of Reference 3, which has a 1.27-cm-diameter sensing area, a thin 1.1 x 9.5 mm column cross section, and column length 2.54 cm.

This was designed for a sensing range up to 3.5 MPa (500 psi). With the Young's modulus of aluminum (Reference 4) and a normal stress p of 2 MPa (≈300 psi), Equation 2.3 gives

$$\delta = 0.009 \text{ mm} \tag{2.4}$$

Taking the anchoring depth d to be the sum of the column length and the piston length, which for this particular gage is 3.8 cm, the inward motion of the gage face with respect to the outer surface of the structure due to $\sigma_y = \sigma_z \approx -\sigma$ with the concrete properties (2.2) is:

$$360(10^{-6})d = 0.014 \text{ mm} \tag{2.5}$$

Comparison of the results (2.4) and (2.5) shows that, in this particular example, lateral stresses have a greater effect on the motion of the gage face with respect to the outer surface of the structure than the normal stress acting on the gage. Naturally, this sort of situation does not necessarily occur in all structures tests; this example merely demonstrates that with deeply anchored gages it is not very unusual for the two effects to be of the same order of magnitude.

Therefore, in order to minimize the effects of soil arching on the registration of a flush-mounted gage in a variety of lateral stress environments in the structure, the following main requirements emerge:

a. The gage should be as stiff as possible, with a small ratio of deflection to the diameter of the sensing area.

b. The gage should be anchored as closely to the surface of the structure as possible; the anchoring depth should at least be smaller than the diameter of the sensing area.

The second requirement (b) minimizes the effects of lateral stresses at the location of the gage in the structure on the interaction of the gage with the soil.

There are also additional requirements. The gage and its mounting system must be such that the lateral stresses exerted on the mount do not in themselves give rise to significant output. The gage should not only be able to survive large acceleration from any direction but should also have low acceleration sensitivity. In order to provide good signal

to noise ratios in explosive test environments, the gage should have high electrical output. The area of the sensing face should be sufficient to average over a large number of sand grains. Since field tests often involve temperature extremes, the functioning of the gage should not be affected by changes in temperature.

2.2 COMPARISON OF COLUMN AND DIAPHRAGM CONCEPTS

Columns are generally thought of as being stiffer than diaphragms, but clearly a thick diaphragm is stiffer than a thin column. A well-designed gage would have a very small ratio of deflection to diameter and would nevertheless give high electrical output. This suggests minimizing the quantity

$$\frac{\delta}{D\varepsilon}$$

where δ is the gage deflection, D is the diameter of the sensing area, and ε is the strain magnitude at the location of the strain gages inside the gage. For a column gage with column length L, $\delta = \varepsilon L$, and therefore

$$\frac{\delta}{D\varepsilon} = \frac{L}{D} \tag{2.6}$$

For a diaphragm gage, the formulas for the deflection δ_m and flexural stress s_m at the midpoint of a fixed-edged plate with radius a, thickness t, Young's modulus E_d and Poisson's ratio ν_d loaded with uniform pressure p give (Reference 5)

$$\delta_m = \frac{3(1 - \nu_d^2)}{16 E_d} \frac{a^4}{t^3} p \tag{2.7}$$

$$s_m = \frac{3}{8}(1 + \nu_d) \left(\frac{a}{t}\right)^2 p \tag{2.8}$$

The maximum flexural stress is in the radial direction at the edge; denoting this by s_e we have (Reference 5)

$$s_e = \frac{3}{4} \left(\frac{a}{t}\right)^2 p \tag{2.9}$$

The strain ε_m at the midpoint of the inner surface of the diaphragm is related to s_m by (Reference 2)

$$\varepsilon_m = \frac{1 - \nu_d}{E_d} s_m$$

and using Equation 2.8

$$\varepsilon_m = \frac{3(1 - \nu_d^2)}{8E_d} \left(\frac{a}{t}\right)^2 p \qquad (2.10)$$

Combining Equations 2.7 and 2.10 gives, for a diaphragm gage

$$\frac{\delta_m}{D\varepsilon_m} = \frac{D}{8t} \qquad (2.11)$$

where $D = 2a$ is the diameter of the sensing area, as before.

A diaphragm gage is usually configured with one or two strain gages at the center sensing flexural tension and one or two near the edge sensing flexural compression. Although the radial compressive strain right at the edge is of higher magnitude than the tensile strain at the center, radial strain varies rapidly with distance near the edge, and it is not practical to position a strain gage of finite size at the edge without getting close to or even partly overlapping the inflection point. Therefore, the compression-sensing strain gages in a small diaphragm gage probably do not contribute more to the total output than the secondary lateral-sensing (Poisson) strain gages in a typical column gage. It follows that comparison of the tensile strain at the center of a diaphragm gage with the magnitude of the compressive strain in a column gage is a realistic indication of the relative magnitudes of electrical output that may be obtained.

It is seen from Equation 2.6 that for a column gage the quantity $\delta/D\varepsilon$ does not depend on any parameters that control its sensing range. On the other hand, since for a given external load the stresses in a fixed-edged plate are proportional to the square of the ratio of the diameter to thickness (Reference 5), it is seen from Equation 2.11 that

the quantity $\delta_m/D\varepsilon_m$ is less for diaphragm gages designed to sense high external stresses than for lower-ranged ones. As an example, for a gage with the diaphragm of the WES SE gage (Reference 6) with D = 1.905 cm and t = 1.905 mm, Equation 2.11 gives a value of 1.25 for $\delta_m/D\varepsilon_m$. By using the properties of the stainless steel SE gage material (Reference 4) in Equation 2.9, a pressure of 10 MPa (≈1500 psi) is predicted to produce a strain of approximately $500(10^{-6})$ at the center of this diaphragm. Similarly, it is predicted that if it is desired to produce the same strain with a pressure of 1.4 MPa (≈200 psi), the ratio D/t has to be raised by a factor of 2.7, resulting in a value of 3.4 for $\delta_m/D\varepsilon_m$. It is interesting to note in passing that these two diaphragm-gage $\delta_m/D\varepsilon_m$ values (1.25 and 3.4) bracket the $\delta/D\varepsilon$ value of 2.0 given by Equation 2.6 for the column gage of Reference 3, which has a 1.27-cm-diameter sensing area and 2.54-cm column length.

However, the effects of soil arching on gage registration are not the same for a rigid-faced piston and a flexing diaphragm with the same midpoint deflection. Due to the deflection discontinuity at the edge of a piston, arching effects can be expected to be considerably greater, especially at the edge of a piston. The results of Askegaard's approximate solutions to the problems of a nonadhering elastic medium pushing on a spring-supported piston and on an elastic diaphragm are given on pp 117-118 of Reference 1. Defining P_e as the difference between the total force that would be exerted on the gage sensing area by the unperturbed normal stress σ_s and the actual total force P, i.e., as

$$P_e = \frac{\pi}{4} D^2 \sigma_s - P$$

Reference 1 gives, for a piston

$$P_e = \delta \frac{DM_s}{1 - \nu_s^2} 3.05 \qquad (2.12)$$

where M_s and ν_s are the Young's modulus and Poisson's ratio of the

external (assumed elastic) medium, and

$$P_e = \delta_m \frac{DM_s}{1 - \nu_s^2} 0.43 \qquad (2.13)$$

for a diaphragm. Defining σ_e as the difference between the unperturbed normal stress and the actual mean stress over the gage sensing area, we have

$$\sigma_e = \frac{P_e}{\frac{\pi}{4}D^2}$$

In terms of this quantity, Equations 2.12 and 2.13 become

$$\sigma_e = \frac{\delta}{D} \frac{4M_s}{\pi(1 - \nu_s^2)} 3.05 \qquad (2.14)$$

for a piston, and

$$\sigma_e = \frac{\delta_m}{D} \frac{4M_s}{\pi(1 - \nu_s^2)} 0.43 \qquad (2.15)$$

for a diaphragm.

Minimizing the gage registration discrepancy while maximizing electrical output suggests minimizing the quantity

$$\frac{\sigma_e}{\epsilon}$$

where ϵ is the strain magnitude at the location of the strain gages inside the gage, as before. Equivalently, since both gage types are assumed to be acted on by the same medium, the respective values of

$$\frac{\sigma_e}{\epsilon} \frac{\pi(1 - \nu_s^2)}{4M_s}$$

may be compared. From Equations 2.6 and 2.14 we have, for a piston

$$\frac{\sigma_e}{\epsilon} \frac{\pi(1 - \nu_s^2)}{4M_s} = \frac{L}{D} 3.05 \qquad (2.16)$$

and from Equations 2.7 and 2.15

$$\frac{\sigma_e}{\varepsilon_m}\frac{\pi(1-\nu_s^2)}{4M_s} = \frac{D}{\delta t}\,0.43 \qquad (2.17)$$

for a diaphragm.

For a gage with the diaphragm of the WES SE gage with D = 1.905 cm and t = 1.905 mm, the right-hand side of Equation 2.17 is 0.5; if the diaphragm thickness is decreased according to Equation 2.10 to give the same strain $\varepsilon_m = 500(10^{-6})$ at 1.4 MPa (≈200 psi) as the SE gage at 10 MPa (≈1500 psi), a value of 1.5 is obtained for the right-hand side of Equation 2.17. Both of these compare very favorably with the column gage of Reference 3 with D = 1.27 cm and column length L = 2.54 cm, which give a value of 6.1 for the right-hand side of Equation 2.16. The column gage can be improved by shortening the column; if L is decreased to 6 mm (≈1/4 inch), the right side of Equation 2.16 becomes 1.44, which is comparable to the corresponding quantity of 1.5 for a diaphragm gage designed for a strain of $500(10^{-6})$ at the center of the diaphragm when loaded by a pressure of 1.4 MPa (≈200 psi).

Clearly, the behavior of a nonadhering elastic medium, on which the Equations 2.12 through 2.17 are based, is only an approximation of the behavior of a real soil. Plastic behavior at the edge of the piston would tend to mitigate the effects of arching on the column gage to some extent. Nevertheless, the foregoing comparison suggests that on the basis of minimizing the effects of arching on gage registration while maximizing electrical output, the diaphragm concept is competitive over much of the soil stress range of interest.

A sensing diaphragm must be isolated from the lateral stresses in the structure. It is also worth noting that the same requirement arises for the base of a shortened column gage. On a long narrow column the strain gages can be positioned sufficiently far from the base to remain unaffected by lateral stresses in the base, but the base of a short, stubby column should be isolated from high lateral stresses.

2.3 OTHER GAGE CONCEPTS

Some other gage concepts which were considered but not adopted are briefly mentioned here.

2.3.1 Fluid-Backed Diaphragm. In this type of gage, a relatively thin diaphragm is backed by a volume of fluid which acts on a small pressure transducer. With this concept, it is possible to obtain very small ratios of deflection to diameter of the sensing area. It is also relatively insensitive to the effects of stones in the soil, whereas a strain-gaged diaphragm is limited to fairly fine-grained and uniform soils. Several free-field soil pressure cells, not intended for dynamic measurements involving high frequencies and accelerations, operate on the basis of this principle (Reference 1).

Aside from possible problems arising from the effects of high lateral acceleration, because liquids possess significantly higher volume coefficients of thermal expansion than most solids (References 7 and 8), this concept is vulnerable to the effects of variations in temperature. For example, suppose that in a field test the structure wall in which the gage is placed is subjected to direct sunshine before backfilling; the temperature of the gage may be above 40 degrees Celsius. After backfilling, equilibrium is eventually reached at a much lower temperature, typically around 10 degrees Celsius or even lower. Due to thermal shrinkage of the fluid, the gage diaphragm moves inward, resulting in loosening of the soil right next to it or even a small gap. It was calculated that even if the fluid volume behind the diaphragm is kept very thin, the deflection due to thermal shrinkage can be of the same order of magnitude as the deflection of an unbacked strain-gaged diaphragm due to the normal stress being measured. It was decided to avoid having to take special precautions to minimize the effects of temperature variations in placement, backfilling, and use.

2.3.2 Diaphragm Acting on Internal Force-Collector Column and Beam. Many commercially available pressure transducers operate by this principle. This concept was rejected because of anticipated vulnerability to high lateral acceleration as well as acceleration sensitivity in the axial direction.

2.3.3 Pressure-Sensitive Paint between Conducting Plates. Also known as the intermetallic resin concept, its operation is based on the change in electrical resistance when pressure is exerted on a granulated conductor suspended in a paint or resin matrix. A previous evaluation of some prototype gages incorporating this principle indicated a severe hysteresis problem (Reference 9). This has apparently been improved in the newer pressure-sensitive paints, but sensitivity to shear and to load eccentricity are known to be serious enough to warrant special precautions. For most pressure-sensitive paints, the load versus resistance relation is nonlinear, although a few are reasonably linear over certain regions. Moreover, the pressure-sensitive paints do not appear to be stiff enough to possess a clear advantage over other concepts on the basis of minimizing gage deflection.

2.3.4 Piezoelectric Transducers. Experience with piezoelectric transducers of other types (such as accelerometers) has indicated that they are not competitive with strain-gaged transducers when it comes to providing a good signal to noise ratio in an explosive test environment. The requirement for high-impedance lines can largely be eliminated by including a shock-resistant amplifier in the gage package, but units of this type that have been tried have nevertheless been prone to drift, and also excessively sensitive to several environmental factors.

2.3.5 Triaxial Array of Embedded Strain Gages. Embedding strain gages directly in the structure material near the surface would not perturb the state of stress in the soil. In an orthogonal coordinate system with the x-direction along the normal to the surface, the normal stress σ_x may be expressed in terms of the three strains ε_x, ε_y, and ε_z as (Reference 2)

$$\sigma_x = \frac{(1 - \nu)E}{(1 + \nu)(1 - 2\nu)} \left[\varepsilon_x + \frac{\nu}{1 - \nu}(\varepsilon_y + \varepsilon_z)\right]$$

Clearly, recording of three separate channels in order to provide one stress measurement is undesirable. Single-channel output could conceivably be obtained by locating the strain gages sensing ε_y and ε_z in a bridge arm opposite to the strain gage sensing ε_x and adjusting

the bridge appropriately by means of fixed resistors, but accurate knowledge of the Poisson's ratio ν would be necessary in any case. Calculations indicated that if reasonable electrical output is to be attained, semiconductor strain gages would have to be used. Some consideration was given to encapsulating a triaxial array of semiconductor strain gages in the center of a flat epoxy slab. Because of the necessity for accurate knowledge of the Poisson's ratio, individual adjustment of each bridge, as well as other anticipated problems, this approach was not pursued.

2.4 SURVEY OF COMMERCIALLY AVAILABLE GAGES

Because of the foregoing considerations, it was decided to limit candidate gages to the strain-gaged diaphragm type. Because of the desire for a stress sampling area of reasonable size and concern over the possible effects of soil granularity on a very small and thin diaphragm, a minimum size requirement was imposed on the sensing area. Because some previous column-type interface stress gages employed a 1.27-diameter sensing area, the minimum requirement for the diaphragm diameter was somewhat arbitrarily set at 1.27 cm (1/2 inch).

The search was based on the perusal of catalogs and specifications, followed by telephone inquiries where further information seemed desirable. There are many strain-gaged diaphragm type pressure transducers commercially available, but none were found with a diaphragm diameter of 1.27 cm or greater. One, the Kulite IPT-750, with a 0.76-cm diaphragm, looked like it could easily be modified to have a 1.27-cm diaphragm. In response to an inquiry, the manufacturer indicated interest in offering a modified version with a diaphragm diameter of 1.27 cm. Other requested modifications were an increase in the distance from the sensing face to the mounting flange in order to accommodate a suitable lateral-isolation ring (this is discussed in greater detail in Chapter 3), and waterproofing the back end of the unit. This modified version was designated the VM-750.

The VM-750 has two semiconductor strain gages bonded to the inside of the diaphragm, one sensing tension at the center and the other sensing compression near the edge. The bridge is internally completed, with temperature compensation. A four-arm-active version has also been tried, but it was decided that the increase in electrical output does not justify having to deal with the calibration changing with temperature when shunting across a semiconductor bridge arm. With the usual two-arm-active unit, shunting is always across an inactive arm. The inactive arms do not contain semiconductor elements; the temperature-compensating semiconductors are in the active arms.

The gage is made of 17-4PH stainless steel, H900 condition. The coefficient of thermal expansion of this material, $11(10^{-6})$ per degrees Celsius (Reference 4), is the same as the typical value for concrete (Reference 5). A listing of full-scale rated pressures and nominal diaphragm thicknesses is given in Table 2.1. The diaphragm thickness is sized such that the full-scale rated pressure produces a flexural strain of approximately $500(10^{-6})$ at the midpoint of the inner surface (Equation 2.10). The corresponding maximum flexural stress is in the radial direction at the edge; when stress concentration at the inner corner is ignored, this is given by Equation 2.9, which predicts a stress of 200 MPa (29,000 psi) at the full-scale rated pressure. This stress is much lower than the 1200 MPa (180,000 psi) yield strength of the material (Reference 4). From the point of view of diaphragm survivability, the gage is rated very conservatively; nevertheless, operation at high strain levels is deemed undesirable because of possible problems with strain gage bond reliability that may arise. A maximum pressure of two times the rated pressure is claimed for this gage. Nominal electrical output at rated pressure is 100 millivolts.

Consideration was also given to designing and constructing a prototype gage in-house. This was not pursued because of the absence of in-house capability for techniques such as electron-beam welding and inorganic bonding of strain gages, and because the Kulite VM-750 appeared to fit the general requirements reasonably well. Some thought was given to increasing the size of the gage in order to obtain

a larger sampling area, but this would have also necessitated an increase in the size of the mount, which would make it less useful in tests involving small model structures. The potential for cost savings inherent in being able to incorporate components common to other transducers was an additional reason for keeping requested modifications to a minimum.

Table 2.1. Rated sensing ranges and nominal diaphragm thicknesses for the Kulite VM-750. Diaphragm diameter is 1.27 cm.

Full-Scale Rating		Diaphragm Thickness
MPa	psi	(mm)
0.34*	50*	0.25*
0.7*	100*	0.33*
1.4	200	0.46
3.4	500	0.71
6.9	1000	1.02
10.3	1500	1.24
13.8	2000	1.45
20.7	3000	1.73

* Tests (Chapter 6) have indicated that the diaphragm of the 0.34-MPa-rated version is too flexible to provide acceptable registration with Ottawa 20-40 sand; the same may be true of the 0.7-MPa-rated version. Registrat on of the 1.4-MPa-rated version was considered acceptable.

CHAPTER 3

DESIGN OF THE LATERAL ISOLATION SYSTEM

3.1 GENERAL DESCRIPTION

Preliminary calculations had indicated that if the gage mounting flange were to undergo the same strain as was predicted to occur inside a reasonably sized steel casing subjected to external axisymmetric stress of 40 MPa (≈6000 psi), consequent strains in the diaphragm would result in excessive output. The possibility of redesigning the gage was considered, but the approach of designing the mount to isolate the gage from lateral stresses appeared more promising.

A cross section of the mount, with gage, is shown in Figure 3.1; this particular mount is designed for thin structures, with wall thickness less than 10 cm. Because of the desire to limit the mass of the clamp ring as well as increased machining difficulties inside a longer one-piece mount, a different version was designed for thick structures; this is shown in Figure 3.2. Lateral isolation functions in the same way in both cases. The thread on the outside of the mount was patterned after the shape of the ridges on reinforcing bars. Detailed drawings and specifications for the gage mount parts are in Appendix A and the installation procedure is in Appendix B.

The lateral-isolation ring combines low stiffness in the radial direction with high stiffness and strength in the axial direction and in shear. Because the axial stiffness of this ring is much greater than that of the clamp ring and bolts, effective anchoring of the gage is through the lateral-isolation ring, close to the outer surface of the structure. The six 4-40 high-strength bolts torqued to 2.26 N-m (20 in.-lb) provide a predicted total preload sufficient to keep the lateral-isolation ring in contact up to external pressures of 53 MPa; decrease of the preload due to high lateral stresses and consequent extensional axial strains in the mount was conservatively accounted for in this estimate. The tests on which the bolt preload torque is based are described in Appendix C. Allowing for reasonable variation in thread friction and consequently in the torque versus tension

relationship, the mount may be considered adequate for external pressures up to 40 MPa (≈6000 psi). In view of the claimed maximum pressure of twice the rated pressure for the Kulite VM-750, the mount may be considered adequate for rated ranges up to 20.7 MPa (3000 psi).

3.2 CHOICE OF MATERIALS

The material for the mount, AISI Type 416 stainless steel, was chosen because of its easy availability and good machinability, and because its coefficient of thermal expansion, $10(10^{-6})$ per degrees Celsius (Reference 4), is very nearly the same as the $11(10^{-6})$ per degrees Celsius typical value for concrete (Reference 5). Carbon steel was avoided because of possible adverse effects of rusting of the surface in contact with the soil on gage registration. Since the rusting process involves an increase in volume, it was anticipated that rusting of the outer surface during the time between backfilling and the test may result in some preloading of the soil on the mount surface and loosening of the soil on the gage surface.

Because the lateral-isolation ring is subjected to a combination of compressive axial stresses and tensile hoop stresses (due to pressure transmitted by the filler material in the annular space), a stronger material had to be used. Type 17-4PH stainless steel in either H900 or H1150 condition provides both adequate strength and a coefficient of thermal expansion (Reference 4) equal to the typical value for concrete (Reference 5).

The material for the clamp ring was chosen to be 7075-T651 aluminum in order to minimize its mass and also its stiffness relative to the lateral-isolation ring. Because effective anchoring of the gage is through the lateral-isolation ring, thermal expansion properties of the clamp ring are not critical. The strength of the flange was designed to match that of the bolts.

The choice of the filler material for the annular space around the outer end of the gage is discussed in Chapter 4.

3.3 DESIGN OF THE LATERAL-ISOLATION RING

The outer and inner diameters of the ring were sized so as to give a bearing area sufficient to prevent yielding of the mount in the event that the bolts were torqued to their ultimate strength, and yet leave an adequate annular gap around the gage for the filler material.' The purpose of the thin inner flange on the inward end of the ring is to provide automatic centering during installation; there is also a similar feature on the clamp ring (Figures 3.1 and 3.2). In order to insure symmetric clamping of the gage, the outer and inner diameters of the thin portion of the clamp ring match the corresponding dimensions of the lateral-isolation ring.

The axial length of the lateral-isolation ring was chosen on the basis of examining the effect of a lineal axisymmetric radial load on an infinite-length pipe of the same thickness and mean radius as the lateral-isolation ring. Considering the mount undergoing an axisymmetric radial inward displacement at its junction with the lateral-isolation ring (Figure 3.1 or 3.2) it is easy to see that if the preload is assumed sufficient for keeping the ring from lifting off the mount at its inner radius, the boundary conditions at this junction are the same as at the location of the radial load on an infinite-length pipe. Defining the quantity λ as

$$\lambda = \sqrt[4]{\frac{3(1 - \nu_r^2)}{R^2 T^2}} \tag{3.1}$$

where R is the mean radius, T is the thickness, and ν_r is the Poisson's ratio of the material, the radial displacement y as a function of the axial distance x is given by (Reference 5)

$$y = y_o e^{-\lambda x}(\cos \lambda x + \sin \lambda x) \tag{3.2}$$

where y_o is the radial displacement at $x = 0$, where the load is applied.

Equation 3.2 is plotted in Figure 3.3. It is evident that for $\lambda x \geq 2$ the displacement is less than 10 percent of the maximum displacement. With the radial dimensions of the lateral-isolation ring, Equation 3.1 gives a value of 0.315 mm^{-1} (8 $in.^{-1}$) for λ, so that $\lambda x = 2$ corresponds to x = 6.35 mm (1/4 inch). On the other hand, at $\lambda x = 1$ (x = 3.175 mm = 1/8 inch), the displacement is approximately half of maximum displacement. The unmodified IPT-750, with a 6.35-mm (0.250 in.) distance from the sensing face to the mounting flange, could accommodate a lateral-isolation ring of only 3.175-mm (1/8 inch) axial length. The distance from the sensing face to the mounting flange on the gage was increased to 9.525 mm (0.375 inch), in order to accommodate a lateral-isolation ring of 6.35-mm axial length.

3.4 LEAK TESTS

It is clear from Figure 3.1 or 3.2 that due to the small dimensions involved, it was not practical to incorporate O-ring seals. The use of soft copper washers on both ends of the lateral-isolation ring was considered, but was not adopted because of the desire to maintain maximum rigidity in the axial direction, as well as to keep the installation process as simple as possible. It was also recognized that sealing at these points does not need to be absolutely watertight. Nevertheless, the leak rate should not be great enough to make it possible for an initially water-saturated soil to locally desaturate when subjected to pressures and pulse durations typical of explosive-generated stress waves.

Conservative leak tests were done by subjecting the outer faces of five gage-and-mount assemblies to water under high pressure, without any filler material in the annular space around the outer end of the gage. This was done by attaching a field calibration fixture (Figure B.2 in Appendix B) to each mount, and hooking them up to a manifold. The mounts were positioned such that the gage sensing faces were in the upward direction. The manifold was carefully filled with water in such a way as to eliminate any air in the system. The pressure was increased in increments of 0.7 MPa (100 psi) while observing the lower

ends of the mounts for any water droplets, until a pressure of 10.3 MPa (1500 psi) was reached. This took place over a period of 20 minutes; the pressure was then held at 10.3 MPa for 10 minutes before it was lowered back down. A careful close-up visual check of the lower ends of the mounts did not reveal any sign of leakage.

However, after dissassembly it was noticed that there had been small leaks in two out of the five mounts. The total amount in each of these was estimated at one or possibly two droplets. The amount of water had not been great enough to migrate a sufficient distance downward to be visible without disassembling the mount. Since the duration in this test (≈10 minutes) exceeded the typical pulse duration in an explosive-generated stress wave (≈10 milliseconds) by four orders of magnitude, the amount of water that might be leaked during such a stress wave is expected to be insignificant.

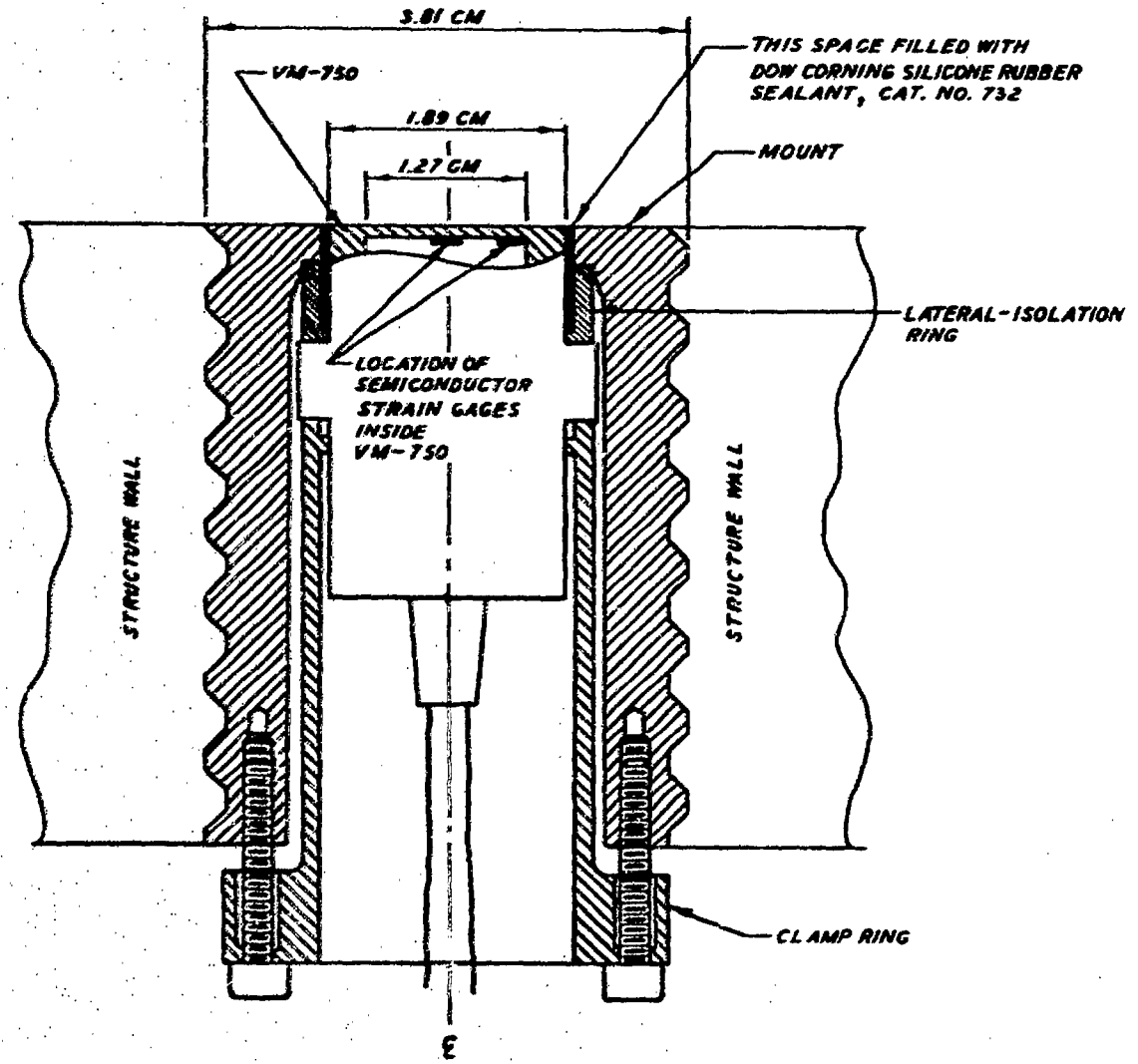

Figure 3.1. Gage in mount designed for thin structures, wall thickness less than 10 cm.

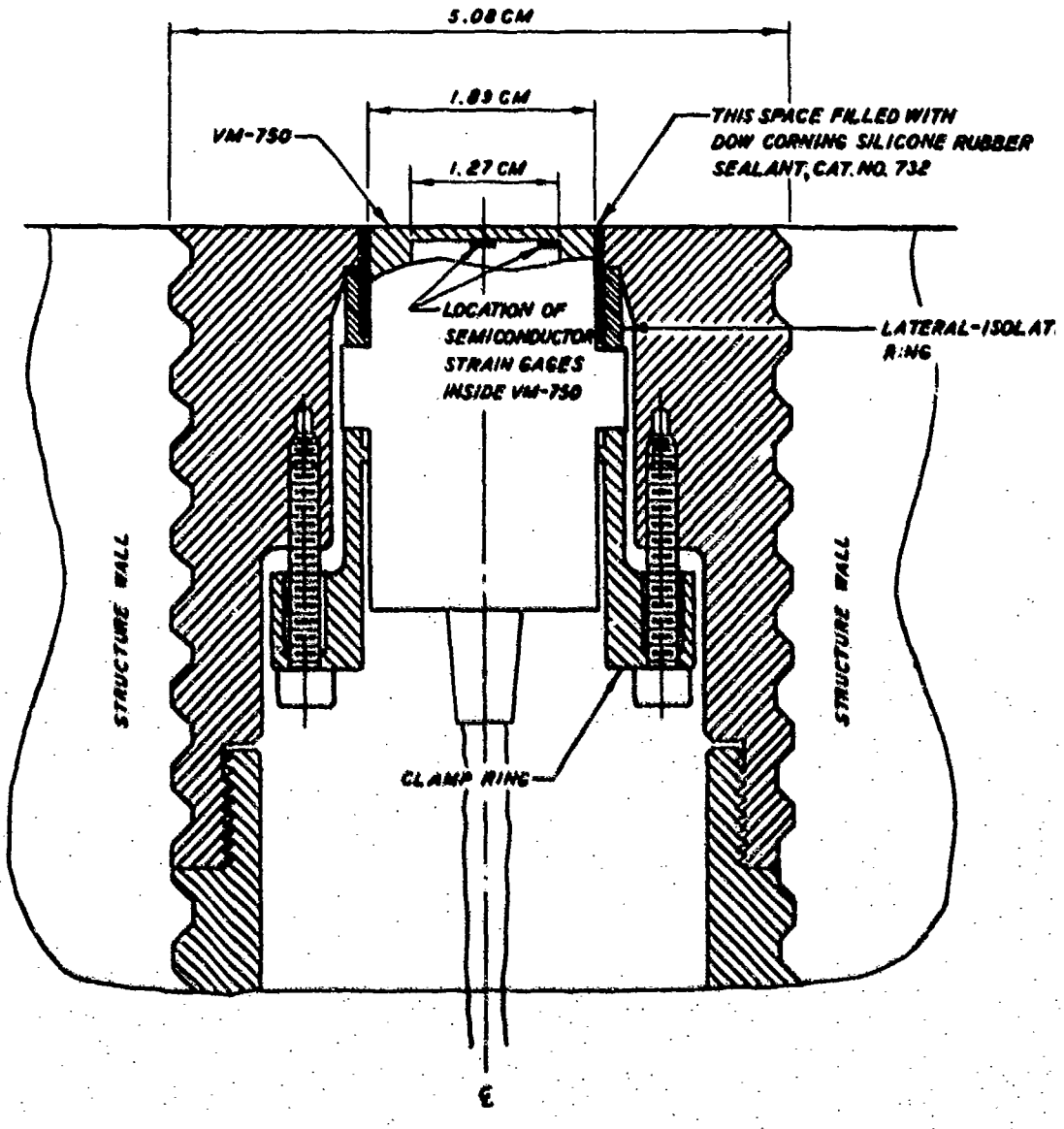

Figure 3.2. Gage in mount designed for thick structures, wall thickness 10 cm or greater.

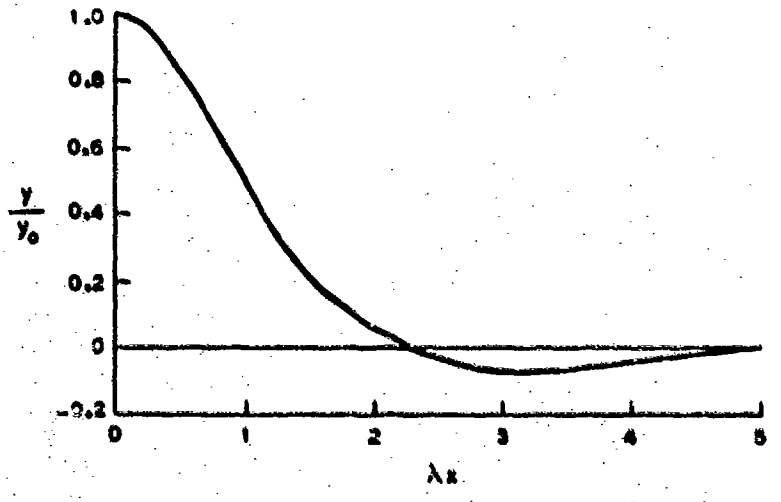

Figure 3.3. Plot of Equation 3.2

CHAPTER 4

EVALUATION OF LATERAL ISOLATION

The same 25.4-cm-diameter dynamic fluid chamber that was used to investigate gage registration was also used as the loading device in evaluating lateral isolation. Cross-sections of the test configuration are shown in Figures 4.1 and 4.2. Loading the circular plate supported on a ring at its edge produces axisymmetric lateral stresses in the mount. The tangential strain in the mount close to the anchoring of the gage was monitored by two strain gages located 90 degrees apart. A thin cap equipped with an O-ring seal isolated the gage from direct pressure on the sensing face. A typical dynamic loading pulse is shown in Figure 4.3.

The first tests were done with concrete-and-steel composite plates. The neutral axis was designed to be at the concrete-and-steel interface so that the steel would be in tension and the concrete in compression. The gage was mounted in a shortened version of the mount designed for thick structures, which was fastened to the steel plate before casting the concrete. Shear studs, 0.635 cm (1/4 inch) diameter, were spaced approximately one per 6.5 square centimetre (one per square inch) on the rest of the inner surface of the steel plate. The concrete was a strong granite-filled mix having a Young's modulus of approximately 27,000 MPa (4,000,000 psi).

In order to keep the soil out of the annular space around the outer end of the gage and yet minimize the lateral forces transmitted through it, the filler material should be very nearly incompressible and yet possess low dynamic stiffness in shear. The material should also be reasonably convenient to use and, ideally, would also act as a sealant. Materials of extremely low shear strength, such as grease or jellied water, were ruled out because of anticipated difficulties with soil placement. In the absence of known dynamic properties of candidate materials, it was recognized that selection would have to be largely on the basis of trial. The dynamic stiffness of several candidate materials was qualitatively compared by impacting cubes of

identical size with a hammer. The drop height was adjusted until the hammer would just barely touch spacers placed beside the specimen on the anvil. If, upon changing the material, the hammer would not touch the spacers when dropped from the same height, the second material was considered to be stiffer than the first. This rough comparison procedure was used to narrow the number of candidate materials down to two: a modeling-clay-like substance with the trade name "Plastilina," and a one-component silicone rubber sealant, Dow Corning Catalog No. 732.

Care was taken to fill the annular space in such a way as to eliminate air-voids. With the Plastilina, this proved to be rather time-consuming. Injection of the silicone rubber sealant proved to be much easier. A simple injection fixture having two holes is placed on the gage and mount such that the holes are diametrically opposed on the annular space being filled. A syringe is inserted into one of the holes and pressure is maintained on the syringe until the sealant flows out of the other hole. A more detailed description of the injection procedure as well as a drawing of the injection fixture is included in Appendix B. The effectiveness of this injection procedure in reliably eliminating even small bubbles irrespective of spatial orientation (the gage facing upward, sideways, and downward) was confirmed by means of a transparent plexiglas model of the annular space.

The silicone rubber sealant, Dow Corning Catalog No. 732, solidifies when in contact with air. A solid "skin" is formed in approximately one hour, and the soil may be placed after that time. Ordinarily, there would be no objection to having the deeper part of the filler material remain liquid at test time, but it was desired to evaluate lateral sensitivity with the filler material solidified throughout. In order to check on the solidifying rate, several steel nuts of the same height as the annular space in the gage mount were placed flat upon a metal plate and the holes filled with the silicone rubber sealant. Solidifying of the deeper part of the sealant was checked by

picking up one of these nuts. It was found that ten days were sufficient for the material to solidify throughout the 9-mm depth. All lateral sensitivity tests with the silicone rubber sealant were done more than ten days after the injection of the material into the annular space in the mount.

Results of lateral sensitivity tests with the concrete-and-steel composite plates are summarized in Table 4.1. The circumferential strain on the inner surface of the mount corresponding to failure of 40-MPa (6000-psi) concrete around the mount under axisymmetric loading was predicted by means of thick-pipe formulas (Reference 5). For the thinner-walled mount (Figure 3.1), this strain magnitude was predicted to be $750(10^{-6})$. Assuming the strain to be proportional to the distance from the neutral axis of the plate, a strain of $750(10^{-6})$ at the junction of the mount with the lateral-isolation ring corresponds to a strain of $700(10^{-6})$ at the strain gage location (Figure 4.1). The lateral sensitivity data, expressed in terms of peak VM-750 output as a percentage of full-scale rating, were linearly extrapolated to this strain level (last column in Table 4.1).

The data in Table 4.1 imply that the silicone rubber sealant is a slightly better isolator than the Plastilina. In view of this, as well as the much easier installation of the silicone rubber sealant, the choice of filler material settled on the Dow Corning silicone rubber sealant, Catalog No. 732.

However, the measured strains in Table 4.1 are approximately three times lower than predicted. Slight gaps (less than 0.1 mm) between the concrete and steel around the periphery of the plates suggested that the mix had shrunken slightly during setting, and consequently the concrete was not anchored to the steel in such a way as to prevent all relative movement. It was expected that increased loading pressures would result in destruction and possible jamming of the composite plate in the test chamber. Although the measured lateral sensitivites were considered encouragingly low, they are based on relatively low input strains, and

the possibility of nonlinear behavior had not been excluded. Evaluation of lateral sensitivity at strain levels corresponding to destruction of concrete around the mount was considered highly desirable. Rather than reattempt the casting of composite plates, it was decided to use metal plates, as shown in Figure 4.2.

The results of lateral sensitivity tests in metal plates are summarized in Table 4.2. As expected, the measured circumferential strains in the mount were in reasonable agreement with predictions (Reference 5). In these plates, a strain of $750(10^{-6})$ at the junction of the mount with the lateral-isolation ring corresponds to a strain of $670(10^{-6})$ at the strain gage location (Figure 4.2). The lateral sensitivity data, expressed in terms of peak VM-750 output as a percentage of full-scale rating, were linearly extrapolated to this strain level (last column in Table 4.2). These findings do not exceed one percent of full-scale rating. Allowing for some variation in lateral sensitivity among individual gages, the lateral sensitivity of the gage-and-mount system under axisymmetric loading corresponding to failure of 40-MPa (6000-psi) concrete around the mount may be conservatively stated as not exceeding two percent of full-scale rating.

Measured lateral sensitivity was consistently higher in dynamic tests than in static tests with the same filler material. This is probably due to viscoelasticity of the filler material. The typical loading pulse is shown in Figure 4.3; because of their high natural frequency (≈4000 Hz) the plates responded quasi-statically and the strain gage output records have the same rise time and shape as the loading pressure pulse. Although the rise time in explosion-generated loading pulses is sometimes shorter, the tested structures are usually sufficiently large so that the time to reach maximum lateral stress usually exceeds the rise time in Figure 4.3. Shorter structural response times may be obtained only with relatively stiff model structures, with natural frequencies greater than 200 Hz.

Table 4.1. Results of lateral sensitivity tests in concrete-and-steel composite plates.

Type of Test	Filler Material	VM-750 Full Scale Rating (MPa)	Peak Pressure in Fluid (MPa)	Peak Circumferential Strain in Mount Times 10^6	Peak VM-750 Output (MPa)	Peak VM-750 Output as % of Full Scale Rating: Actual	Peak VM-750 Output as % of Full Scale Rating: Extrapolated to Strain of 700 (10^{-6})
Dynamic	None	1.4*	3.51	106	0.0028	0.20	1.3
Dynamic	Plastilina	1.4*	3.65	111	0.0074	0.54	3.4
Dynamic	None	10.3	3.32	83	0.0094	0.09	0.8
Dynamic	Plastilina	10.3	1.99	45	0.0123	0.12	1.8
Dynamic	DC 732**	10.3	2.56	58	0.0121	0.12	1.4
Dynamic	DC 732**	10.3	5.28	109	0.0186	0.18	1.2
Static	DC 732**	10.3	3.14	56	0.0079	0.08	1.0

* The 1.4-MPa-rated gage was a 4-arm-active version; two-arm-active versions are normally used.
** DC 732 denotes Dow Corning silicone rubber sealant, Cat. No. 732.

Table 4.2. Results of lateral sensitivity tests in metal plates. The 0.34-MPa-rated and 1.4-MPa-rated gages were mounted in aluminum plates and the 13.8-MPa-rated gage was mounted in a stainless steel plate. The filler material was Dow Corning silicone rubber sealant, Cat. No. 732.

Type of Test	VM-750 Full Scale Rating (MPa)	Peak Pressure in Fluid (MPa)	Peak Circumferential Strain in Mount Times 10^6	Peak VM-750 Output (MPa)	Peak VM-750 Output as % of Full Scale Rating	
					Actual	Extrapolated to Strain of 670(10^{-6})
Dynamic	0.34*	3.83	406	0.0019	0.56	0.92
Dynamic	0.34*	6.40	654	0.0031	0.90	0.92
Static	0.34*	6.36	639	0.0004	0.12	0.13
Dynamic	1.4	1.05	130	0.0008	0.06	0.29
Dynamic	1.4	6.15	645	0.0042	0.30	0.31
Dynamic	1.4	9.46	905	-0.0065	-0.48	-0.35
Static	1.4	5.81	588	0.0021	0.15	0.17
Dynamic	13.8	4.95	235	-0.049	-0.35	-1.00
Dynamic	13.8	10.83	499	-0.067	-0.48	-0.63
Dynamic	13.8	12.70	595	-0.090	-0.65	-0.73
Static	13.8	9.18	402	-0.048	-0.35	-0.58

* Tests (Chapter 6) have indicated that the diaphragm of the 0.34-MPa-rated version is too flexible to provide acceptable registration with Ottawa 20-40 sand. Registration of the 1.4-MPa-rated version was considered acceptable.

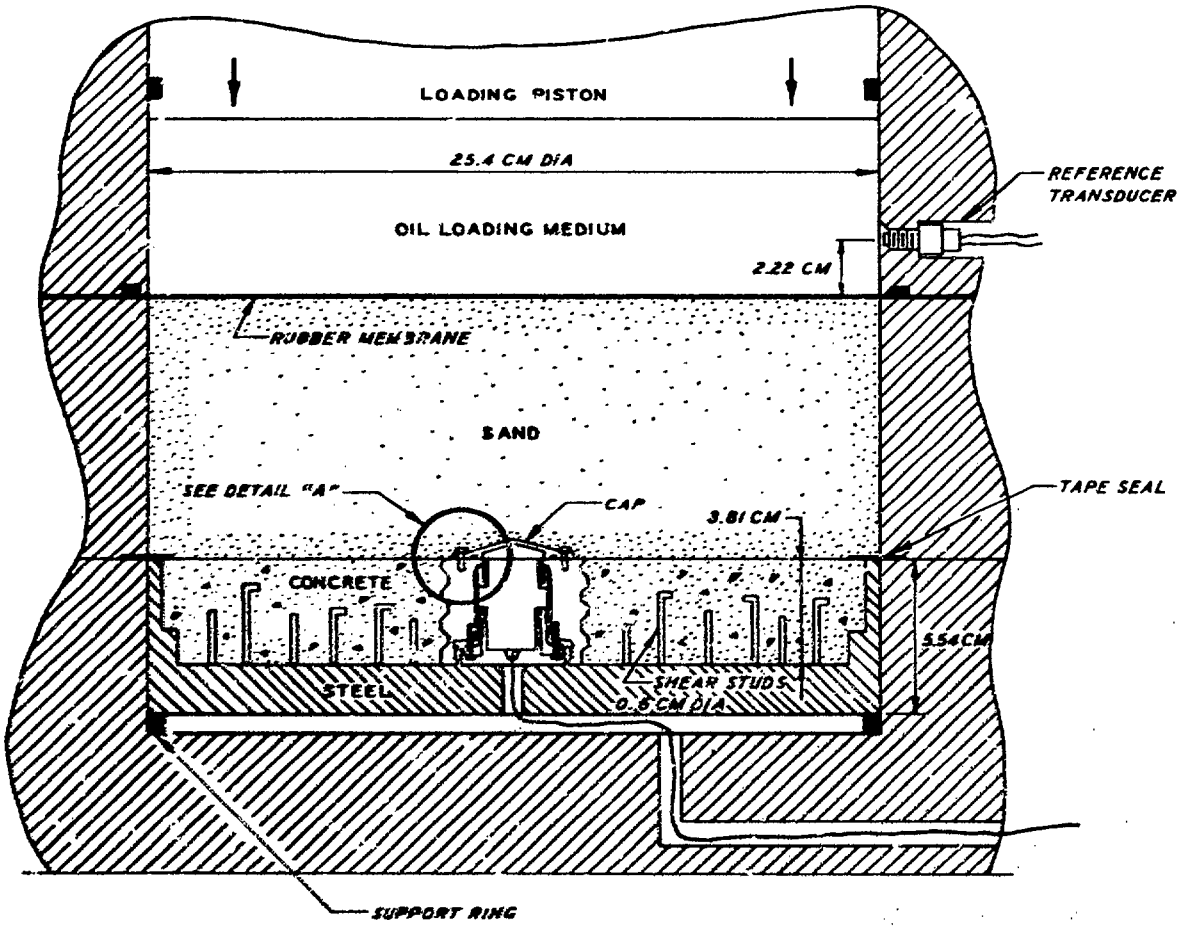

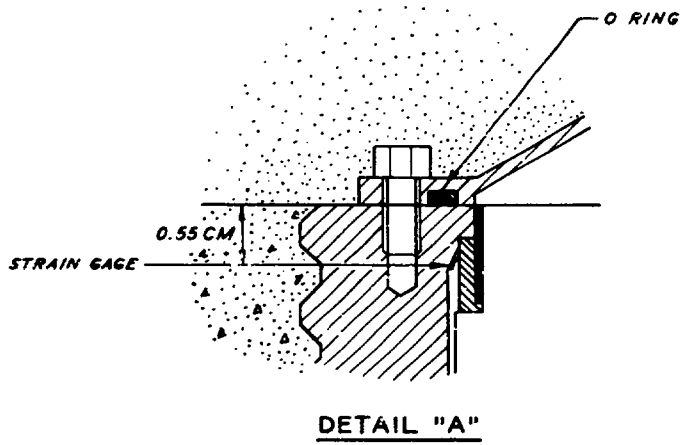

Figure 4.1. Evaluation of lateral sensitivity in concrete and steel composite plate.

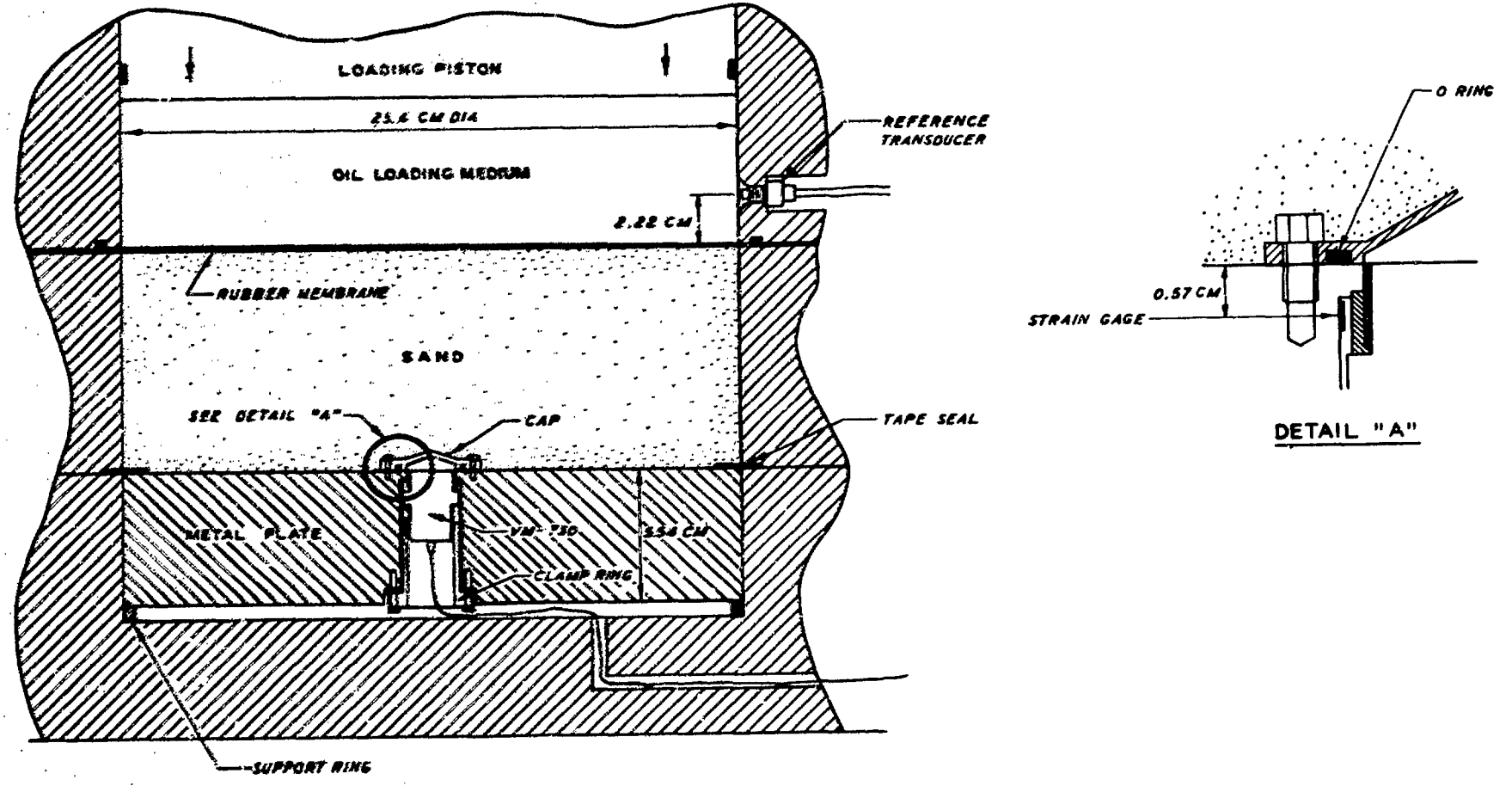

Figure 4.2. Evaluation of lateral sensitivity in metal plate.

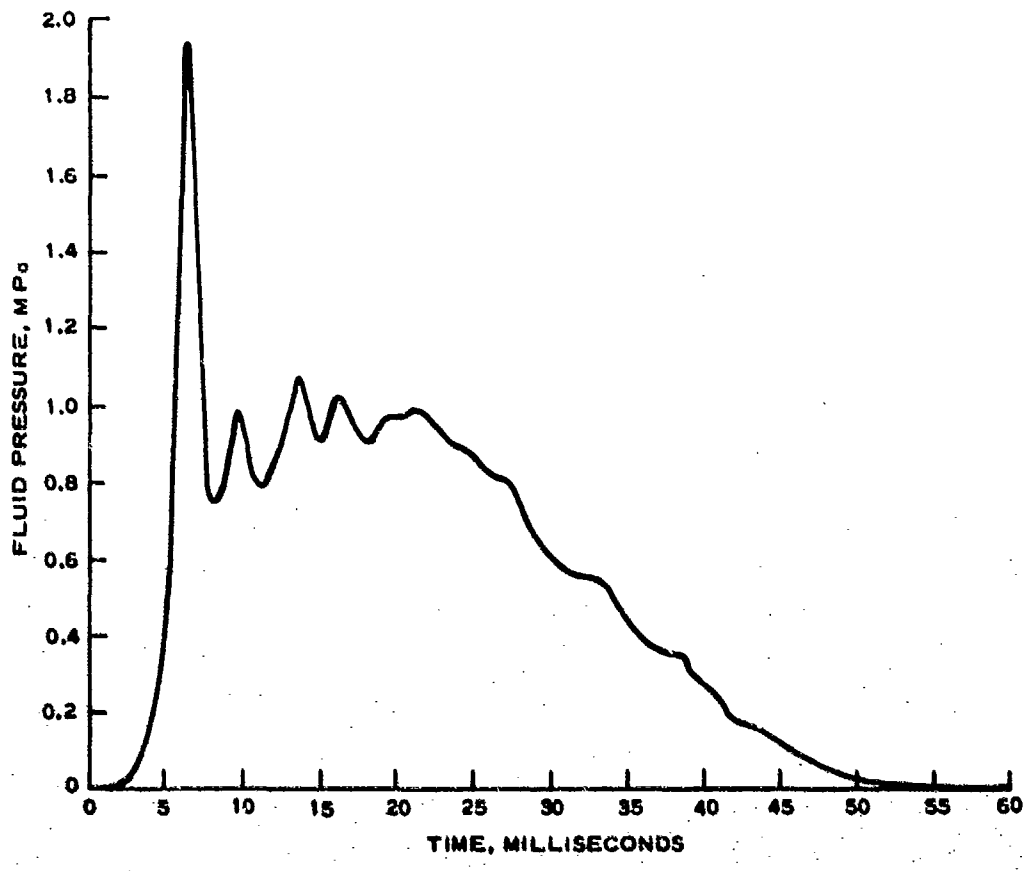

Figure 4.3. Typical loading pulse shape in the 25.4-cm fluid chamber.

CHAPTER 5

ACCELERATION SENSITIVITY

The acceleration sensitivity of a fixed-edged strain-gaged diaphragm in air is easily computed from the mass per unit area of the diaphragm. Clearly, any variation in edge fixity (rolling of the edge) in response to high acceleration would invalidate such a simple calculation.

The acceleration sensitivity of two gages, a 1.4-MPa-rated and a 20.7-MPa-rated version, was measured on a spin table which subjected them to approximately 1000 g's of acceleration. Each gage mount (the version for thick structures was used) was fastened to the spin table by means of a bracket with bolts threading into the holes on the outer face intended to accommodate a field calibration fixture. The bracket had a relief hole in the center, so that it did not touch the gage. Each mount was positioned so that the gage sensing face was toward the center of the spin table.

The results are given in Table 5.1. The excellent agreement with the corresponding calculated values implies that the gage case is sufficiently rigid to maintain diaphragm edge fixity under high acceleration and, consequently, the calculated acceleration sensitivities for the intermediate rated pressure ranges (Table 5.1) are also expected to be realistic. These acceleration sensitivities are not high enough to significantly affect soil stress measurements.

Calculated natural frequencies, computed from the formula for the natural frequency of a fixed-edged plate (Reference 5) are also included in Table 5.1.

Table 5.1. Acceleration sensitivity and diaphragm natural frequency for the Kulite VM-750.

Full-Scale Rating		Acceleration Sensitivity in Air (kPa/g)		Calculated Natural Frequency (Hz)
MPa	psi	Calculated	Measured	
1.4	200	0.03	0.02 (0.003 psi/g)	28,000
3.4	500	0.05	--	43,000
6.9	1000	0.08	--	62,000
10.3	1500	0.10	--	76,000
13.8	2000	0.11	--	88,000
20.7	3000	0.13	0.13 (0.019 psi/g)	107,000

CHAPTER 6

GAGE REGISTRATION WITH SAND

Three varieties of sand were used in these tests: Ottawa 20-40, Ottawa 50-200, and Reid-Bedford Model sand. Reid-Bedford Model sand has been extensively used as backfill in structures tests in the WES large blast load generator, and its properties have been described in greater detail elsewhere (Reference 10). Grain-size distribution curves for these three varieties of sand are presented in Figures 6.1, 6.2, and 6.3, respectively. The results of static and dynamic uniaxial strain tests are presented in Figures 6.4 through 6.9. Comparison of static and dynamic uniaxial test results does not indicate any rate-dependence: except for the effects of oscillations in the dynamic loading pulses, there are no significant differences between the stress versus strain curves from the static and the dynamic tests. Most of the gage testing was done with Ottawa 20-40, the stiffest of these three varieties of sand.

A 25.4-cm-diameter dynamic fluid chamber was used to subject the sand over a flush-mounted gage to a known stress input. The test configuration was the same as in Figures 4.1 and 4.2 except that the cap shown over the gage was removed. Supporting the plate evenly on its lower surface might be considered an ideal test condition; however, a face cut on a lathe does not normally produce a perfectly flat surface but one that is slightly concave or convex. Calculations indicated that placing these very stiff plates on the fluid chamber bottom would not have guaranteed even support. Supporting the plate at or near its center would cause it to deflect so as to become slightly convex upward under load, which would tend to subtract from the effects of the gage diaphragm deflection, resulting in indicated gage registration somewhat closer to ideal, one-to-one registration than might actually be the case. Rather than go to special machining techniques in order to insure even support, it was decided to provide a somewhat conservative test

environment by supporting these stiff plates under their edges, so that the effects of plate and gage deflections would be additive. The sand was always placed by sprinkling.

Most of the test results are expressed in terms of plots of the fluid pressure versus the stress indicated by the VM-750, together with plots of the fluid pressure versus the registration ratio (Figures 6.10-6.24). The measured registration ratio is taken to be the stress indicated by the VM-750 divided by the fluid pressure. Due to the effects of error propagation, the measured registration ratios are not considered to be very reliable at fluid pressures less than fifteen percent of the peak value. The general features of these gage registration test results are as expected for a flush-mounted gage: somewhat hysteretic behavior with underregistration during loading changing to overregistration during unloading, as the gage diaphragm pushes the sand back outward. The overlapping lines in the unloading portion of the curves from the dynamic tests correspond to oscillations after the main peak in the dynamic loading pulse (Figure 4.3).

Significant effects of plate deflection and chamber wall friction would become noticeable upon varying the depth of the sand. The results of a dynamic and a static test with 5.08 cm of Ottawa 20-40 sand over a 1.4-MPa-rated gage are shown in Figure 6.10 and the results of a dynamic and a static test with the sand depth increased to 9.52 cm are shown in Figure 6.11. There are no significant differences between the results of the static tests. Except for the effects of oscillations after the main peak in the dynamic loading pulse, the differences between the static and dynamic test results are believed to be due to wave-propagation effects in the test chamber, and, as expected, these are more noticeable with the greater sand depth. For example, the truncated apex in the plot of fluid pressure versus indicated stress from the dynamic test in Figure 6.11 is due to the two peaks not being coincident in time. In actuality, they were separated by 0.2 msec, which is the transit time required for a wave traveling at 600 metres per second to propagage from the height of the reference transducer to the bottom of a 9.52-cm-high sand sample. Compared to the rise time of a typical

dynamic loading pulse (Figure 4.3), this 0.2 msec transit time is nevertheless not long enough for wave-propagation effects to influence measurements of registration ratio at the peak by more than a few percent. All the other gage registration tests, both static and dynamic, were done with 9.52-cm sand depth.

Comparison of test results with the three different sands indicates greater underregistration during loading with Ottawa 20-40 than with the less stiff Ottawa 50-200 and Reid-Bedford Model sands. This is evident upon comparing test results with these three sands on the same 1.4-MPa-rated gage: with Ottawa 20-40 sand in Figures 6.10-6.14, with Ottawa 50-200 sand in Figure 6.15, and with Reid-Bedford Model sand in Figures 6.16-6.19. Similarly, the characteristic upward concavity of the loading portion of the fluid pressure versus indicated stress curves (clearest in the static test results) reflects the upward concavity of the stress versus uniaxial strain behavior of the sand (Figures 6.4-6.9). That is, as the stiffness of the sand increases with the applied stress, so does the departure from ideal registration. When the loading is not carried to high peak stresses, as in Figure 6.16 where the peak is 0.2 MPa, the registration remains close to ideal up to the peak. Upon repeated loadings, with each pulse packing the sand more tightly, there is a tendency toward slightly greater underregistration. This is more clearly noticeable with the Ottawa 50-200 sand (Figure 6.15) and Reid-Bedford Model sand (Figure 6.18).

It has already been pointed out in Chapter 2 that diaphragm gages designed to sense high external stresses are expected to perform with smaller deviations from ideal registration than the less stiff lower-ranged versions. This is also borne out by the test results. The results of tests with a 0.34-MPa-rated VM-750 are summarized in Table 6.1. It is evident from Table 6.1 that the diaphragm of the 0.34-MPa-rated version is too flexible to provide acceptable registration with Ottawa 20-40 sand. With the same sand, the 1.4-MPa-rated version produced loading registration ratios of approximately 0.8 at applied stresses close to its rated range (Figures 6.10-6.13), and its registration with this relatively severe medium was considered acceptable. Not

surprisingly, closer to ideal registration was obtained in tests with the stiffer 10.3-MPa-rated (Figures 6.20-6.23) and 13.8-MPa-rated versions (Figures 6.24).

A relatively high degree of repeatability is another noteworthy feature of the gage registration test results. Tests with the free-field SE gage in sand and clay (References 6 and 11) yielded significantly more data scatter. This suggests that the placement of a free-field stress gage on the soil is a more severe problem than the placement of backfill on the gage. Regarding interface stress measurements, high accuracy may be expected to be obtainable most easily on the roofs of buried structures, while measurements on footings and floors present the most severe problems. Vertical walls may be considered to present an intermediate degree of placement difficulty.

When considering other types of soil, it should be kept in mind that the presence of stones next to a strain-gaged diaphragm is likely to result in erratic measurements. The use of a properly proportioned pocket of a finer-grained, stone-free soil covering the gage is discussed in Reference 1. Ideally, the mechanical properties of the pocket soil should be representative of the field soil, but a perfect match should not be expected or assumed. In some cases, it may be sufficient to merely remove stones from the immediate vicinity of the gage or to use sieved field soil in covering the gage. Repeatability may also be expected to diminish with sands that are significantly more coarse-grained than Ottawa 20-40, which was the coarsest sand in the tests reported here. Perhaps the most severe problems are presented by moistened backfills that cement together and shrink nonuniformly around the buried structure; a large array of gages would be needed in order not to be misled by the effects of the consequent unpredictably uneven loading of the structure.

Some laboratory measurements of gage registration with the same soil as in the field application make it possible to correct for systematic deviations from ideal registration. Clearly, the configuration of any small pocket of unrepresentative soil covering the gage should also be duplicated. If the mechanical behavior of the soil(s) is not

significantly rate-dependent, static tests would be preferred since wave-propagation effects in the sample are thereby avoided. With such a plot of fluid pressure versus indicated stress, correction of the peak stress as well as the entire loading portion up to the first peak is straightforward: for various values of indicated stress (abscissa), reading off the fluid pressure (ordinate) from the loading portion of the curve gives the corresponding corrected stress. Correction of a monotonically decreasing unloading portion is similarly straightforward provided that the laboratory test was carried to the same peak value in indicated stress as in the field record. Correction of an oscillatory record is more difficult; nevertheless, a plot of fluid pressure versus indicated stress from a laboratory test can be used to set upper and lower limits in the oscillating portion of the record.

Table 6.1. Registration of 0.34-MPa-rated VM-750 with Ottawa 20-40 sand.

Sand Density (gm/cc)	Type of Test	Peak Pressure in Fluid (MPa)	Peak Indicated Stress (MPa)	Registration Ratio at Peak
1.8037	Dynamic	0.131	0.066	0.50
1.8030	Static	0.336	0.136	0.40
1.8042	Static	0.379	0.145	0.38

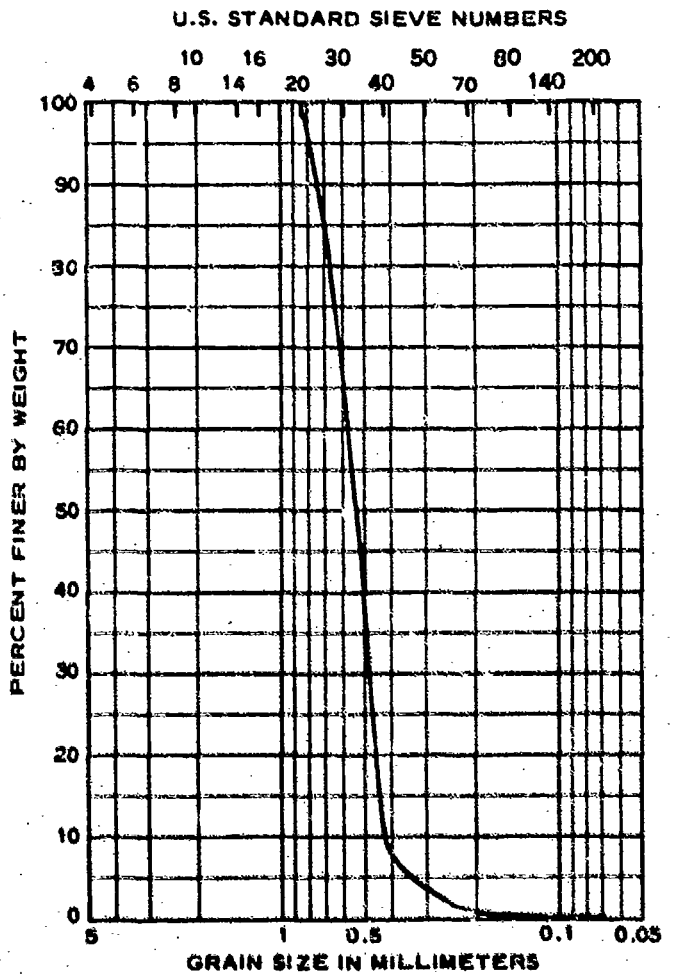

Figure 6.1. Grain-size distribution for Ottawa 20-40 sand.

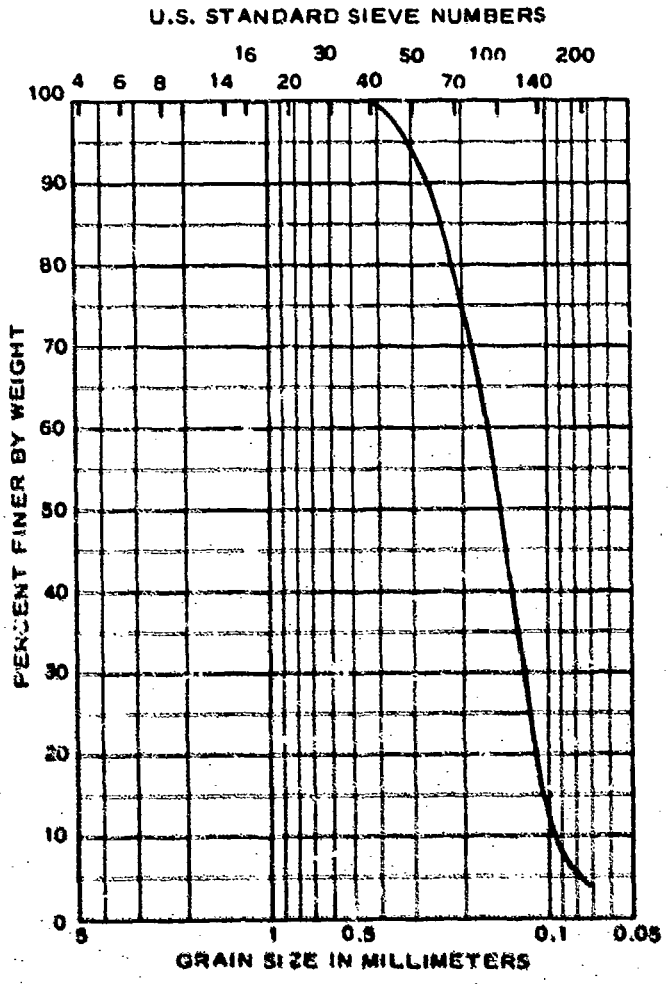

Figure 6.2. Grain-size distribution for Ottawa 50-200 sand.

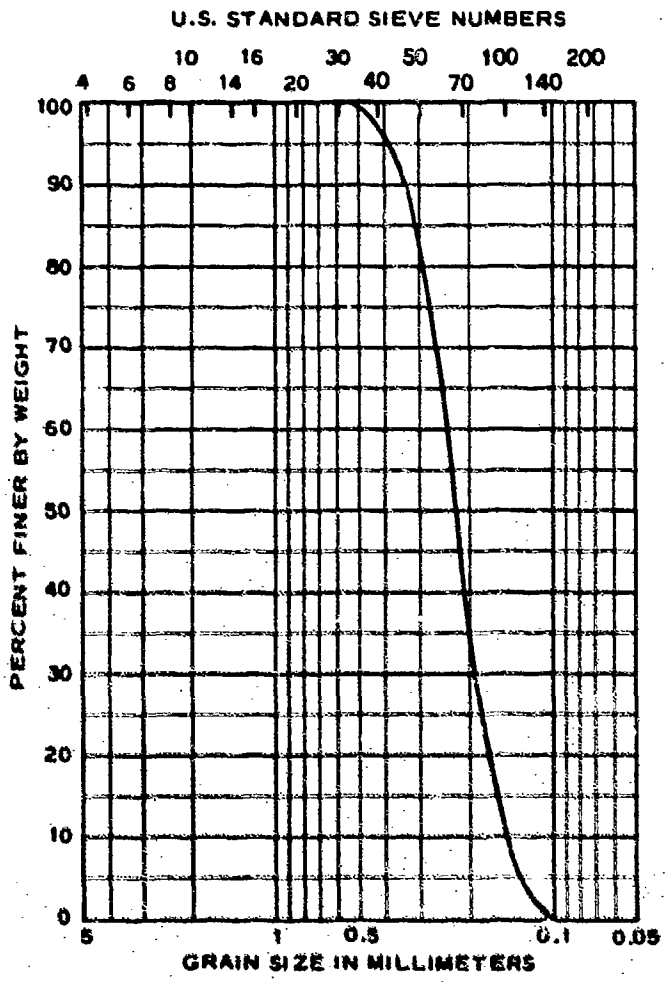

Figure 6.3. Grain-size distribution for Reid-Bedford model sand.

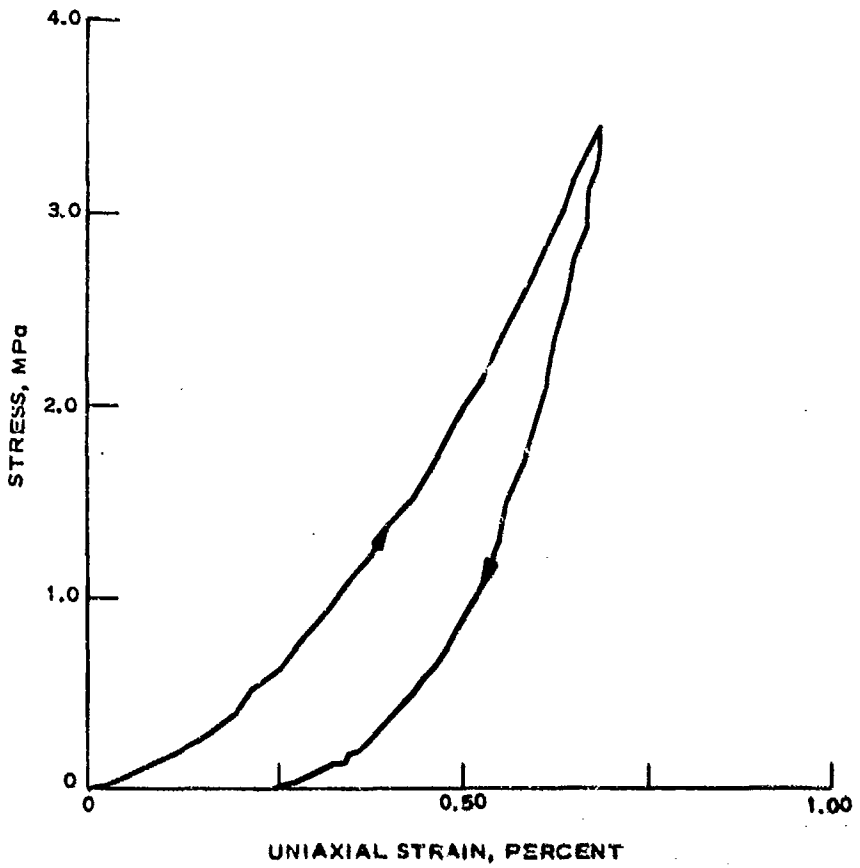

Figure 6.4. Static uniaxial stress-strain for Ottawa 20-20 sand. Density = 1.8072 gm/cc.

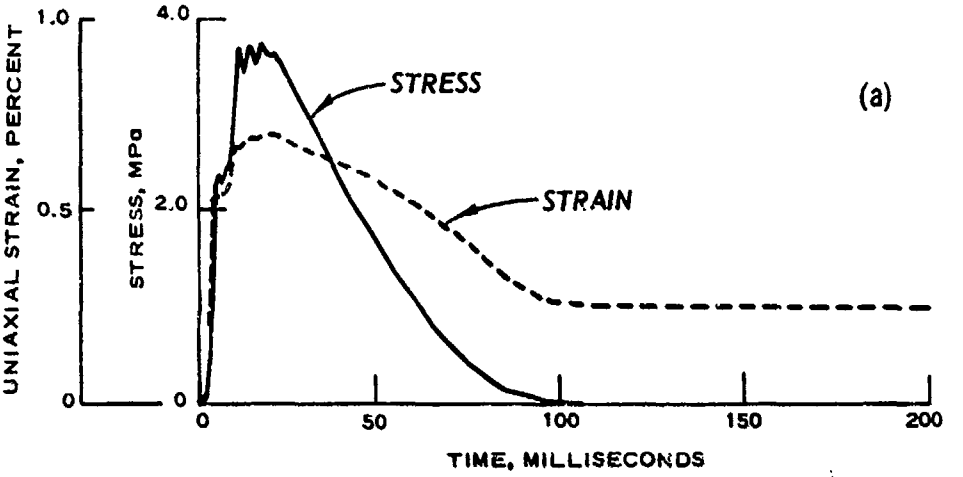

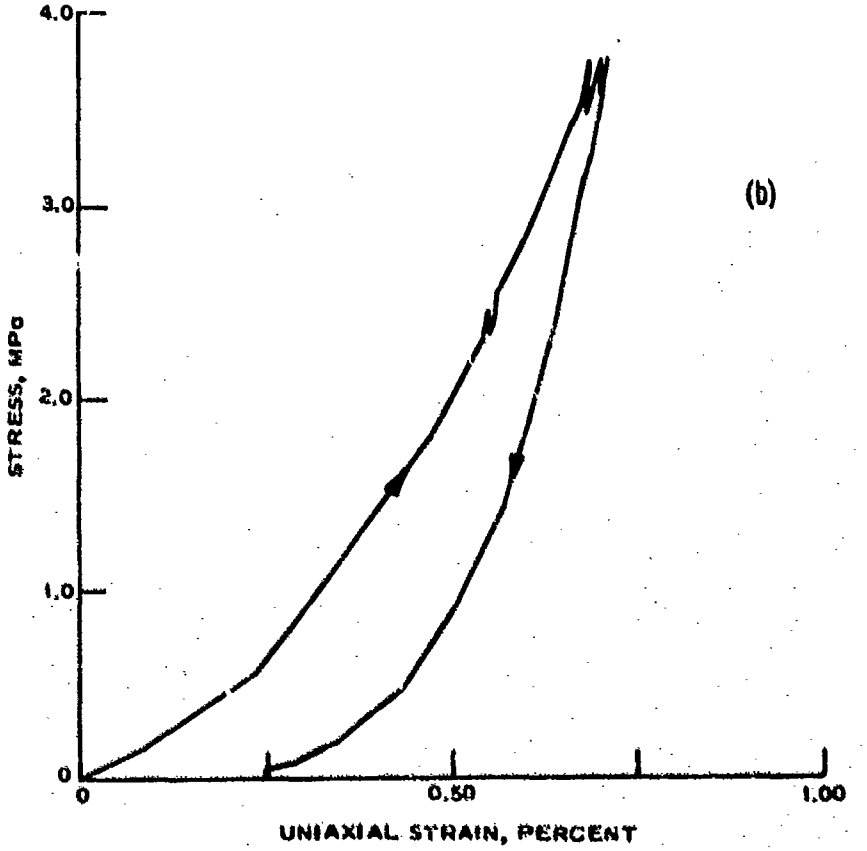

Figure 6.5. Dynamic uniaxial test results on Ottawa 20-40 sand. (a) Stress and strain time histories, (b) stress versus strain. Density = 1.7997-gm/cc.

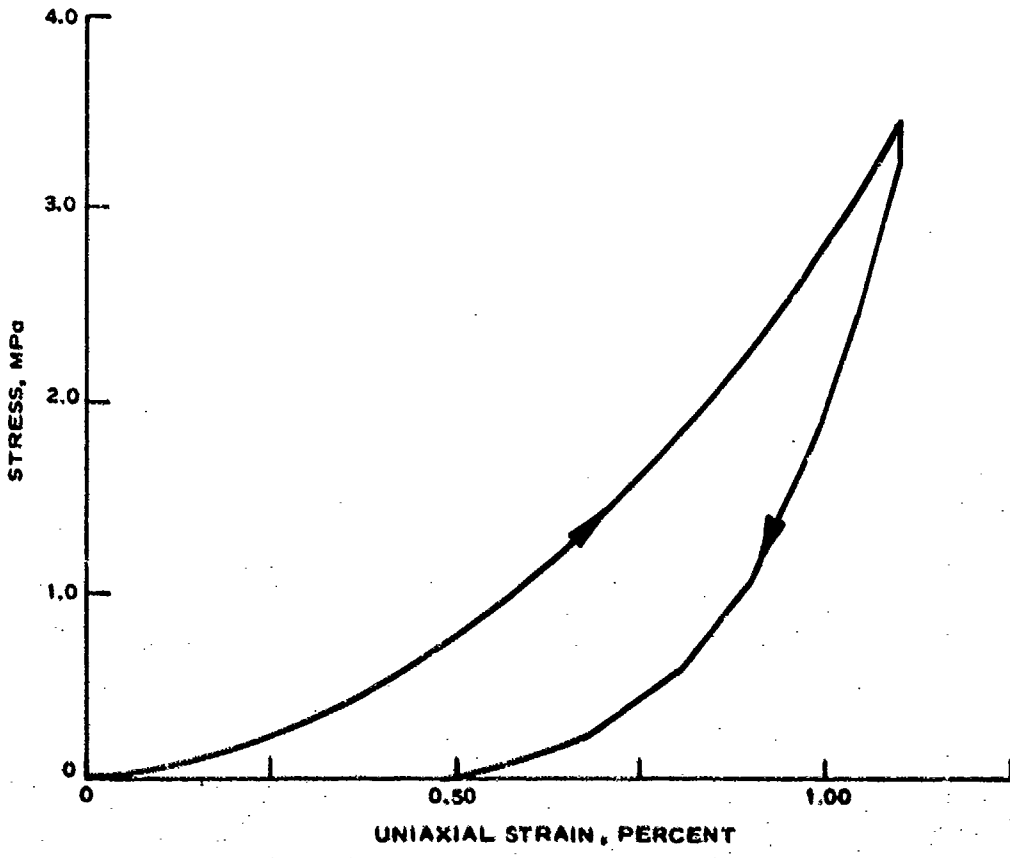

Figure 6.6. Static uniaxial stress-strain for Ottawa 50-200 sand. Density = 1.6944-gm/cc.

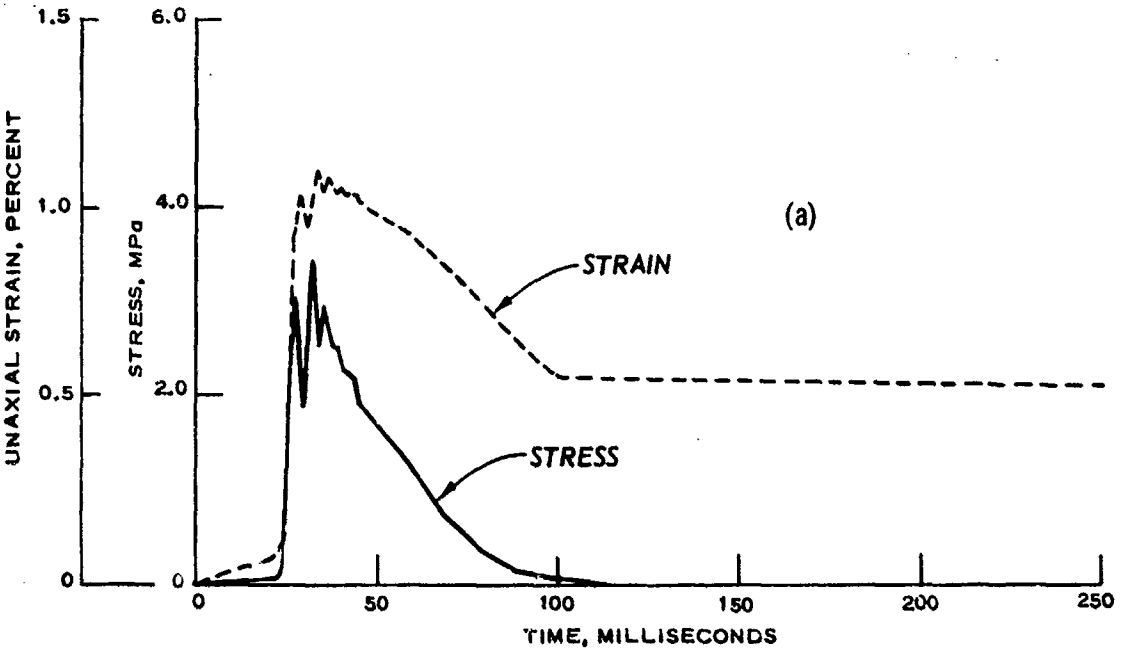

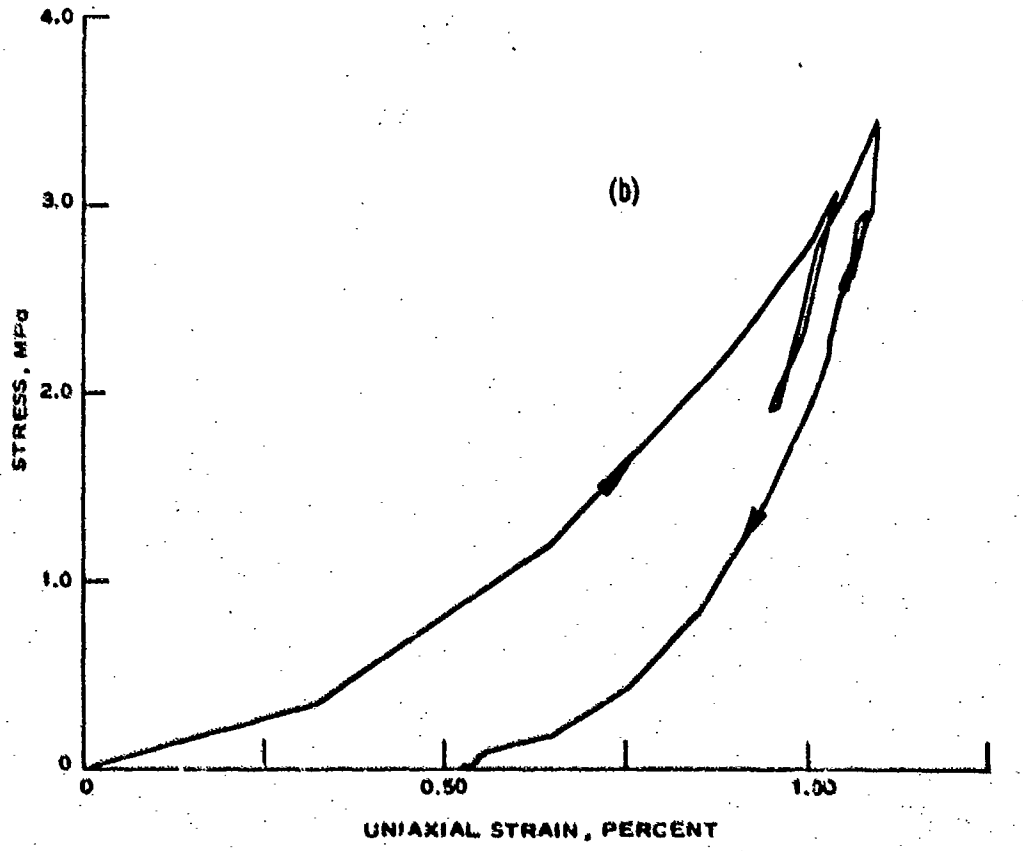

Figure 6.7. Dynamic uniaxial test results on Ottawa 50-200 sand. (a) Stress and strain time histories, (b) stress versus strain. Density = 1.6908 gm/cc.

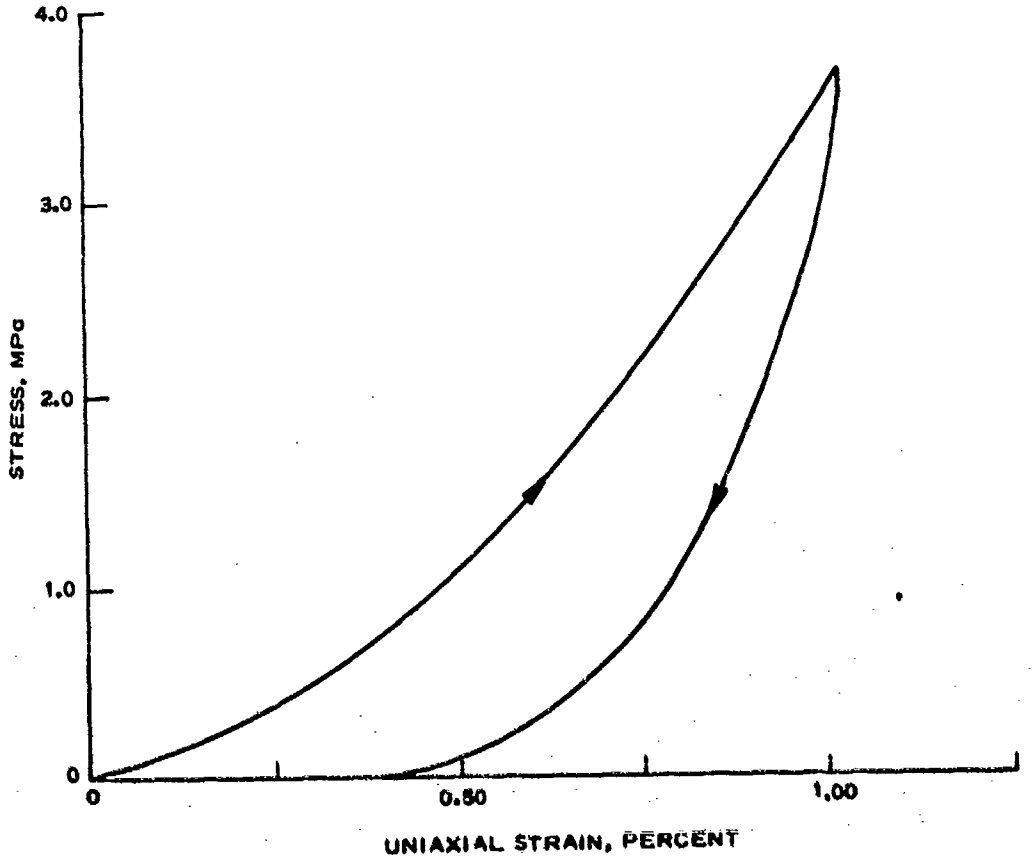

Figure 6.8. Static uniaxial stress-strain for Reid-Bedford Model sand. Density = 1.6363-gm/cc.

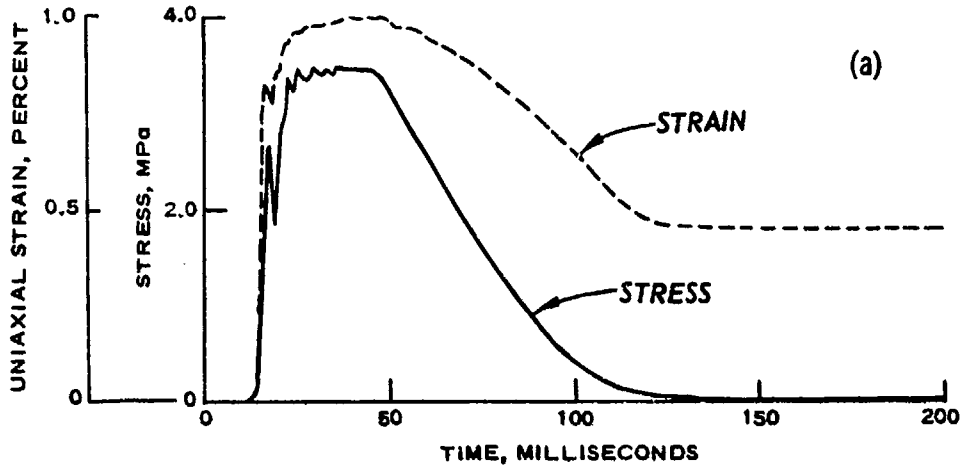

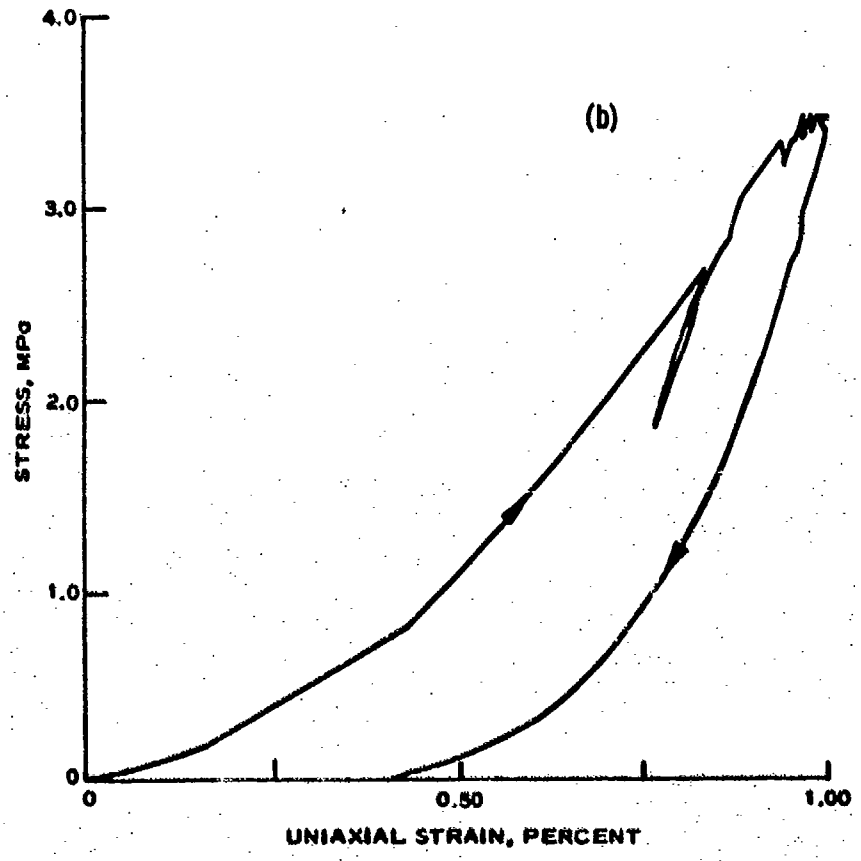

Figure 6.9. Dynamic uniaxial test results on Reid-Bedford Model sand. (a) Stress and strain time histories (b) stress versus strain. Density = 1.6401 gm/cc.

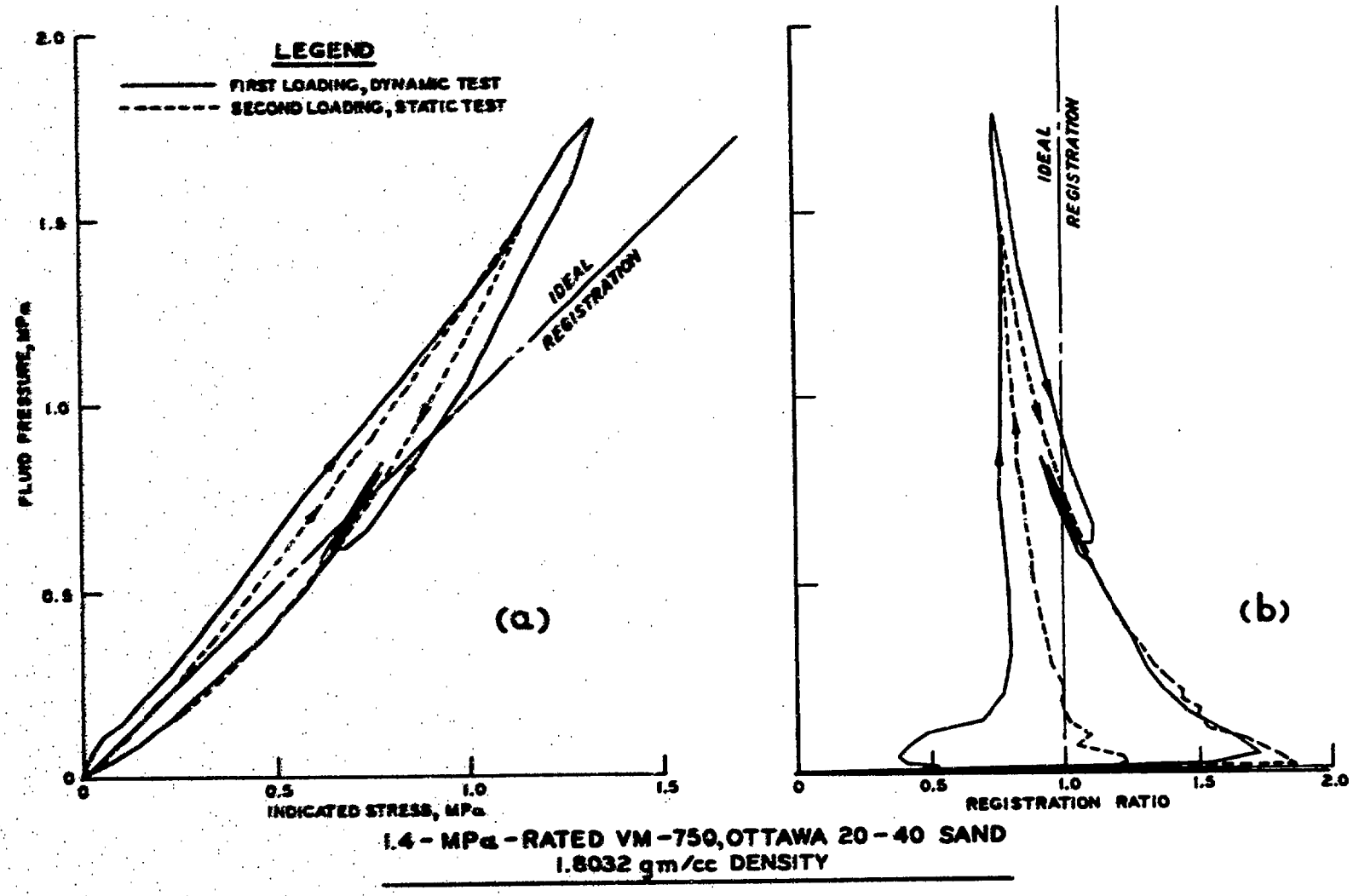

Figure 6.10. Registration of 1.4-MPa-rated VM-750 with Ottawa 20-40 sand. Sand depth was 5.08 cm in these tests; in all other tests it was 9.52 cm. (a) Fluid pressure versus indicated stress, (b) fluid pressure versus registration ratio.

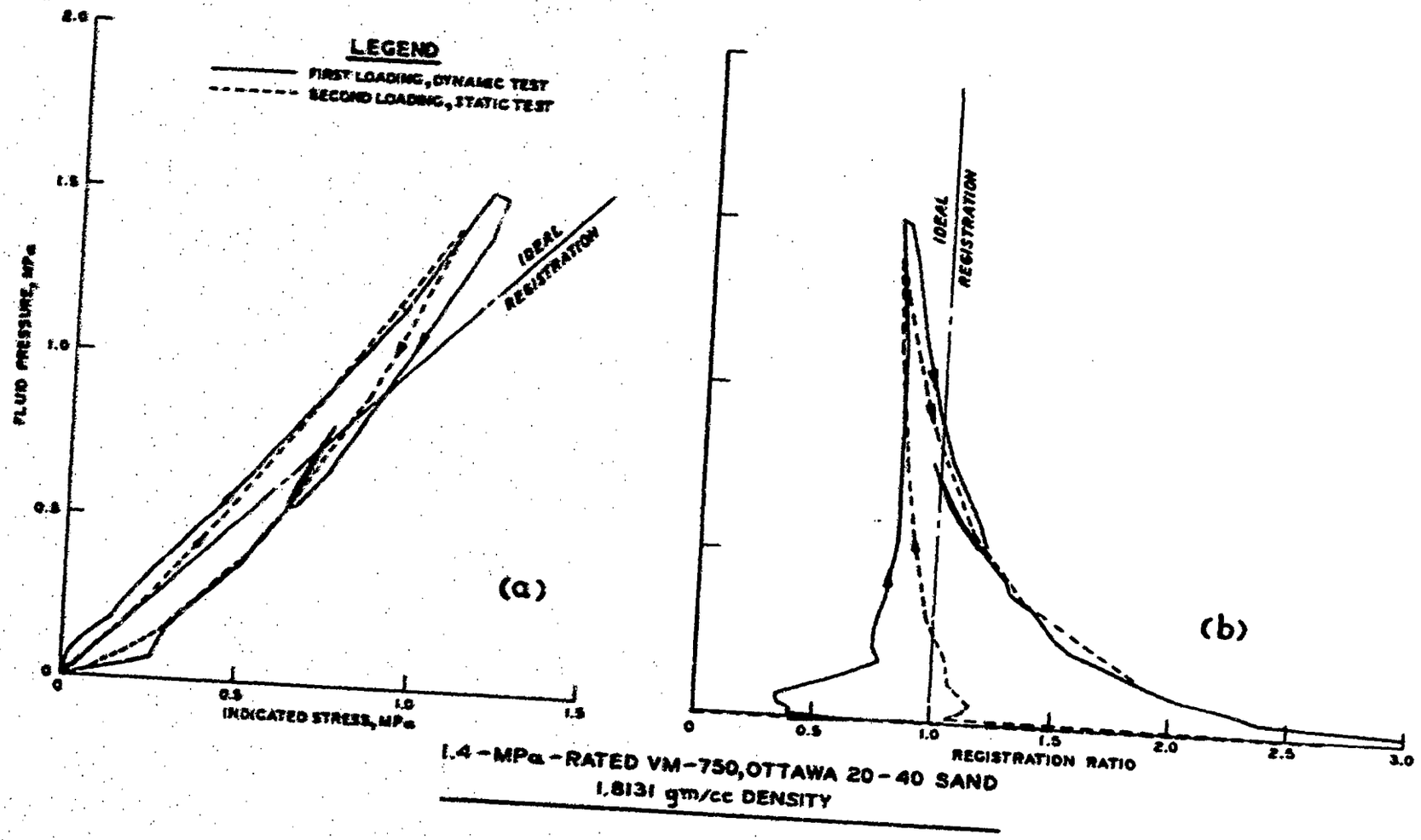

Figure 6.11 Registration of 1.4-MPa-rated VM-750 with Ottawa 20-40 sand. (a) Fluid pressure versus indicated stress, (b) fluid pressure versus registration ratio.

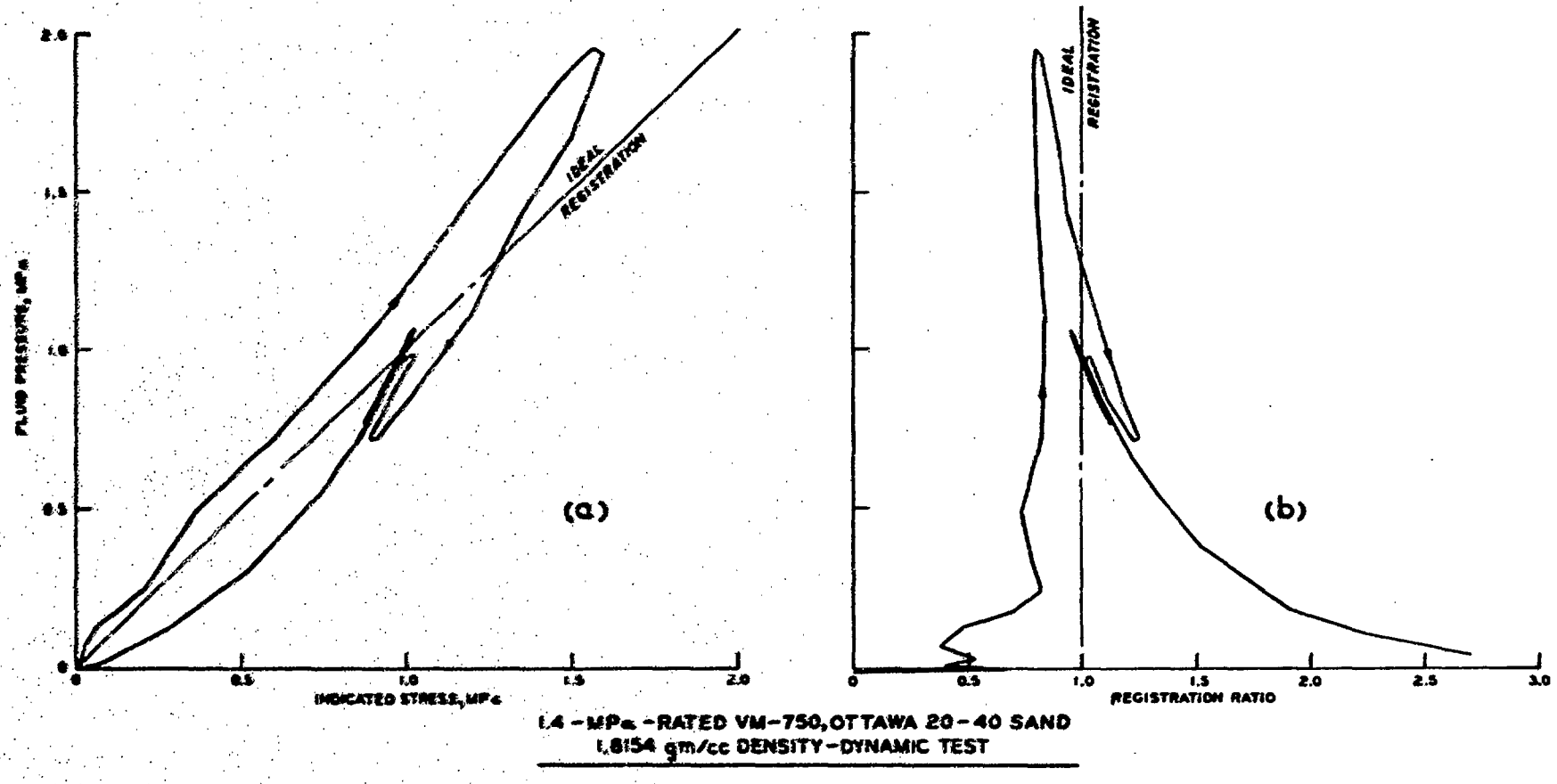

Figure 6.12 Registration of 1.4-MPa-rated VM-750 with Ottawa 20-40 sand. (a) Fluid pressure versus indicated stress, (b) fluid pressure versus registration ratio.

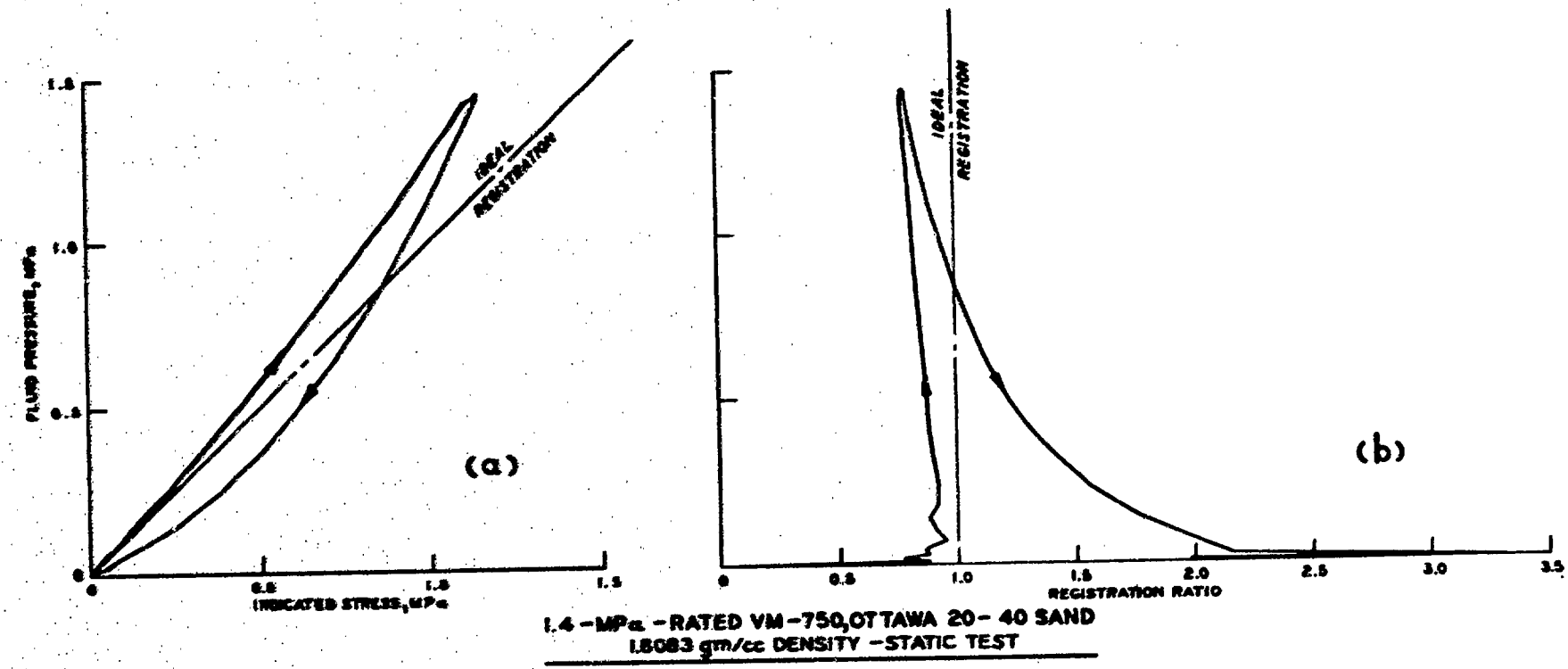

Figure 6.13. Registration of 1.4-MPa-rated VM-750 with Ottawa 20-40 sand. (a) Fluid pressure versus indicated stress, (b) fluid pressure versus registration ratio.

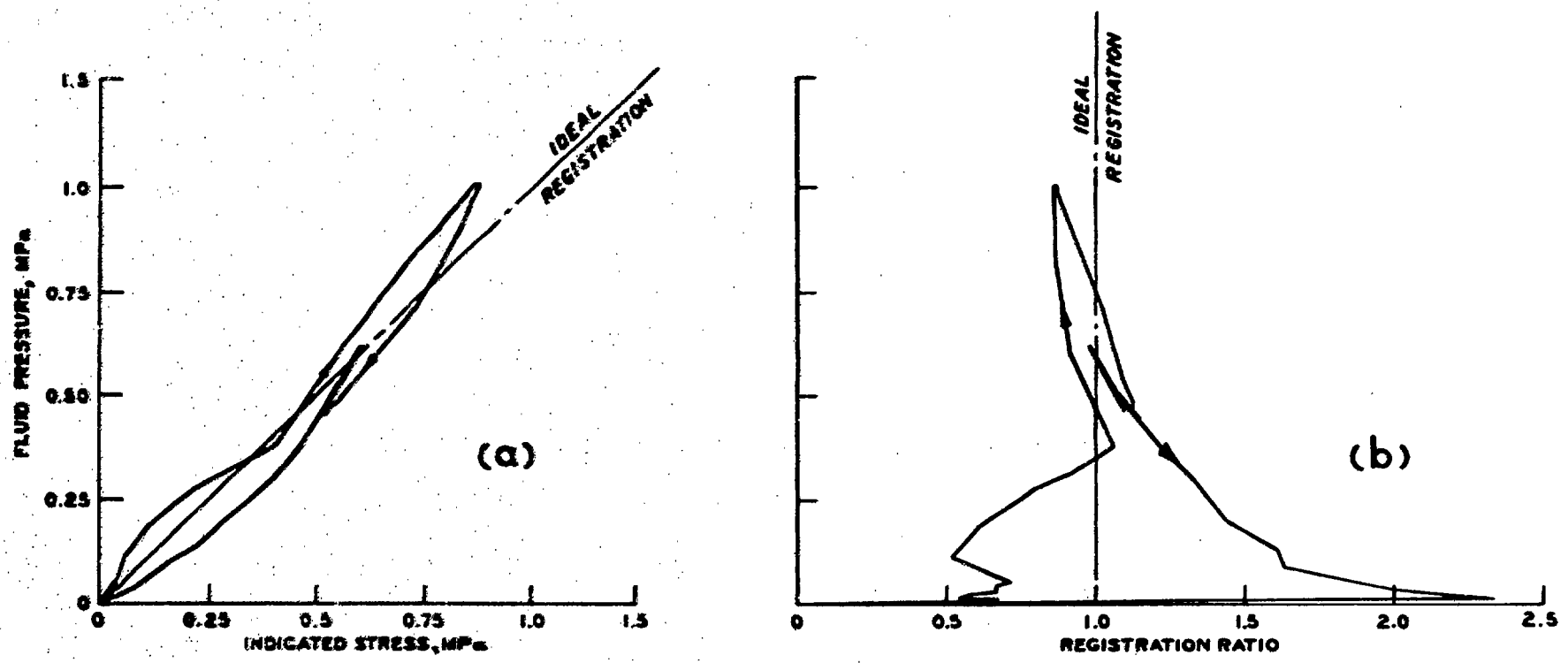

Figure 6.14. Registration of 1.4-MPa-rated VM-750 with Ottawa 20-40 sand. (a) Fluid pressure versus indicated stress, (b) fluid pressure versus registration ratio.

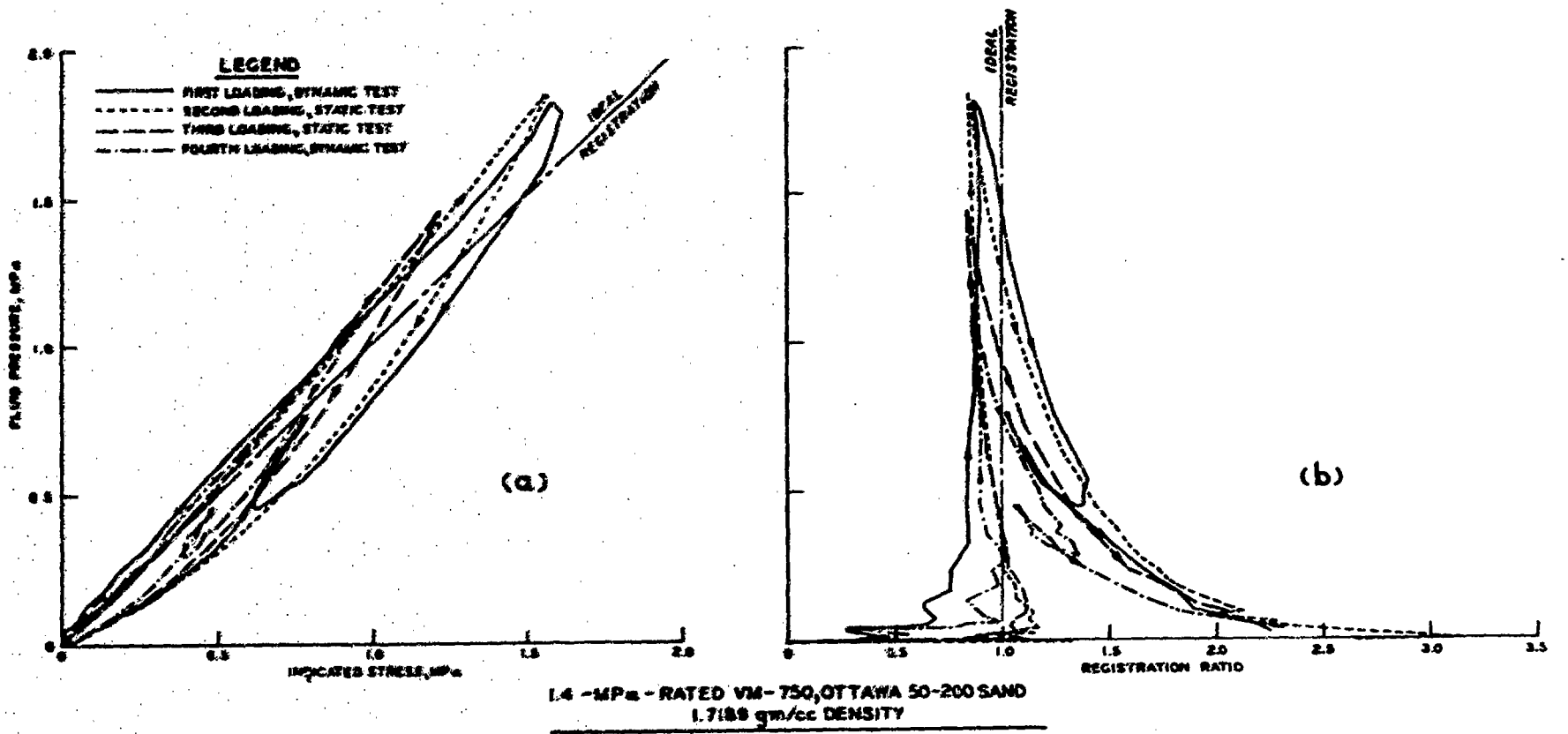

Figure 6.15. Registration of 1.4-MPa-rated VM-750 with Ottawa 50-200 sand. (a) Fluid pressure versus indicated stress, (b) fluid pressure versus registration ratio.

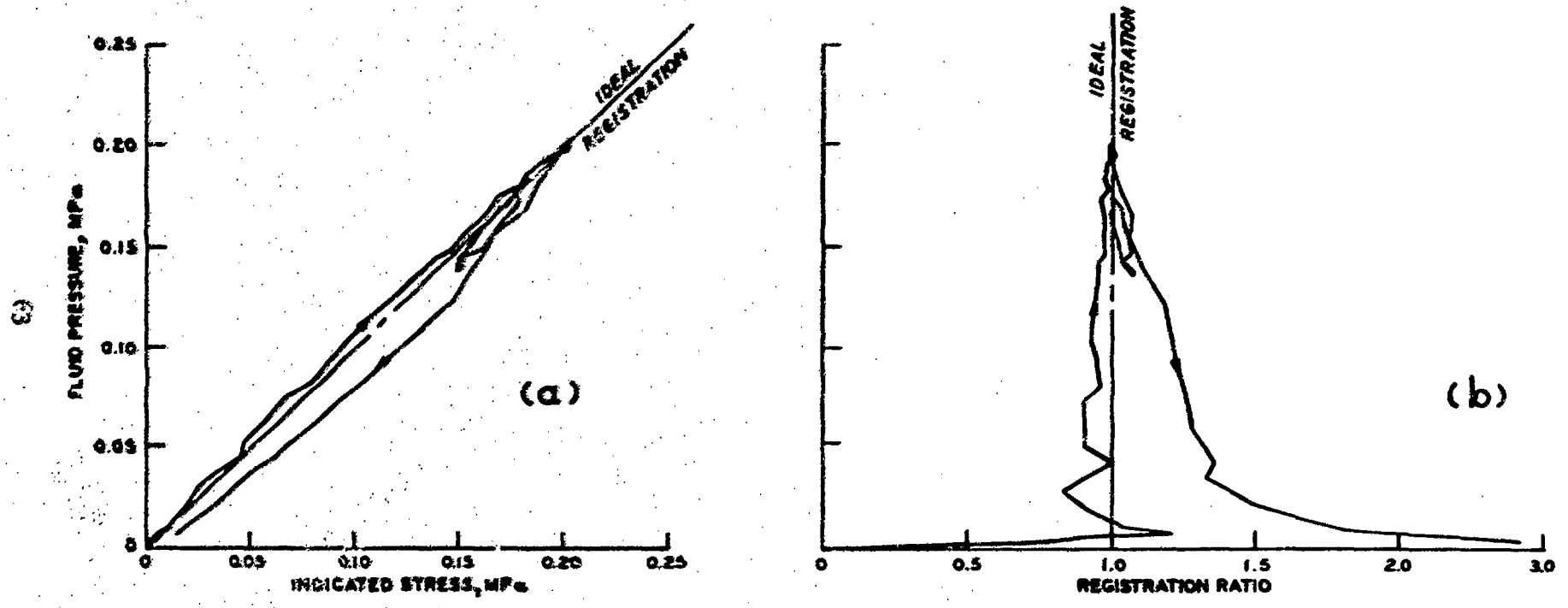

1.4-MPa-RATED VM-750, REID-BEDFORD MODEL SAND, DYNAMIC TEST

Figure 6.16. Registration of 1.4-MPa-rated VM-750 with Reid-Bedford Model sand. (a) Fluid pressure versus indicated stress, (b) fluid pressure versus registration ratio.

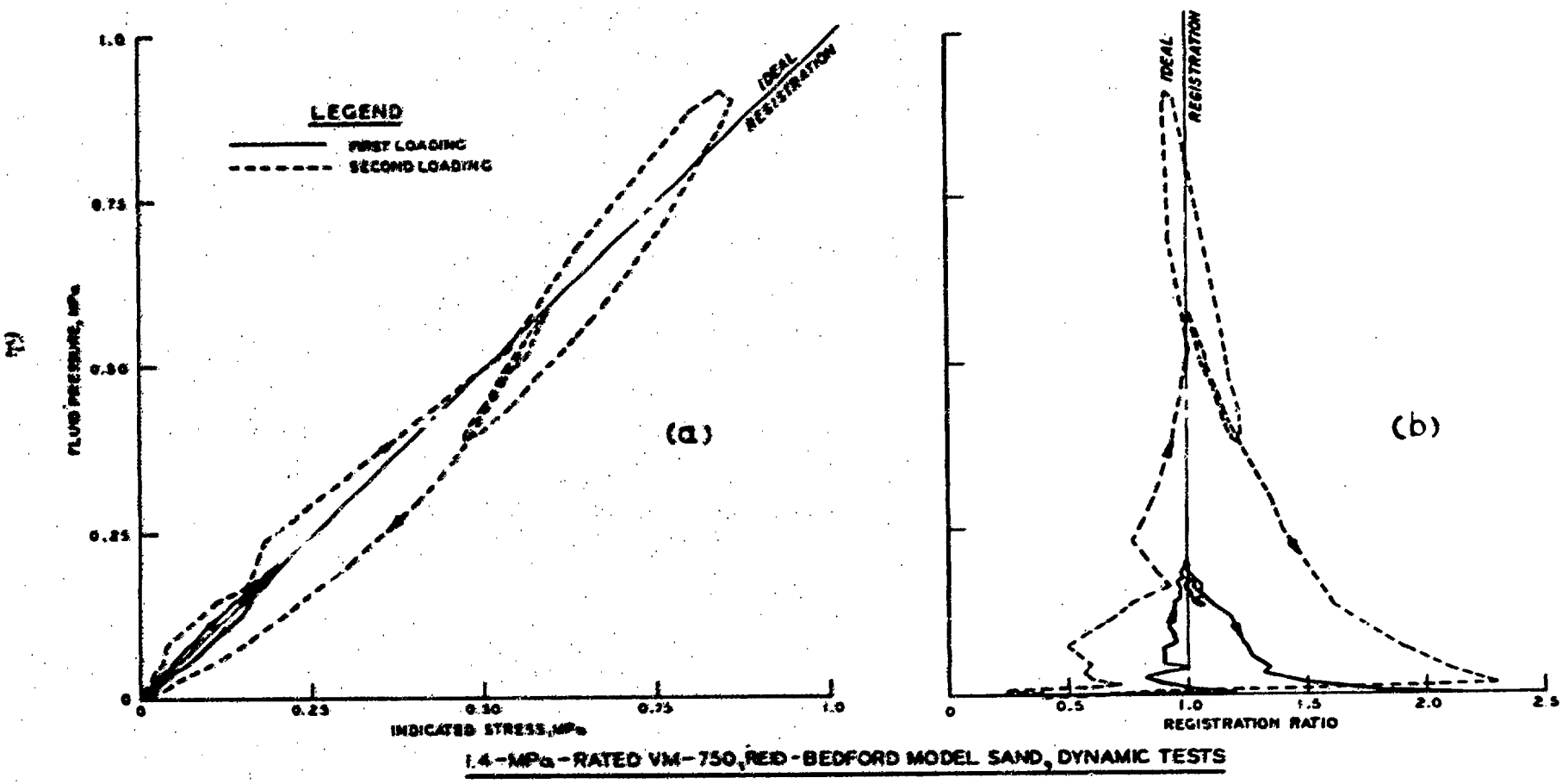

Figure 6.17. Registration of 1.4-MPa-rated VM-750 with Reid-Bedford Model sand. (a) Fluid pressure versus indicated stress, (b) fluid pressure versus registration ratio.

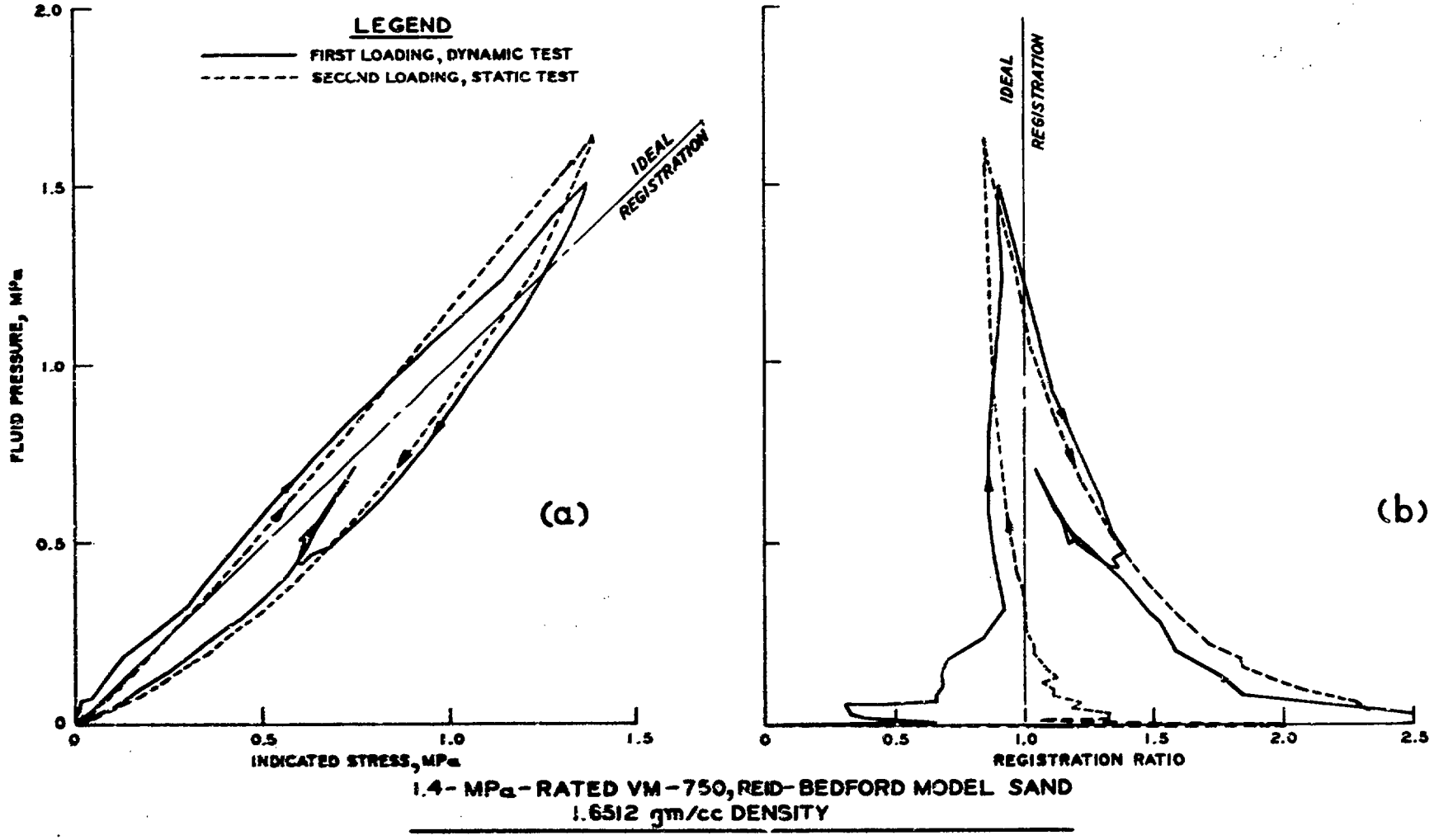

Figure 6.18. Registration of 1.4-MPa-rated VM-750 with Reid-Bedford Model sand. (a) Fluid pressure versus indicated stress, (b) fluid pressure versus registration ratio.

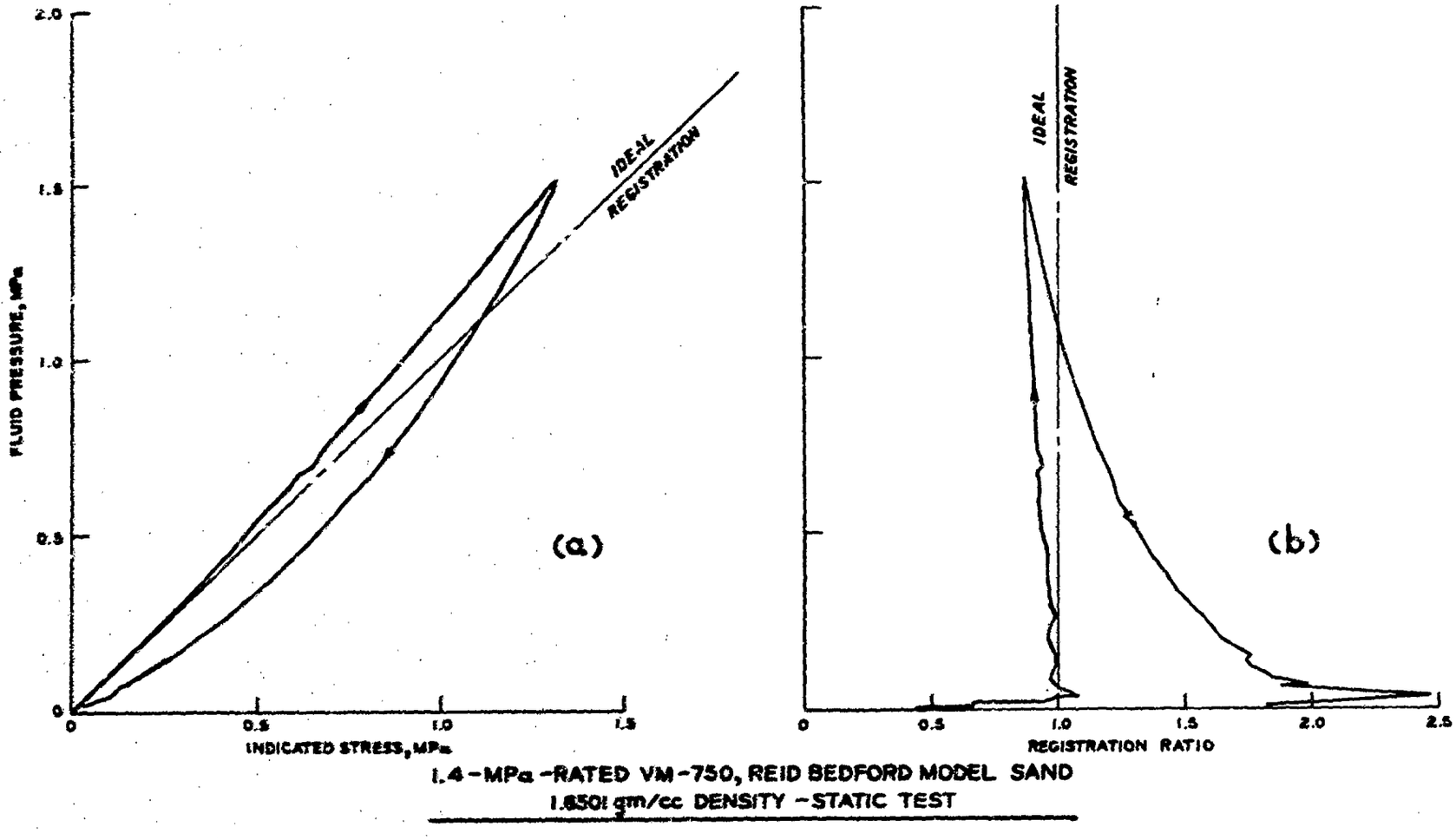

Figure 6.19. Registration of 1.4-MPa-rated VM-750 with Reid-Bedford Model sand. (a) Fluid pressure versus indicated stress, (b) fluid pressure versus registration ratio.

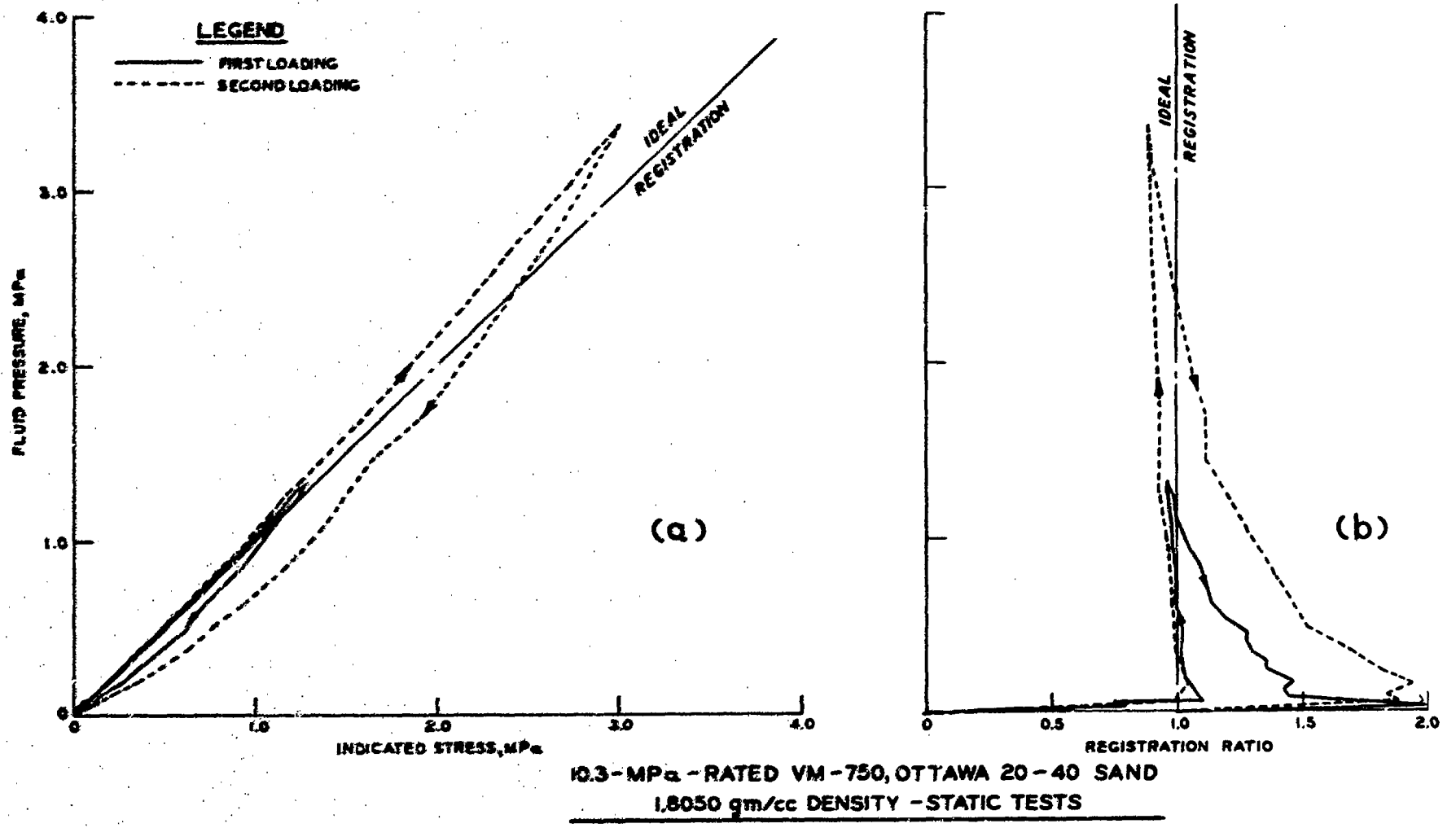

Figure 6.20. Registration of 10.3-MPa-rated VM-750 with Ottawa 20-40 sand. (a) Fluid pressure versus indicated stress, (b) fluid pressure versus registration ratio.

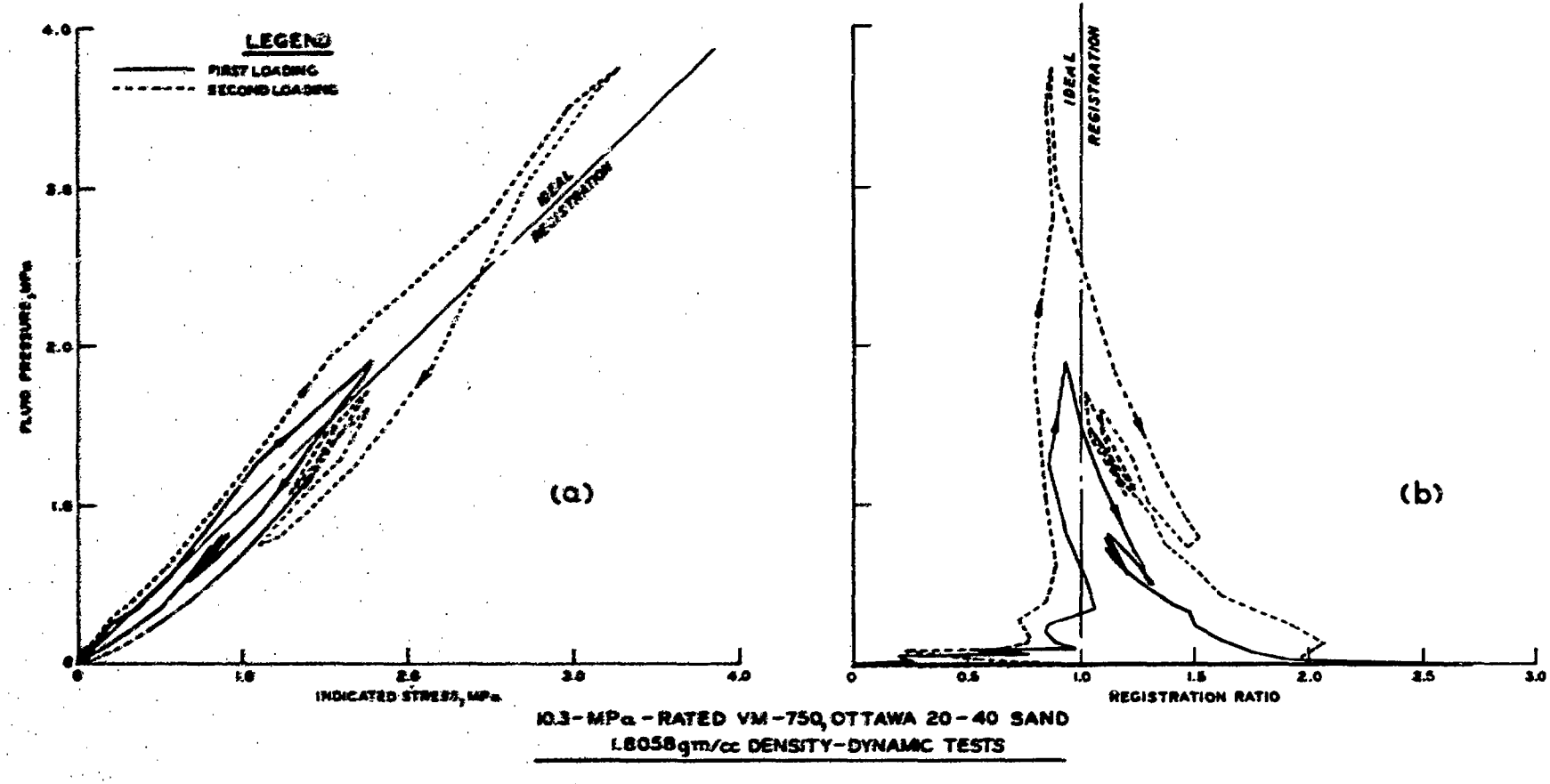

Figure 6.21. Registration 10.3-MPa-rated VM-750 with Ottawa 20-40 sand. (a) Fluid pressure versus indicated stress, (b) fluid pressure versus registration ratio.

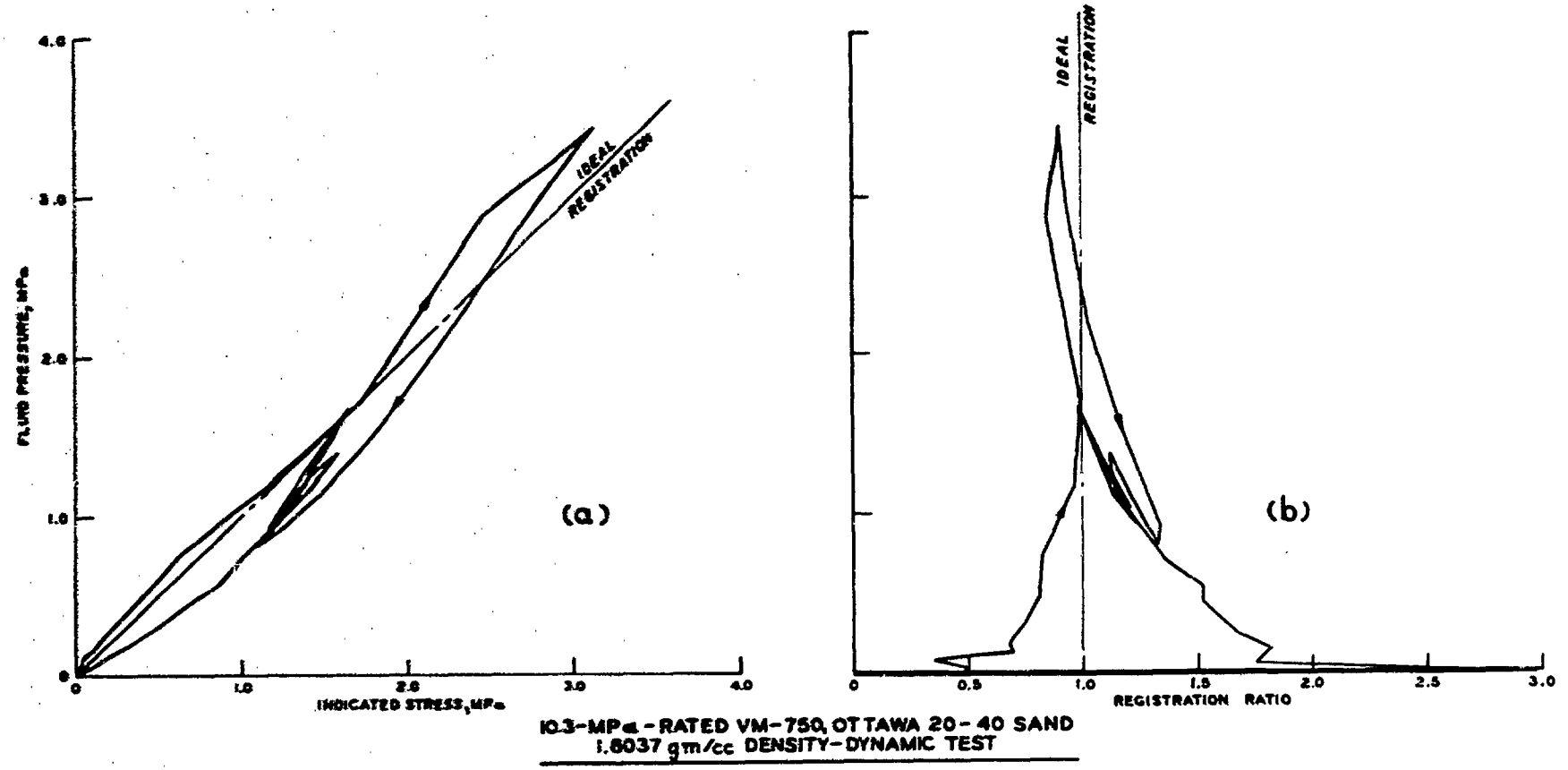

Figure 6.22. Registration of 10.3-MPa-rated VM-750 with Ottawa 20-40 sand. (a) Fluid pressure versus indicated stress, (b) fluid pressure versus registration ratio.

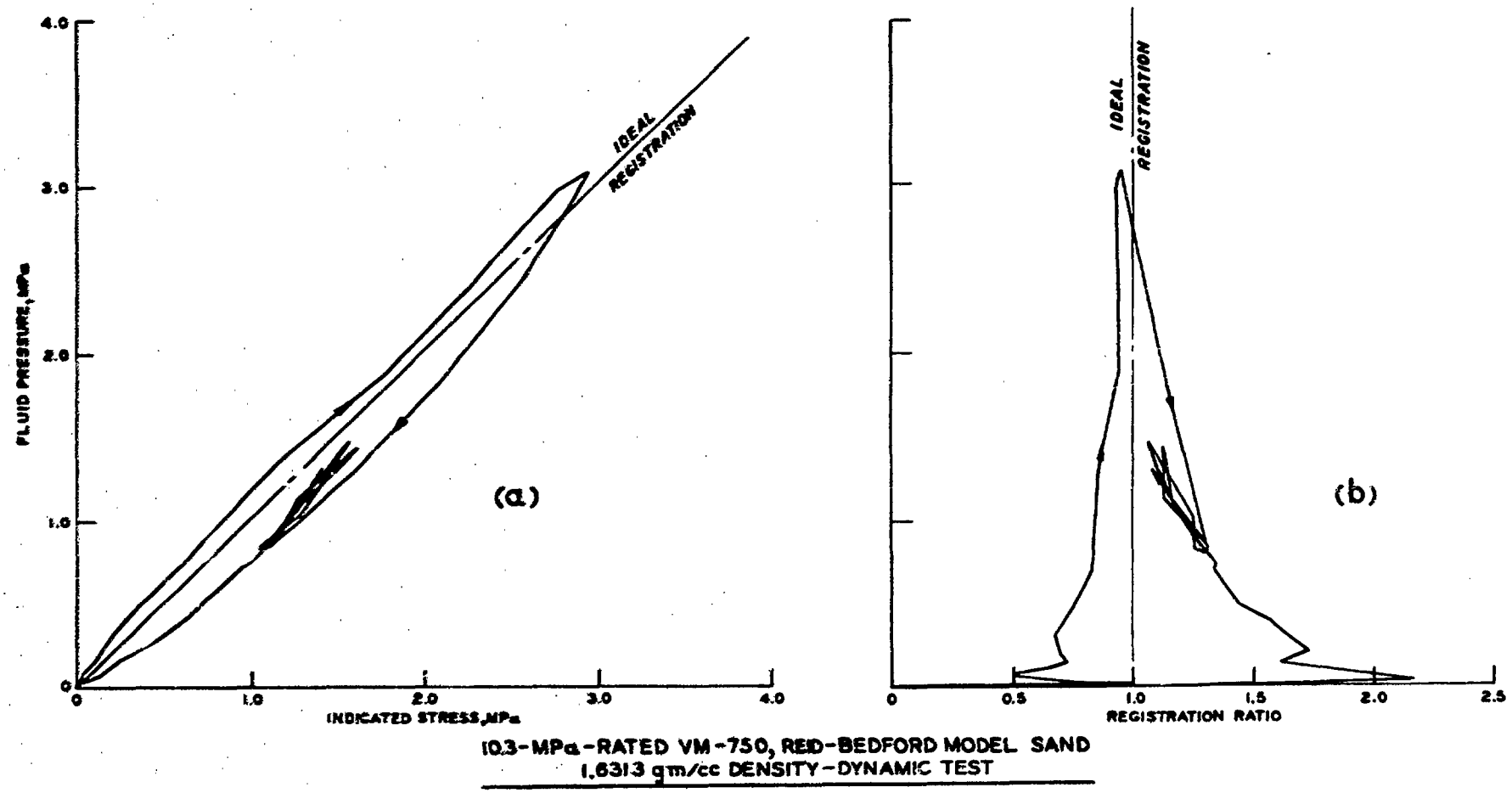

Figure 6.23. Registration of 10.3-MPa-rated VM-750 with Reid-Bedford Model sand. (a) Fluid pressure versus indicated stress, (b) fluid pressure versus registration ratio.

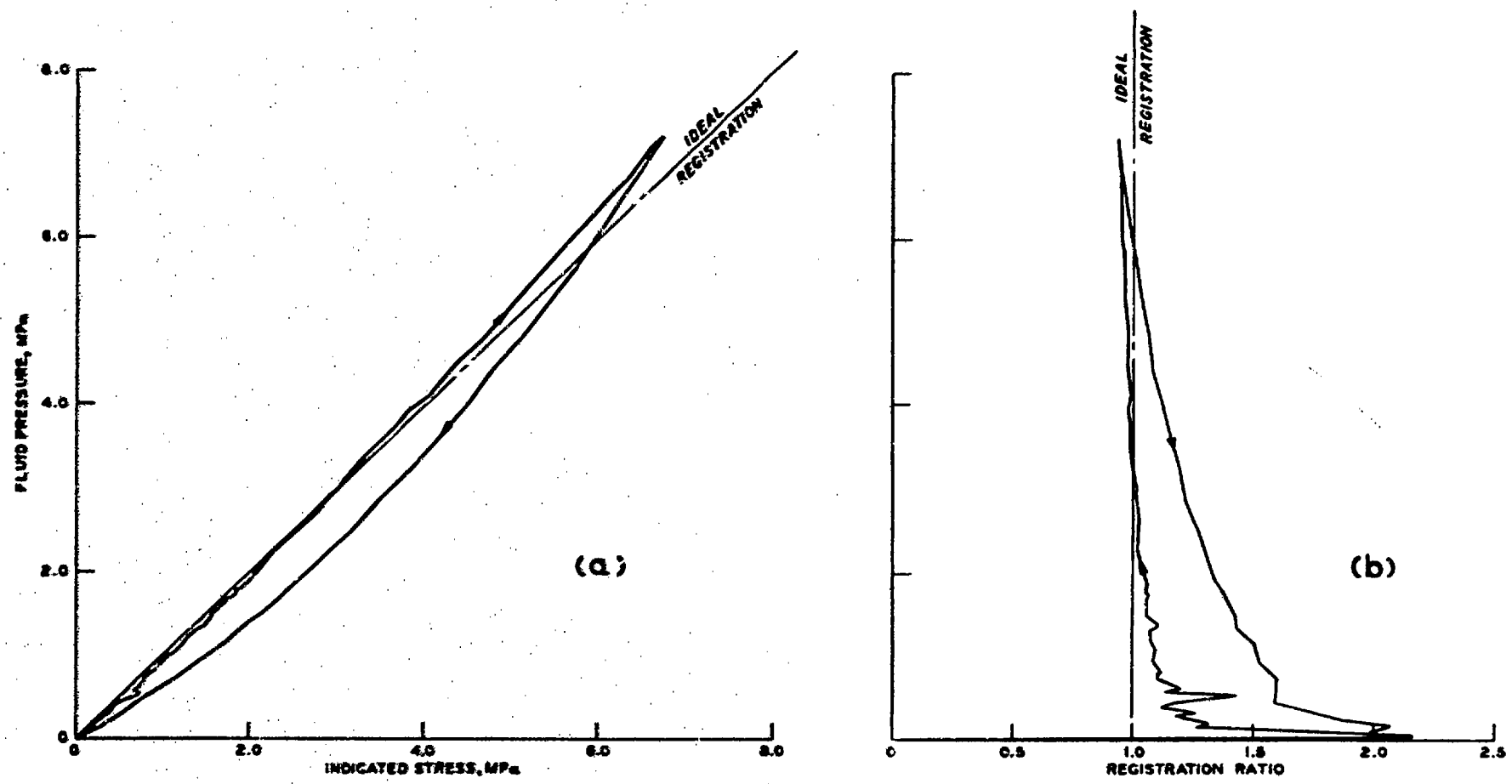

Figure 6.24. Registration of 13.8-MPa-rated VM-750 with Ottawa 20-40 sand. (a) Fluid pressure versus indicated stress, (b) fluid pressure versus registration ratio.

CHAPTER 7

SUMMARY AND CONCLUSIONS

Consideration of the effects of lateral stresses in the structure wall on the interaction of the gage with the soil leads to the basic requirements of high gage stiffness and anchoring as closely to the surface of the structure as possible. Theoretical comparison of the interaction of diaphragm and column type gages with an external non-adhering elastic medium implies that on the basis of minimizing the effects of soil arching on gage registration while maximizing electrical output, the strain-gaged diaphragm concept is competitive over much of the soil stress range of interest. Several other gage concepts were also considered. A survey of commercially available gages turned up a candidate gage that appeared to be suitable after certain requested modifications. This modified version was designated the VM-750 by its manufacturer, Kulite Semiconductor, Inc.

The VM-750 has two semiconductor strain gages bonded to the inside of the diaphragm, and temperature compensation in the inactive bridge arms. The diaphragm and gage case material is 17-4PH stainless steel, H900 condition; its thermal expansion is very nearly the same as that of concrete. Nominal electrical output at rated pressure is 100 millivolts. Claimed maximum pressure is twice the rated pressure. A listing of rated pressures and nominal diaphragm thicknesses is given in Table 2.1.

The mounting system anchors the gage close to the outer surface of the structure and isolates it from lateral stresses in the structure. Cross sections of two versions of the mount are shown in Figures 3.1 and 3.2. The strength of the mount is adequate for rated ranges up to 20.7 MPa (3000 psi). Measured lateral sensitivity under axisymmetric loading corresponding to failure of 40-MPa (6000-psi) concrete around the mount did not exceed one percent of full-scale rating. Allowing for some variation in lateral sensitivity among individual gages, two percent of full-scale rating may be considered a more conservative limit

under these conditions. The tests included static tests plus dynamic tests with a rise time of approximately two milliseconds; a typical dynamic loading pulse is shown in Figure 4.3. With shorter rise times in lateral stress, the lateral sensitivity may be higher. However, such short structural response times may be obtained only with relatively stiff model structures, with natural frequencies greater than 200 Hz.

Measured acceleration sensitivities are in excellent agreement with predictions based on the mass per unit area of the diaphragm. These are not high enough to significantly affect soil stress measurements. Calculated and measured acceleration sensitivities as well as calculated diaphragm natural frequencies are given in Table 5.1.

Gage registration tests (Chapter 6) involved three varieties of sand: Ottawa 20-40, Ottawa 50-200, and Reid-Bedford Model sand. Most of the tests were done with Ottawa 20-40, the stiffest of these three varieties. These tests indicated that a gage diaphragm designed for a full-scale rating of 0.34 MPa (50 psi) is too flexible to provide acceptable registration with Ottawa 20-40 sand. Registration of the 1.4-MPa-rated version with this relatively severe medium was considered acceptable; measured registration ratios during loading were approximately 0.8 at applied stresses close to its rated range. Closer to ideal registration was obtained in tests with the stiffer 10.3-MPa-rated and 13.8-MPa-rated versions. With the possible exception of soils of much lower shear strength (such as wet clays), the use of versions of this gage rated for less than 1.4 MPa (200 psi) is not recommended. In view of the 100-millivolt nominal full-scale output, this should not be a severe limitation on measurements below 1.4 MPa.

The gage registration test results also demonstrate a relatively high degree of repeatability. However, these tests were conducted under laboratory conditions and with the gage in an upward-facing surface. Due to increased difficulties in soil placement, the same degree of repeatability should not be expected with measurements on vertical walls. Measurements on downward-facing surfaces present even more severe placement problems.

When considering other types of soil, it must be kept in mind that the presence of stones next to the diaphragm is likely to result in erratic measurements. If the backfill should contain stones, a properly proportioned small pocket of stone-free soil may be used to cover the gage. In some cases, it may be sufficient to merely remove stones from the immediate vicinity of the gage or to use sieved field soil in covering the gage. Perhaps the most severe problems are presented by moistened backfills that cement together and shrink nonuniformly around the structure.

Some laboratory measurements of gage registration (such as the tests reported in Chapter 6) with the same soil as in the field application make it possible to correct for systematic deviations from ideal registration. The configuration of any small pocket of unrepresentative soil covering the gage should also be duplicated in the laboratory tests.

An investigation of the effects of various field backfill placement and compaction techniques on gage registration and data scatter would yield much useful information on the accuracy and limitations of soil-structure interface stress measurements under field conditions.

REFERENCES

1. M. J. Hvorslev; "The Changeable Interaction Between Soils and Pressure Cells; Tests and Reviews at the Waterways Experiment Station;" Technical Report No. S-76-7, June 1976; U. S. Army Engineer Waterways Experiment Station, CE, Vicksburg, MS.

2. S. P. Timoshenko and J. N. Goodier; Theory of Elasticity, 3rd ed., McGraw-hill, New York, NY, 1970.

3. R. W. Faust and J. K. Ingram; "Development of On-Structure Stress Gages;" Technical Report No. 1-801, November 1967; U. S. Army Engineer Waterways Experiment Station, CE, Vicksburg, MS.

4. "Materials Selector 76," Materials Engineering; Vol 82, No. 4, September 1975.

5. R. J. Roark and W. C. Young; Formulas for Stress and Strain, 5th ed., McGraw-Hill, New York, NY, 1975.

6. J. K. Ingram; "Development of a Free-Field Soil Stress Gage for Static and Dynamic Measurements;" Technical Report No. 1-814, February 1968; U. S. Army Engineer Waterways Experiment Station, CE, Vicksburg, MS.

7. Handbook of Chemistry and Physics; 54th ed., The Chemical Rubber Co., Cleveland, OH, 1973.

8. American Institute of Physics Handbook; McGraw-Hill, New York, NY, 1967.

9. J. R. Stagner and R. Obenchain; "Concepts for On-Structure Shear Gage and On-Structure Self-Recording Stress-Gage;" Technical Documentary Report No. AFSWC-TDR-62-148, August 1963; Air Force Special Weapons Center, Kirtland AFB, NM.

10. T. E. Kennedy, C. E. Albritton, and R. E. Walker; "Initial Evaluation of Free-Field Response of the Large Blast Load Generator;" Technical Report No. 1-723, 1966; Appendix A; U. S. Army Engineer Waterways Experiment Station, CE, Vicksburg, MS.

11. P. F. Hadala; "The Effect of Placement Method on the Response of Soil Stress Gages;" Technical Report No. 3-803, November 1967; U. S. Army Engineer Waterways Experiment Station, CE, Vicksburg, MS.

APPENDIX A

GAGE MOUNT PARTS

A detailed drawing of the lateral-isolation ring is given in Figure A.1. Detailed drawings of the mount and clamp ring for use in thin structures, with wall thicknness less than 4 inches, are given in Figures A.2 and A.3 respectively. Dimension T in Figures A.2 and A.3 should be equal to or slightly less than the thickness of the structure, depending on the method of fastening the mount to the form. For example, for most measurements on a horizontal roof of a buried structure, it is convenient to make the length of the mount equal to the roof thickness and attach it to the form on the bottom end, while for most measurements on vertical or sloping walls it is more expedient to make the length of the mount approximately 1/16 to 1/8 inch less than the wall thickness, and attach it to the outer wall of the form. Detailed drawings of the mount and clamp ring for use in thick structures are given in Figures A.4 and A.5 respectively. Dimension C in Figure A.4 should be equal to or slightly less than the thickness of the structure minus 2 inches, depending on the method of fastening the mount to the form. Installation is discussed in greater detail in Appendix B.

The specifications for the bolts are as follows: No. 4-40 socket head cap screws, length under head 5/8 inch, minimum tensile strength 180,000 psi.

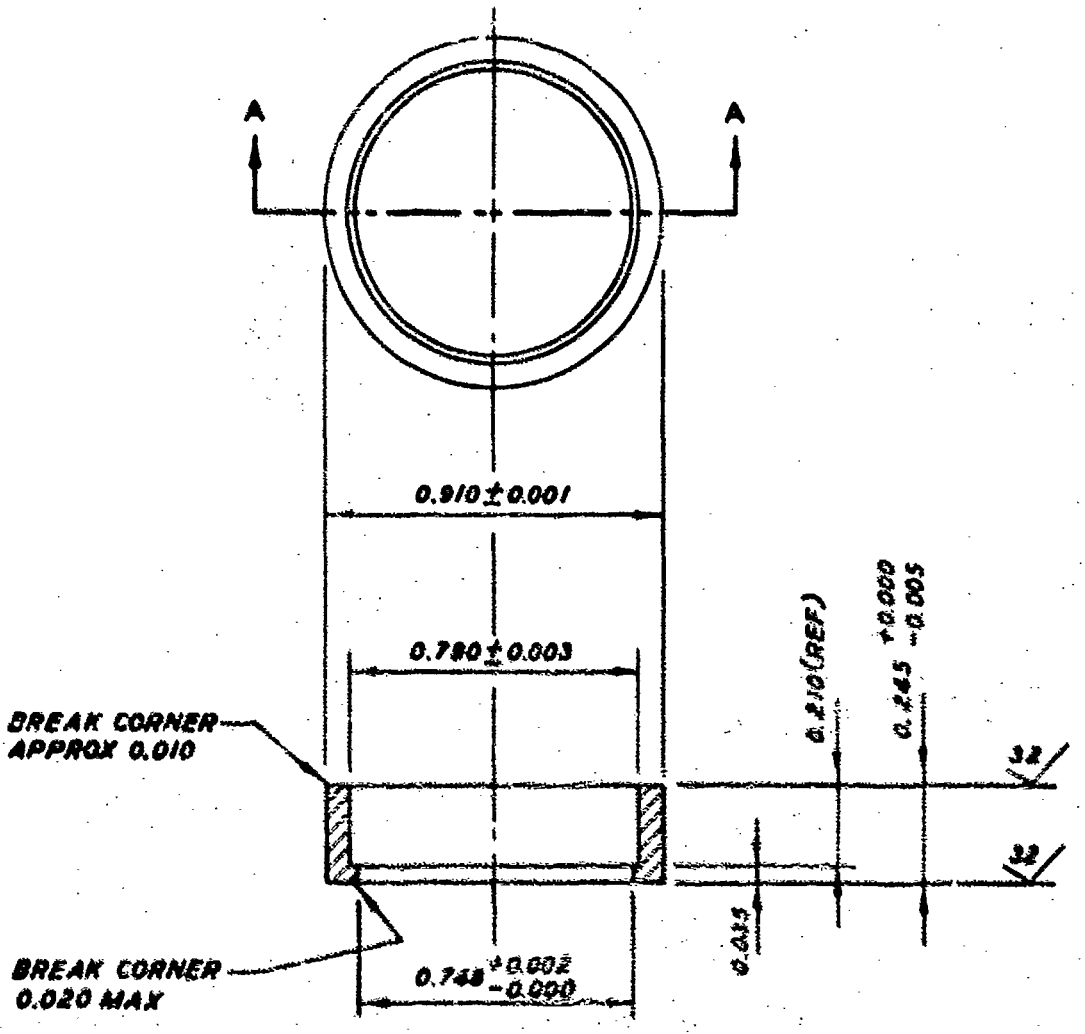

SECTION A - A

LATERAL-ISOLATION RING FOR SOIL-STRUCTURE INTERFACE STRESS GAGE

MATERIAL: 17-4 PH STAINLESS STEEL CONDITION H1150 OR H900
ALL DIMENSIONS ARE IN INCHES
TOLERANCES: ± 0.010 UNLESS OTHERWISE SPECIFIED

Figure A.1. Lateral-isolation ring.

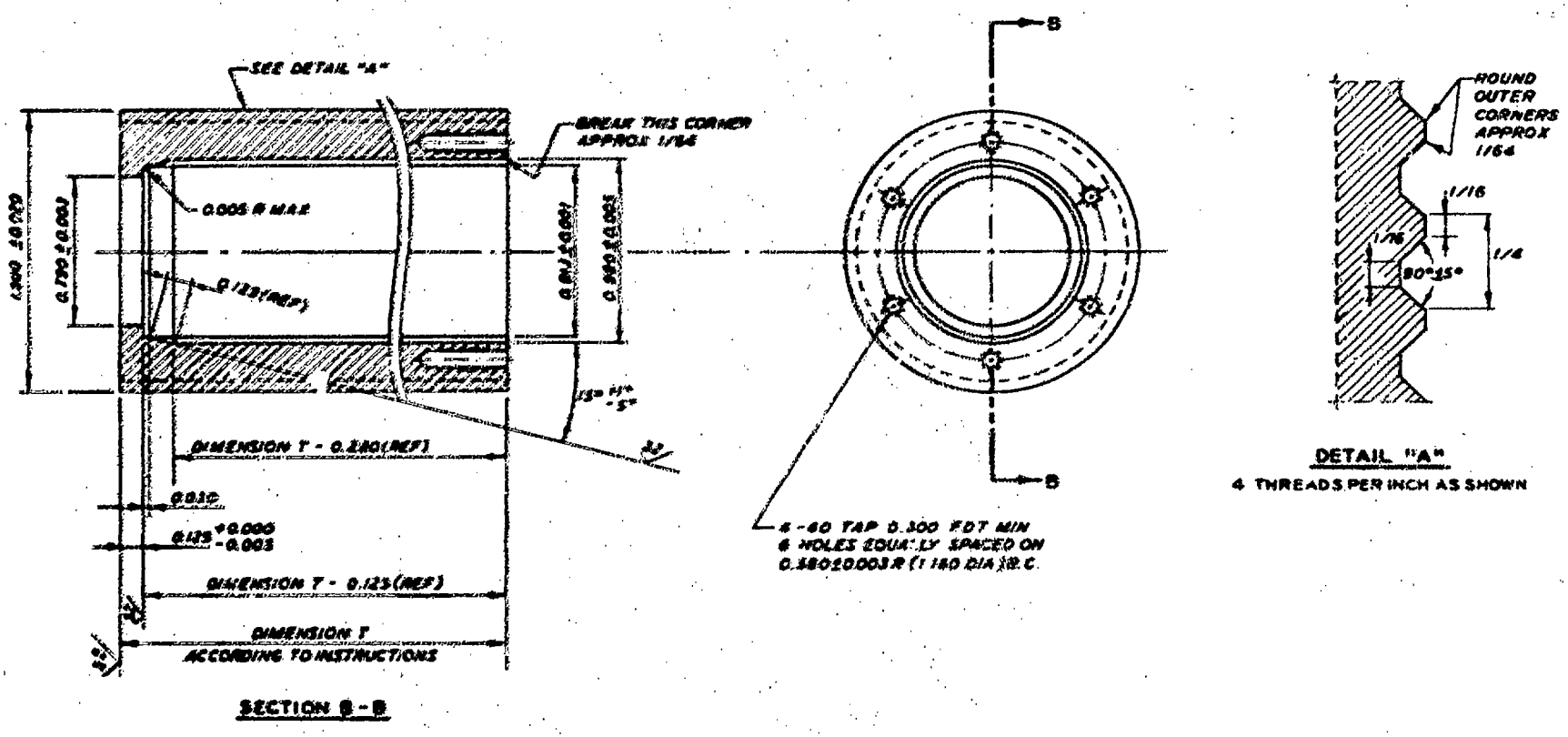

MOUNT FOR
SOIL-STRUCTURE INTERFACE STRESS GAGE
IN THIN STRUCTURES (LESS THAN 4 INCH WALL)

MATERIAL: AISI TYPE 416 STAINLESS STEEL

ALL DIMENSIONS (EXCEPT ANGLES) ARE IN INCHES
TOLERANCES ±0.010 UNLESS OTHERWISE SPECIFIED

Figure A.2. Mount for use in thin structures.

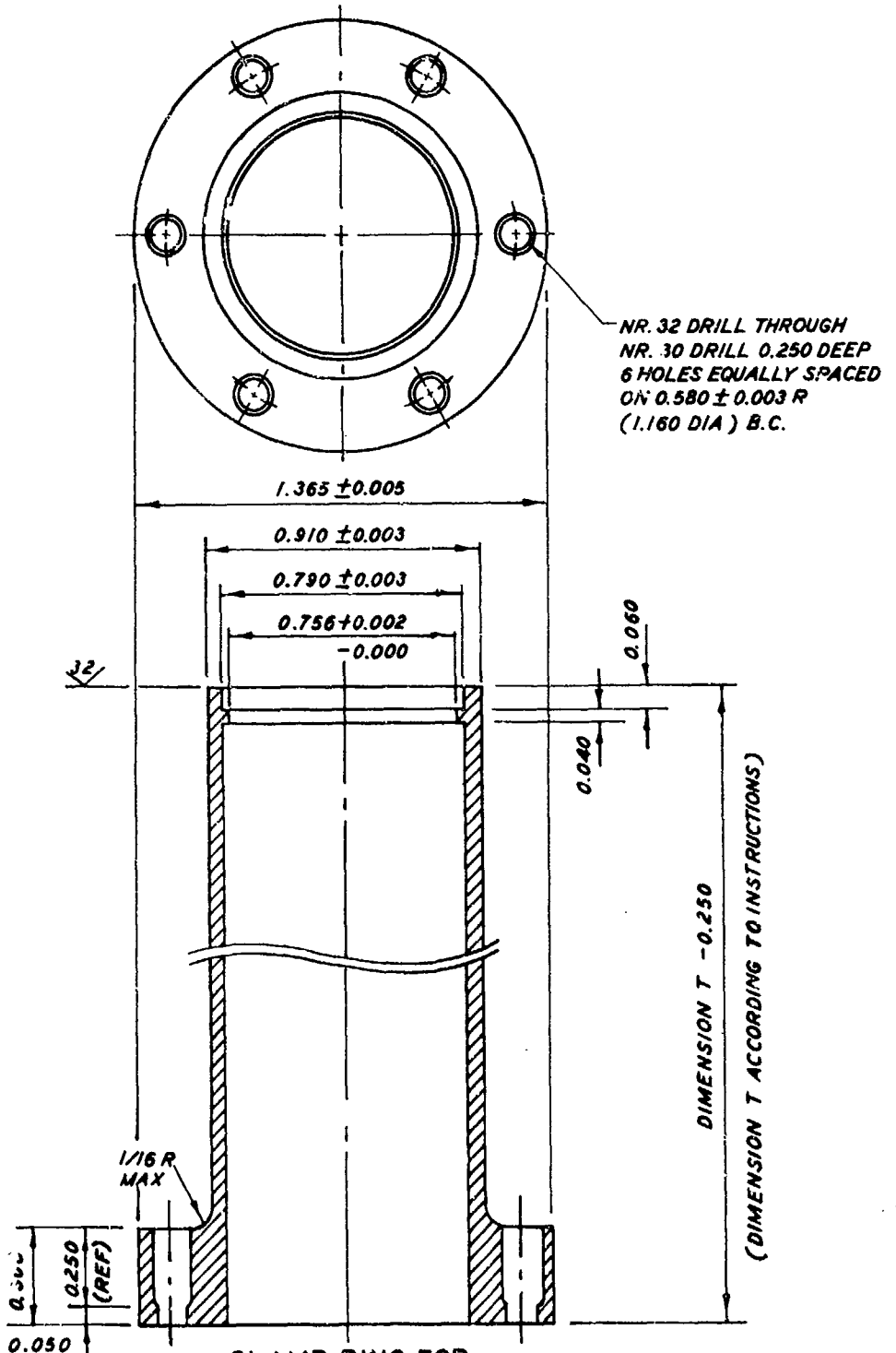

CLAMP RING FOR
SOIL-STRUCTURE INTERFACE STRESS GAGE
IN THIN STRUCTURES (LESS THAN 4 INCH WALL)

MATERIAL: 7075-T6 (OR -T651) ALUMINUM
ALL DIMENSIONS ARE IN INCHES
TOLERANCES: ±0.010 UNLESS OTHERWISE SPECIFIED

Figure A.3. Clamp ring for use in thin structures.

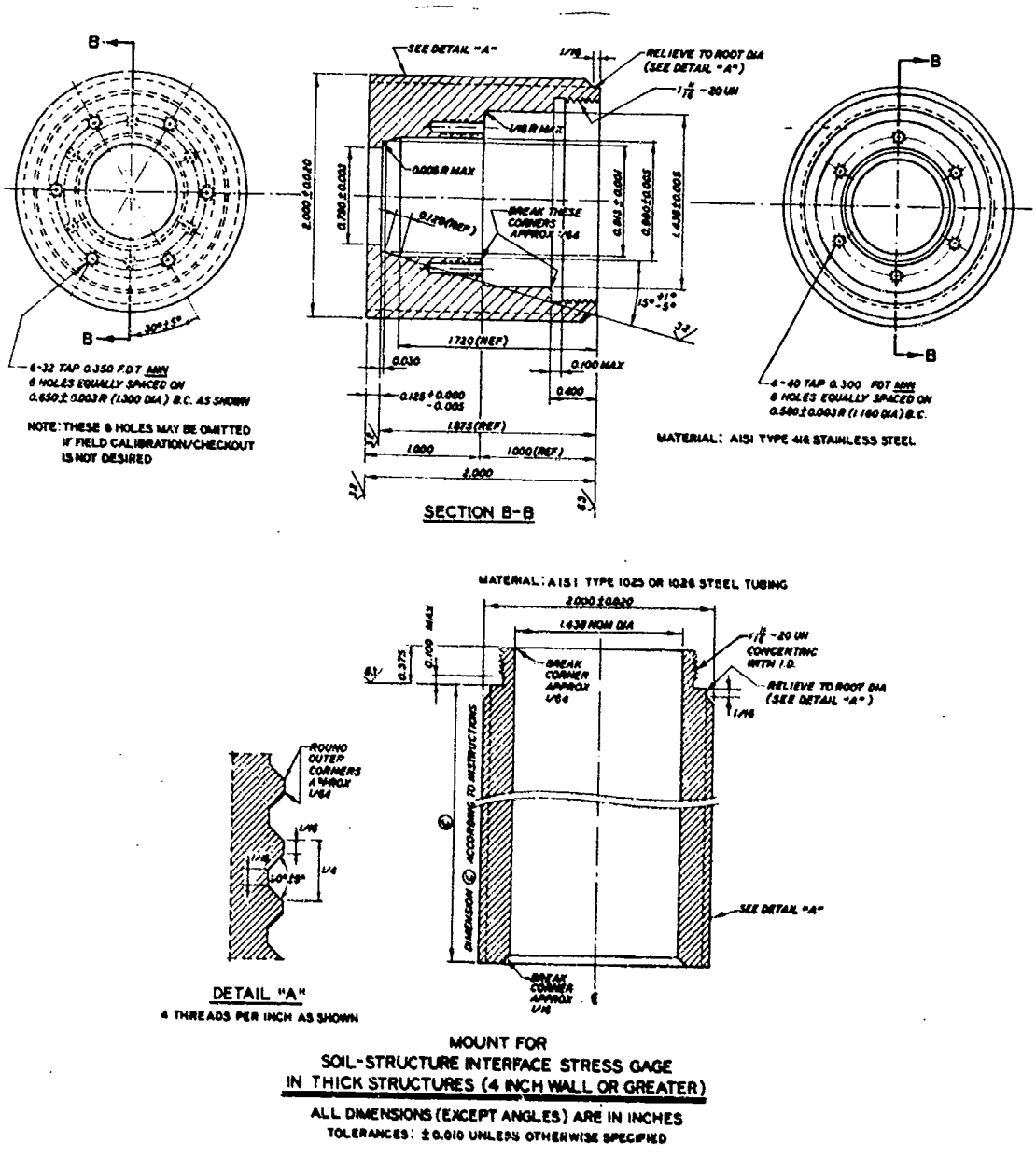

MOUNT FOR
SOIL-STRUCTURE INTERFACE STRESS GAGE
IN THICK STRUCTURES (4 INCH WALL OR GREATER)

ALL DIMENSIONS (EXCEPT ANGLES) ARE IN INCHES
TOLERANCES: ±0.010 UNLESS OTHERWISE SPECIFIED

Figure A.4. Mount for use in thick structures.

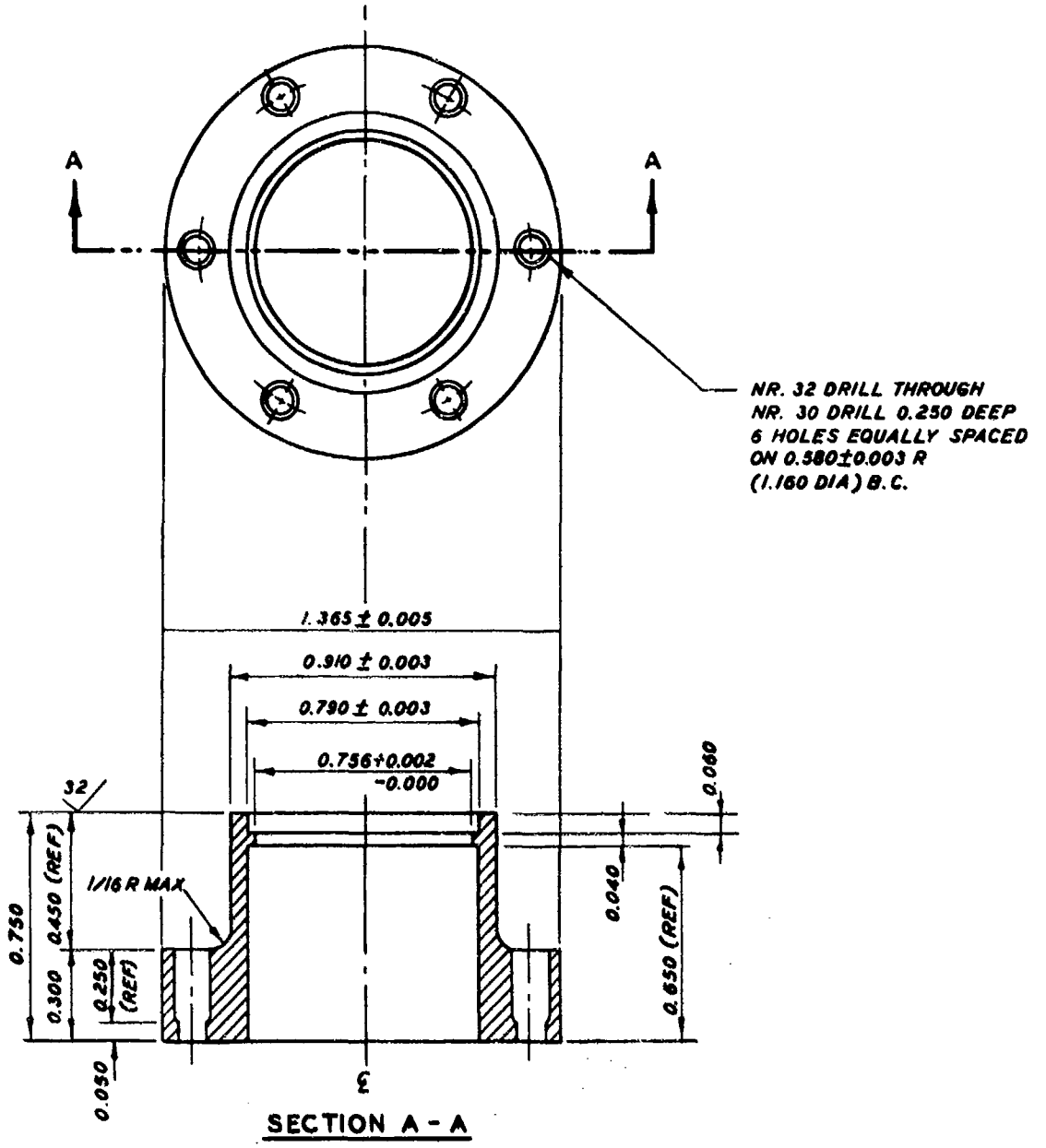

SECTION A - A

CLAMP RING FOR
SOIL-STRUCTURE INTERFACE STRESS GAGE
IN THICK STRUCTURES (4 INCH WALL OR GREATER)

MATERIAL: 7075 - T6 (OR -T651) ALUMINUM
ALL DIMENSIONS ARE IN INCHES
TOLERANCES: ±0.010 UNLESS OTHERWISE SPECIFIED

Figure A.5. Clamp ring for use in thick structures.

APPENDIX B

INSTALLATION PROCEURE

B.1 CALIBRATION OPTIONS

Most users prefer to calibrate a gage of this type in the laboratory prior to installation. A detailed drawing of a convenient laboratory calibration fixture is given in Figure B.1. With the mount designed for thick structures (Figure A.4) field calibration after installation is also possible. The field calibration fixture, shown in Figure B.2, fastens to the outer surface of the mount with six 6-32 high-strength socket head cap screws, length under head one inch, torqued to 35 in.-lbs. Prior to placing the backfill, the holes for attaching the field calibration fixture should be plugged; 6-32 set screws are convenient for this purpose.

B.2 INSTALLATION OF THE MOUNT IN THE STRUCTURE

It is preferable not to have the gage installed in the mount while the structure is being cast, but to install the gage once the structure has been completed and the form is off. The mount must be thoroughly cleaned and degreased. Because of possible relative movement during pouring and vibration of the mix, attachment of both ends of the mount to the corresponding walls of the form is not desirable. Since the outer surface of the mount should be flush with the structure, it follows that the mount should be fastened to the outer wall of the form whenever possible. Making the mount slightly shorter than the structure thickness eliminates interference with the inner wall of the form. However, if the form has no outer wall, such as in the case on a flat roof, then the mount length must be the same as the roof thickness.

Attachment of the mount to the outer wall of the form is usually most convenient with a single 1/4-20 bolt through the form. The special nut shown in Figure B.3 may be used with both versions of the gage mount; it fits onto the surfaces mating with the lateral-isolation ring. In order to insure subsequent firm anchoring of the gage to the

mount, it is important to avoid trapping burr-raising dirt or grit between this nut and the gage mount. The inner end of the mount must be plugged with a rubber stopper or blocked off with pressure-sensitive tape. The tape must be trimmed such that it does not overlap the threaded outer diameter of the mount.

For installation in a flat roof, the mount may be fastened with a single long bolt running all the way through, or by small screws running into tapped holes in the inner end. In the latter case, the outer end must be plugged with a rubber stopper or blocked off with pressure-sensitive tape. As always, the tape must be trimmed such that it does not overlap the threaded outer diameter of the mount.

B.3 INSTALLATION OF THE GAGE IN THE MOUNT

Because stiff anchoring of the gage to the mount is absolutely essential, all bearing surfaces must be free of dirt or grit. This is especially important in the case of the lateral-isolation ring and the corresponding mating surfaces on the mount and on the gage.

The mount parts are made such that centering is automatic. The small centering flange on the inside of the lateral-isolation ring must always be inward, i.e., next to the mounting flange of the gage, as shown in Figures 3.1 and 3.2.

In the mount designed for thin structures (Figure 3.1) the clamp ring extends to the inside of the structure and installation is straight-forward. In case of upward-facing and sideways-facing measurements, the most expedient procedure is as follows. The wire lead is threaded through the clamp ring, and the clamp ring and lateral-isolation ring are positioned on the gage. Holding the clamp ring by its flange and keeping the gage in place by maintaining a small pulling force on the wire, all three pieces are now inserted into the mount. The clamp ring is held in position while the bolts are inserted and made finger-tight. Although the taper in the mount facilitates seating of the lateral-isolation ring, it is nevertheless advisable to check the outer face of the mount before tightening the bolts. Improper

seating or jamming inside the mount would be indicated by the gage not extending all the way to the outer surface. The bolts are torqued to 20 in.-lbs.

The installation procedure with the mount designed for thick structures (Figure 3.2) is similar, except that the clamp ring can not be hand-held during insertion and the bolts must be engaged and tightened by means of a long wrench. A plastic tube that jams into the inner diameter of the flange end of the clamp ring has been used successfully as an insertion tool. Again, maintaining a small pulling force on the wire lead passing through the clamp ring and tube helps keep the gage in place in the clamp ring. The plastic tube is not removed until at least some of the bolts are in place. The bolts are torqued to 20 in.-lbs.

Injection of the silicone rubber sealant, Dow Corning Catalog No. 732, into the annular space around the outer end of the gage is facilitated by the injection tool shown in Figure B.4. The injection tool is positioned over the gage and mount such that the holes are diametrically opposed on the annular space. A syringe filled with the silicone rubber sealant is inserted into one of the holes and pressure is maintained on the syringe until the sealant flows out of the other hole. In case any bubbles were injected into the annular space, pressure on the syringe should be maintained until the bubbles are seen emerging from the other hole. All excess sealant must be removed from the outer surfaces of the gage and mount. It is expedient not to attempt to wipe this off immediately, but to scrape it off with a fingernail or a piece of wood or plastic after the sealant has solidified to some extent. In any case, the backfill should not be placed until at least a solid outer "skin" has formed; minimum time is approximately one hour.

B.4 INSTALLATION OF PREVIOUSLY USED GAGES

Upon recovery, the silicone rubber sealant and lateral-isolation ring usually stay attached to the gage. It is not necessary to remove the lateral-isolation ring before reusing the gage. However, because

stiff anchoring of the gage to the mount is absolutely essential, the possibility of trapping any solidified sealant between the lateral-isolation ring and the mount should be avoided by trimming off any attached sealant outward (toward the sensing face) from the lateral-isolation ring. This space is then filled by injection after the gage is in place.

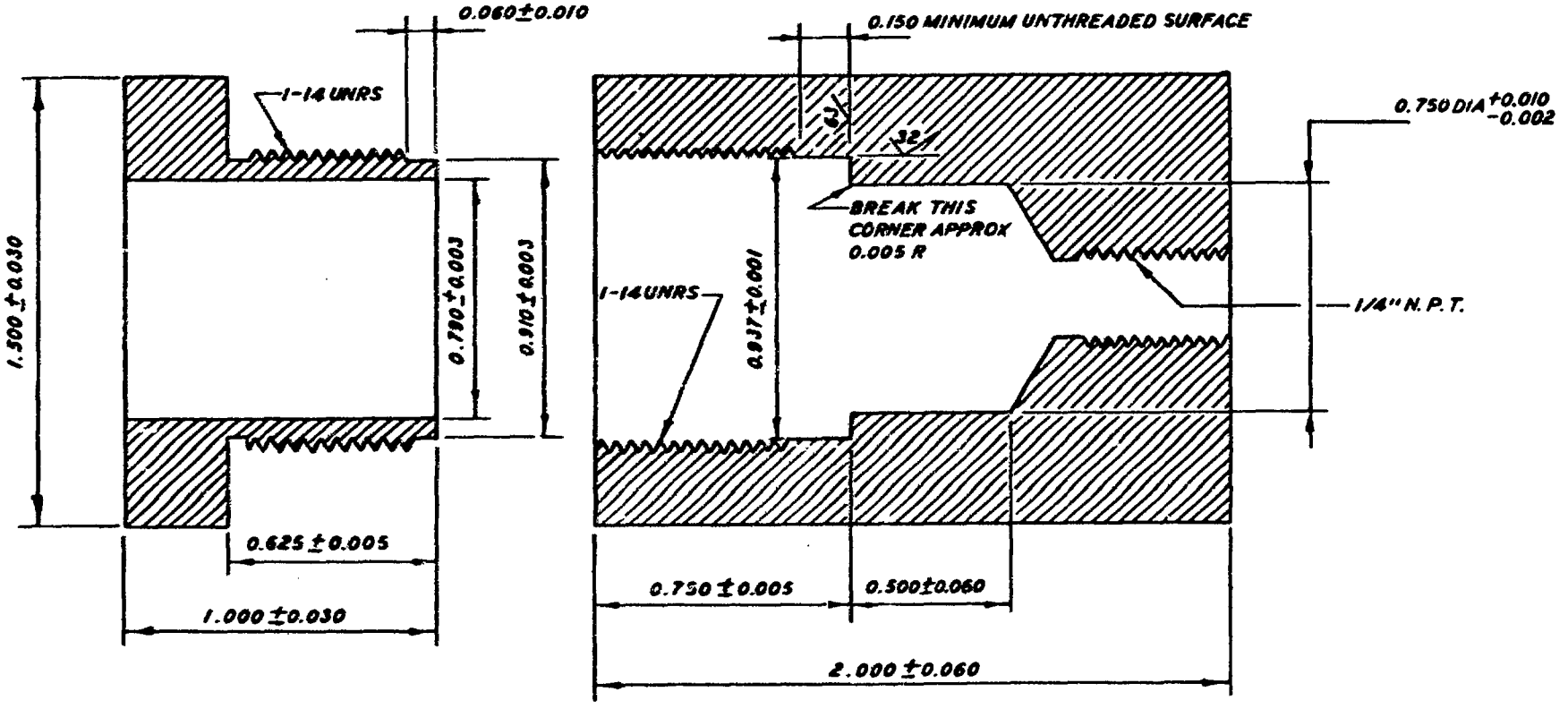

LABORATORY CALIBRATION FIXTURE FOR SOIL-STRUCTURE INTERFACE STRESS GAGE

MATERIAL: MILD STEEL
ALL DIMENSIONS ARE IN INCHES

Figure B.1. Laboratory calibration fixture. An O-ring with Parker size No. 2-116 is required.

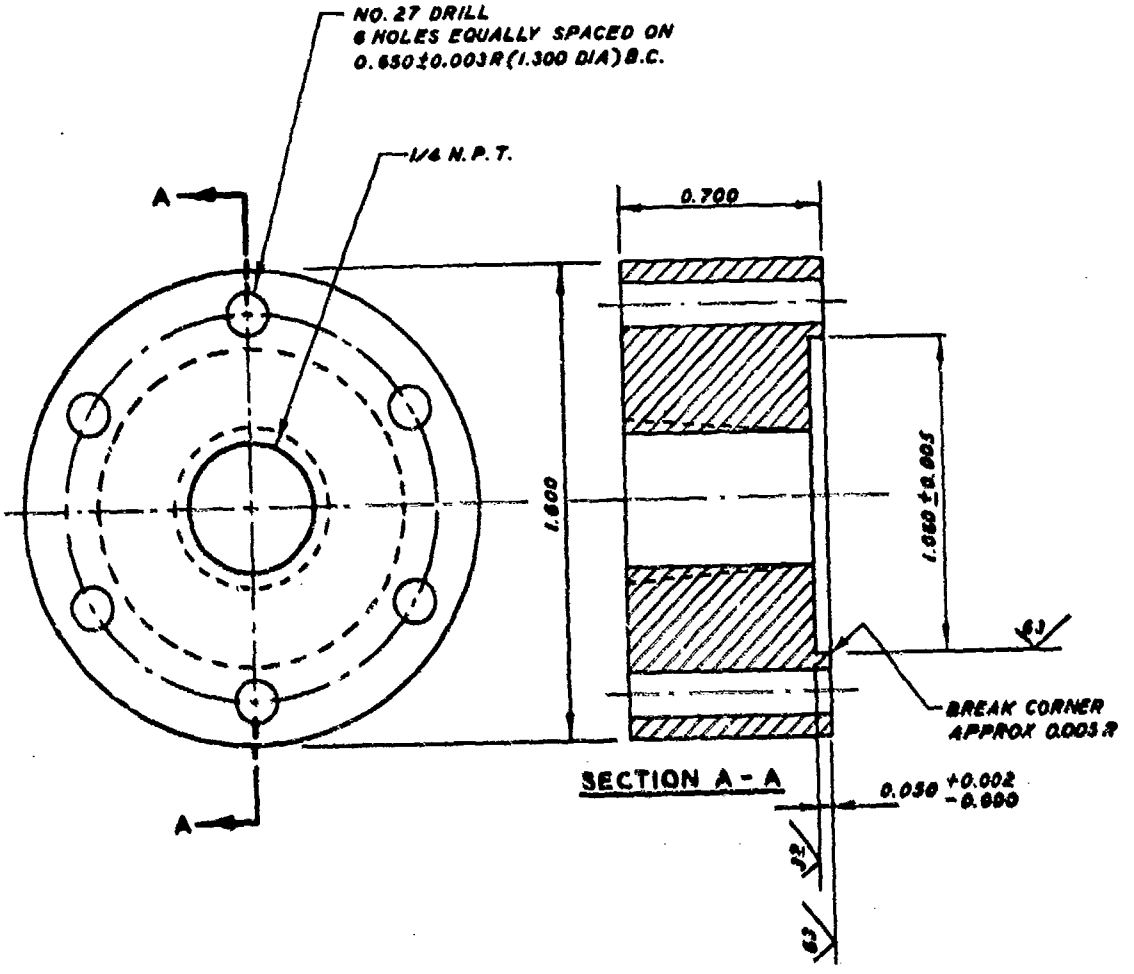

FIELD CALIBRATION FIXTURE FOR
SOIL-STRUCTURE INTERFACE STRESS GAGE

MATERIAL: AISI TYPE 416 STAINLESS STEEL
ALL DIMENSIONS ARE IN INCHES
TOLERANCES: ±0.010 UNLESS OTHERWISE SPECIFIED

Figure B.2. Field calibration fixture. An O-ring with Parker size No. 2-021 is required.

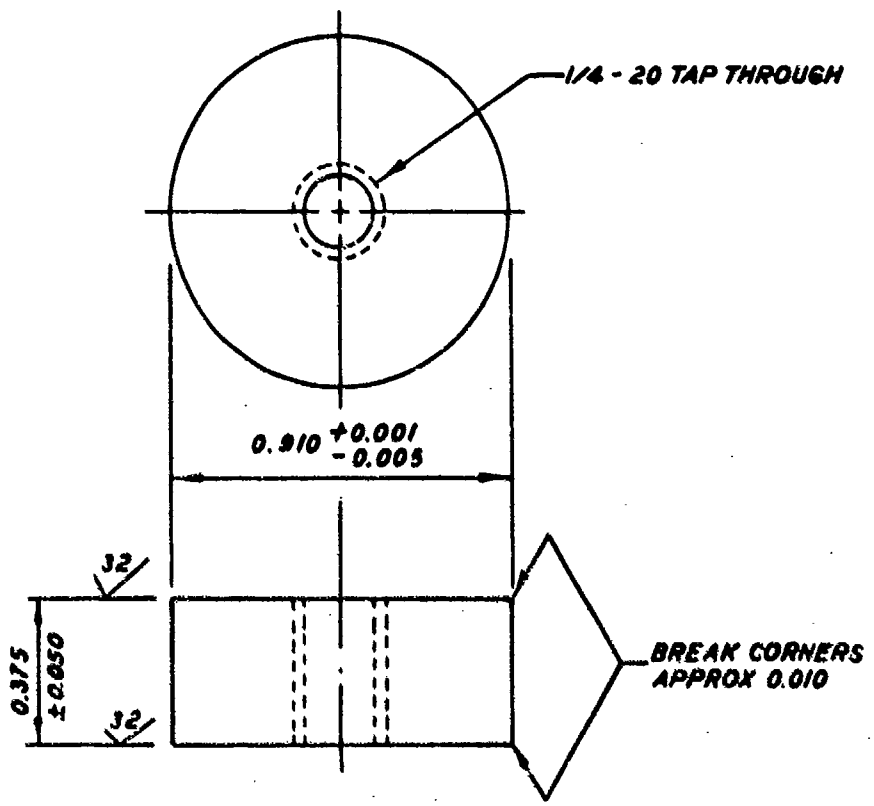

Figure B.3. Nut for fastening mount to outer wall of the structure form.

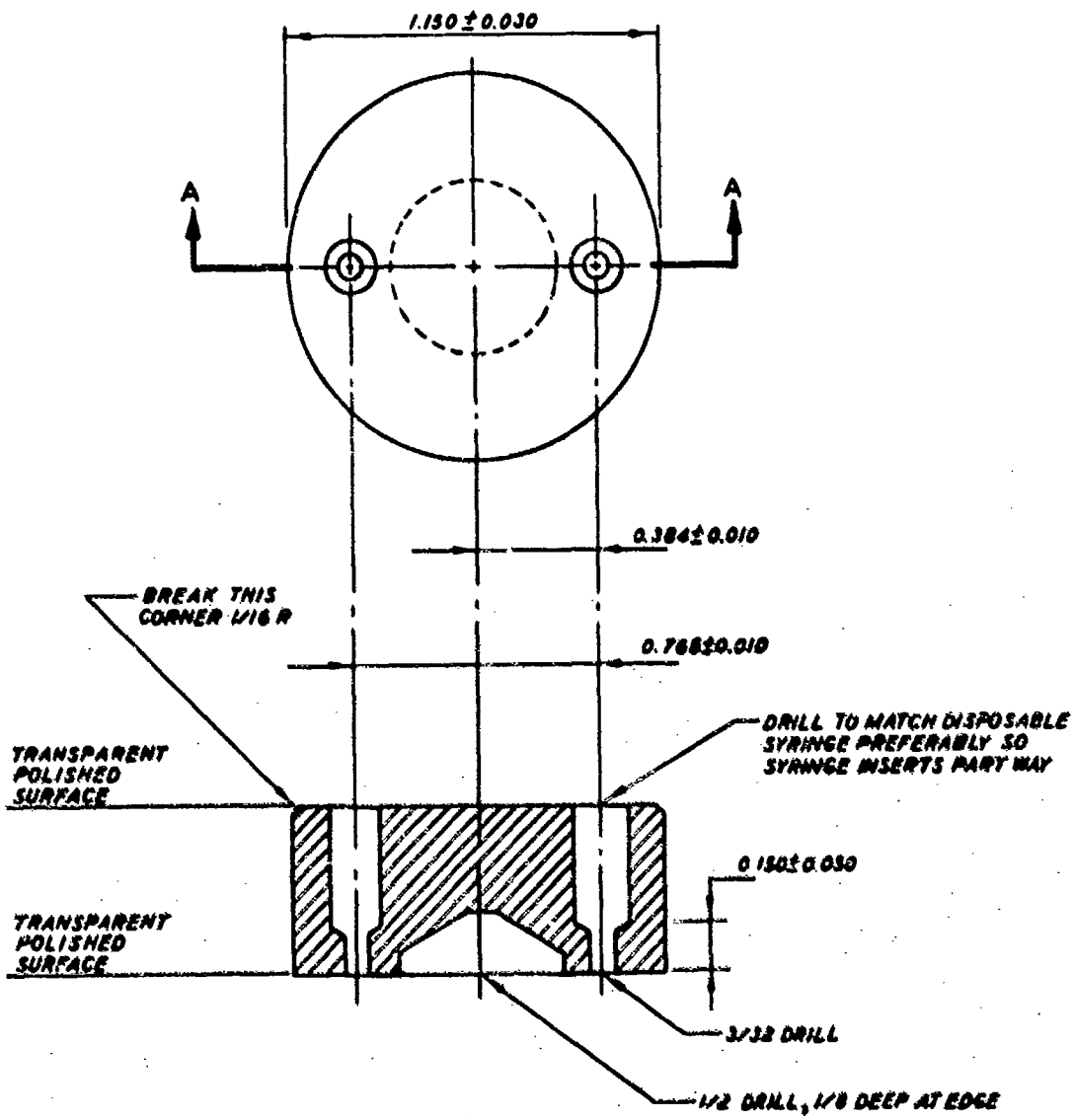

Figure B.4. Injection tool. 1/16-inch-thick rubber or neoprene (a somewhat transparent variety is best) with two holes matching the 3/32 drill holes glued to the bottom side.

APPENDIX C

TESTS TO ESTABLISH THE BOLT PRELOAD TORQUE

The bolt preload torque of 2.26 N-m (20 in.-lb) was chosen as 2/3 of the mean torque in a sample of 22 bolts torqued to failure in a simple test fixture involving the same materials and thread engagement length as in the mount. Surfaces of the test fixture, including the threads, had been cleaned with Freon 113; the bolt surfaces were in the same condition as in their shipping container. All tests involved virgin surfaces; there were no "repeat" tests with previously used surfaces.

In the actual mount, the bolts are additionally subjected to some flexure because of the elastic deformation (rolling) of the clamp ring during tightening. Further tests were done with three gage-and-mount assemblies. In each of these, the six bolts were tightened in a diametrically opposing sequence in small increments until one failed. The mean failure torque thus obtained, 3.1 N-m, was very nearly the same as the mean of the lowest four out of the 22 failure torques (4/22 = 1/6) obtained in the simple test fixture.

DISTRIBUTION LIST

DEPARTMENT OF DEFENSE

Assistant to the Secretary of Defense
Atomic Energy
ATTN: Executive Assistant

Defense Advanced Rsch. Proj. Agency
ATTN: TIO

Defense Intelligence Agency
ATTN: DB-4C, E. O'Farrell
ATTN: DB-4N

Defense Nuclear Agency
2 cy ATTN: SPSS
4 cy ATTN: TITL

Defense Technical Information Center
12 cy ATTN: DD

Field Command
Defense Nuclear Agency
ATTN: FCTMOF
ATTN: FCPR

Field Command
Defense Nuclear Agency
Livermore Division
ATTN: FCPRL

Undersecretary of Def. for Rsch. & Engrg.
ATTN: Strategic & Space Systems (OS)

DEPARTMENT OF THE ARMY

BMD Advanced Technology Center
Department of the Army
ATTN: ATC-T
ATTN: ICRDABH-X

Chief of Engineers
Department of the Army
ATTN: DAEN-MCE-D
ATTN: DAEN-RDM

U.S. Army Concepts Analysis Agency
ATTN: CSSA-ADL

Harry Diamond Laboratories
Department of the Army
ATTN: DELHD-I-TL
ATTN: DELHD-N-P

U.S. Army Ballistic Research Labs.
ATTN: DRDAR-BLE, J. Keefer
ATTN: DRDAR-TSB-S
ATTN: DRDAR-BLV

U.S. Army Engineer Center
ATTN: DT-LRC

U.S. Army Engineer Div., Huntsville
ATTN: HNDED-SR

U.S. Army Engineer Div., Ohio River
ATTN: ORDAS-L

DEPARTMENT OF THE ARMY (Continued)

U.S. Army Engr. Waterways Exper. Station
ATTN: WESSE, L. Ingram
ATTN: J. Strange
ATTN: WESSD, G. Jackson
ATTN: Library
ATTN: WESSA, W. Flathau
ATTN: J. Drake

U.S. Army Material & Mechanics Rsch. Ctr.
ATTN: Technical Library

U.S. Army Materiel Dev. & Readiness Cmd.
ATTN: DRXAM-TL

U.S. Army Missile Command
ATTN: RSIC

U.S. Army Nuclear & Chemical Agency
ATTN: Library

DEPARTMENT OF THE NAVY

Naval Construction Battalion Center
ATTN: Code L51, S. Takahashi
ATTN: Code L51, R. Odello
ATTN: Code L08A

Naval Electronic Systems Command
ATTN: PME 117-21

Naval Facilities Engineering Command
ATTN: Code 03T
ATTN: Code 04B
ATTN: Code 09M22C

Naval Material Command
ATTN: MAT 08T-22

Naval Postgraduate School
ATTN: Code 0142

Naval Research Laboratory
ATTN: Code 2627

Naval Surface Weapons Center
ATTN: Code F31

Naval Surface Weapons Center
ATTN: Tech. Library & Info. Services Branc

Naval Weapons Evaluation Facility
ATTN: Code 10

Newport Laboratory
Naval Underwater Systems Center
ATTN: Code EM, J. Kalinowski

DEPARTMENT OF THE AIR FORCE

Air Force Geophysics Laboratory
ATTN: LWW, K. Thompson

Air Force Institute of Technology
ATTN: Library

DEPARTMENT OF THE AIR FORCE (Continued)

Air Force Systems Command
ATTN: DLW

Air Force Weapons Laboratory
Air Force Systems Command
ATTN: NTES, J. Shinn
ATTN: SUL
ATTN: DEO-I
ATTN: DED-I

Ballistic Missile Office
Air Force Systems Command
ATTN: MNN

Deputy Chief of Staff
Research, Development, & Acq.
Department of the Air Force
ATTN: AFRDSM

Foreign Technology Division
Air Force Systems Command
ATTN: NIIS Library

Vela Seismology Center
ATTN: G. Ullrich

DEPARTMENT OF ENERGY

Department of Energy
Nevada Operations Office
ATTN: Mail & Records for Technical Library

DEPARTMENT OF ENERGY CONTRACTOR

Sandia National Laboratories
ATTN: L. Hill
ATTN: A. Chabai
ATTN: 3141

DEPARTMENT OF DEFENSE CONTRACTORS

Agbabian Associates
ATTN: M. Agbabian

Applied Theory, Inc.
2 cy ATTN: J. Trulio

AVCO Research & Systems Group
ATTN: Library A830

BDM Corp.
ATTN: Corporate Library
ATTN: T. Neighbors

Boeing Co.
ATTN: Aerospace Library

California Institute of Technology
ATTN: T. Ahrens

DEPARTMENT OF DEFENSE CONTRACTORS (Continued)

California Research & Technology, Inc.
ATTN: K. Kreyenhagen
ATTN: Library

California Research & Technology, Inc.
ATTN: D. Orphal

Civil Systems, Inc.
ATTN: S. Blouin

EG&G Washington Analytical Services Center, Inc.
ATTN: Library

Eric H. Wang
Civil Engineering Rsch. Fac.
ATTN: N. Baum

General Electric Company—TEMPO
ATTN: DASIAC

IIT Research Institute
ATTN: Documents Library
ATTN: R. Welch

Kaman Sciences Corp.
ATTN: Library

Merritt CASES, Inc.
ATTN: Library
ATTN: J. Merritt

Nathan M. Newmark Consult. Eng. Svcs.
ATTN: N. Newmark

Physics International Co.
ATTN: Technical Library
ATTN: F. Sauer

R & D Associates
ATTN: C. MacDonald
ATTN: Technical Information Center
ATTN: J. Carpenter
ATTN: J. Lewis
ATTN: P. Haas

Science Applications, Inc.
ATTN: Technical Library

Science Applications, Inc.
ATTN: D. Maxwell

Southwest Research Institute
ATTN: W. Baker

SRI International
ATTN: D. Keough
ATTN: Y. Gupta

TRW Defense & Space Sys. Group
ATTN: P. Dai